CURRENT INSTABILITIES IN CADMIUM SULPHIDE

THESIS PRESENTED FOR THE DEGREE OF

DOCTOR OF PHILOSOPHY IN THE UNIVERSITY OF LONDON

BY

ABDUL QAYYUM

ROYAL HOLLOWAY COLLEGE

February, 1972

BIBL. LONDIN. UNIV.

ProQuest Number: 10097586

All rights reserved

INFORMATION TO ALL USERS
The quality of this reproduction is dependent upon the quality of the copy submitted.

In the unlikely event that the author did not send a complete manuscript
and there are missing pages, these will be noted. Also, if material had to be removed,
a note will indicate the deletion.

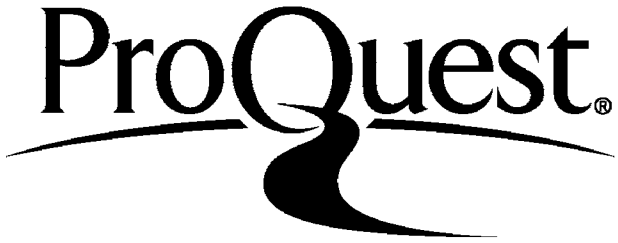

ProQuest 10097586

Published by ProQuest LLC(2016). Copyright of the Dissertation is held by the Author.

All rights reserved.
This work is protected against unauthorized copying under Title 17, United States Code.
Microform Edition © ProQuest LLC.

ProQuest LLC
789 East Eisenhower Parkway
P.O. Box 1346
Ann Arbor, MI 48106-1346

ACKNOWLEDGMENTS

I wish to take this opportunity to express my gratitude to Dr. E.R. Wooding for the provision of excellent research facilities. I also thank him for his constant interest and encouragement throughout the course of investigation and without whose collaboration the work described in this thesis would not have been possible. I thank Mr. J. Henley, Mr. W.H. Howell and Mr. R. Mason for their help and co-operation with the construction of apparatus and preparation of specimens.

I also wish to thank the Ministry of Education, Government of Pakistan, for providing personal financial support.

Finally, I thank my wife for much forbearance and my parents for providing me with the opportunities to continue my education.

ABSTRACT

During the investigation of current instabilities in semi-insulating single CdS crystals, caused by applying a high voltage pulse and using various illumination distributions, some completely new phenomena have been observed. The major phenomena are discussed and explanations have been offered for the observed effects with various types of illumination. Phenomena observed have been compared with the results of other workers.

One type of instability was initiated by applying high voltage pulses to CdS specimens in complete darkness. It is observed from the field measurements that the period of oscillation is equal to the transit time of the acoustic wave from the position of high field region to the anode end of the specimen and not related to the wave transit time between electrodes.

High frequency non-sinusodial electrical oscillations were observed in uniformly illuminated specimens. These were attributed to the effect of longitudinal potential gradients which were found when the electric field was measured under oscillatory conditions.

Continuous acousto-electric current oscillations were observed in a specimen by shading a length near to the anode end. Extremely high fields were detected in the high resistivity region so formed when amplification occurred. Obscuring a narrow strip perpendicular to the length of the sample and applying a high voltage pulse resulted in current oscillations and two step saturation of the current. A number of oscillatory modes were often found in a specimen, depending on the position of the shielded strip on the specimen. Extremely high electric

fields were observed near the position of the obscured strip of the specimen.

In two-step current saturation phenomena the changes in current pulses were recorded. Low frequency current oscillations were observed after the current had fallen to a final steady value. The conductivity of the material at different times after the application of a high voltage pulse was recorded and it remained constant below threshold voltages and thereafter differed from the ohmic low voltage value. The electric field reached maximum values 0.5mm from the cathode and 1mm from the anode ends of the specimen.

High frequency non-sinusodial current oscillations were recorded by localised illumination of the specimens with an He-Ne laser beam. With low voltage pulses, the I-V characteristics of these specimens fell below the linear ohmic relation, but at high voltages the current became proportional to the square of the applied voltage.

Qualitative explanations of these oscillations have been given and it has been shown that they are consistent with existing theory.

CONTENTS

Publications

1. INTRODUCTION

In semi-insulating CdS continuous current oscillations with frequencies around 1MHz or less have been observed by many workers,[37,44,51,55,56] if the crystal is illuminated in the vicinity of the negative electrode and a sufficiently large drift field is applied. By illuminating the specimen in various ways, the author of this thesis has shown the existence of a number of phenomena not previously reported, and an explanation of these effects is presented.

Samples of semi-insulating cadmium sulphide obtained from several sources showed considerable variability even if specimens were cut from adjacent sites in a single crystal. In the course of the investigation, observations have been made on the current resulting from the application of a high voltage pulse; measurements being made of its amplitude, oscillation frequency and saturation value. The field distribution through the specimen has been determined enabling the resistivity to be calculated. Absorption spectra were obtained in the range 2.5 to 25 micron so that trapping centres could be identified.

With the aid of these measurements, it has been possible to produce an explanation of the phenomena observed.

It has been known[30-32] that sound waves in semi-insulating and semi-conducting CdS material are strongly attenuated because of their interaction with conduction carriers. The deformation potential or piezoelectric effect may be responsible for such interactions and it becomes strongest when the carriers are drifting near to or faster than the velocity of sound.[31] The degree of attenuation which the acoustic wave undergoes is dependent on the drift velocity of the carriers.

Weinreich,[30] explored this possibility and showed that the carriers would amplify acoustic waves if the drift velocity of the carriers was made to exceed the velocity of sound. His earlier attempts to amplify acoustic waves in Germanium[32] were unsuccessful because of the low gain at the frequency employed. However, later work[33,34] has shown that considerable amplification is possible for both piezoelectric and non-piezoelectric materials.

The first indication of gain was observed by Hutson, McFee and White,[33] who obtained gains of 18db at 15MHz and 38db at 45MHz, in a 7mm length of CdS.

In general, continuous current oscillations in semi-insulating materials occur only when there is a non-uniformity of conductivity along the specimen. The material most frequently utilized and which has been selected for this phenomenon is semi-insulating CdS. The inherent nature of the material permits variation of conductivity over a wide range by varying the illumination so that gradients in the conductivity may easily be achieved.

Several different types of current oscillations have been observed for various materials[36-41] and under different conditions.[35-44,46,57-63] The mechanism of these observed oscillations is not completely understood and much investigation is still in progress around the world.

Acousto-electric current oscillations have been obtained by shading a length of the specimen from the anode end. Obscuring a narrow strip along the length of the specimen often resulted in oscillations and two step saturation in current. A number of frequency modes were often observed in a single specimen. The frequency depended on the position of the dark strip along the length of the specimen. It is suggested

that observance of these frequency modes are due to the presence of irregularities in the specimen. The changes in current pulses, when a high voltage pulse was applied to a specimen were recorded. The conductivity of the material at different times was measured after the application of a high voltage pulse and its dependence on illumination intensity was observed. It is suggested that in two step current saturation phenomena, the acousto-electric interaction is followed by injection of holes from crystal inhomogeneities.

High frequency non-sinusodial electrical oscillations have been obtained in specimens under uniform illumination and localised illumination by a helium neon laser beam. The current voltage characteristics at low voltages fell below the linear ohmic relation. After this the sub-linear region changed into stronger electric fields with current varying as the square of the voltage. The absorption spectra of the material also showed absorption peaks, suggesting the presence of active trapping centres. These instabilities in current have been attributed to the filling and emptying of these trapping centres.

Continuous current oscillations were also observed in two specimens cut from a single CdS crystal, after applying a high voltage pulse in complete darkness. It was observed that the period of oscillation equalled the time taken by the sound wave to travel from the position of high field region to the anode end of the specimen.

In view of the wide variety of oscillations observed it is possible that more than one kind of mechanism is responsible for these oscillations in CdS. However, the main interest is to discuss each phenomena observed and try to formulate a model to explain the effect.

A qualitative discussion on how oscillations occur at different conditions employed and how their frequencies might be effected is included.

2. Solid state plasma

2.1 Plasma

We can define a solid state plasma as any combination of 'mobile' electrons or holes or both that can exist in a crystal. Electrical neutrality of the entire solid is always assumed in the quiescent state. Thus, in a metal such as copper the free electrons comprising the plasma are electrically compensated by the positively ionized copper atoms, whereas in a semi-conductor, with non-equilibrium numbers of electrons and holes, the electrical compensation arises from the electron hole compensation as well as the ionized donors and acceptors. When electric and magnetic fields are applied to this plasma, density gradient and space charge effects can arise. Under these conditions the concept of screening at distances greater than the Debye length, plasma oscillations occur.

There are three types of plasmas that occur in solids. They are:-

a) Uncompensated plasma

b) Compensated plasma

c) Non-equilibrium plasma

Uncompensated plasma

Here electrons (or holes) interacting with themselves in a uniform ion background constitute an 'uncompensated plasma'. The best examples are the electrons in a metal, the electrons (or holes) in an extrinsic semi-conductor, or those of a doped semi-metal. The motion of charge carriers in this type of plasma is always constrained by the necessity to maintain space charge neutrality with the fixed lattice or impurity ions.

Compensated plasma

This type of solid state plasma possesses equal densities of oppositely charged particles, electrons and holes, both of which are highly mobile compared with the positively charged particles of uncompensated plasma, namely the lattice or impurity ions. This type of plasma can be produced in intrinsic semi-conductors and pure semi-metals. Compensated plasma is also constrained though not completely inhibited by space charges from the gross motions the third type of plasma can perpetrate (pinch effect).

Non-equilibrium plasma

The third type of plasma is composed of non-equilibrium carriers in essentially equal densities produced, for example, by injection from current contacts, by optical injection and by impact ionization. These charge carriers are not required to neutralize fixed ionic charges and therefore can readily engage in gross displacements such as occur during the pinch effect.

Sources

Materials in which these effects are observed are:-

1) Metals (i.e. Cu, Na, K)

2) Semi-metals (i.e. Bi, Sb)

3) Semi-conductors (i.e. Ge, Si, InSb)

2.1.1 Sources of solid state plasma

The following have been summarized as the sources of solid state plasma:

1. The injection of electrons or holes or both into semi-conductors from a pn junction. This source has been extensively employed for many semi-conductors. A good example of how this technique

is applied to solid state plasma experiments in InSb is found in the work of Ancker-Johnson et al.[1]

2. Impact ionization across the forbidden energy gap of semi-conductors. This process is called 'avalanche breakdown' and can occur in either bulk material or reverse biased pn junctions. In bulk material, this type of technique has yielded quite dense electron hole plasmas in such low band gap semi-conductors as InSb[2] and InAs.[3-4] For higher band gap semi-conductors such as Ge, Si the avalanche breakdown process is more readily accomplished by reverse biasing a pn junction to develop the very high electric fields needed. Such experiments have been extensively pursued in Ge and Si.[5] This particular generation technique was employed with InSb in the first studies of the pinch effect in solids.[6] It was also used extensively in the pioneer experiments that exhibited microwave emission from InSb.[7]

3. Impact ionization of impurity levels in semi-conductors. This technique is useful when low density plasmas are needed. When the thermal energy of the lattice becomes of order of the impurity ionization energy, most of the electrons (for donors impurities) become frozen out on the impurities. But for shallow impurities in semi-conductors, such as Ge, this requires a very low temperature ($T \ll 20^{\circ}K$). If the remaining electrons in the conduction band are then drifted to high enough kinetic energies, they can cause impact ionization of the frozen out levels, thereby increasing the mobile carrier density by order of magnitude. This position can be achieved by drifting electric fields of the order 10V/cm in such materials as Ge[8], where the shallow impurities have energies of about 10^{-2}eV. The plasmas produced by this method consist of only one species of mobile carrier (electrons or holes for n- or p-type impurities respectively) in contrast to the technique of band gap ionization which gives electron hole pairs.

4. Ionizing radiation for the production of electron-hole pairs. If a semi-conductor with a forbidden energy gap of E_G is exposed to radiation of energy $\hbar\omega$ such that $\hbar\omega > E_G$ electron-hole pairs can be produced. This technique can be applied to any semi-conductor. With intense optical laser beams it should become a very convenient source for studying high density solid state plasma effects.

The solid state plasma differs from the gaseous plasma in two respects, namely the parameters are often of an entirely different order of magnitude and the physical laws are operating on a different scale.

2.1.2 Range of parameters

Some of the important parameters are discussed below:

Carrier density

The plasma density in solids can range over many orders of magnitude, from metals such as copper having $\simeq 10^{28}$ electrons/m^3, to a very pure semi-conductor such as Germanium or silver having $\simeq 10^{14}$ electrons/m^3 at low temperatures. It is rather easy to change the plasma density in a given solid by several orders of magnitude in a controlled fashion, using the methods described above.

Effective mass of carriers

Because of the periodic potential of the crystal lattice the effective mass m^* of the mobile carriers is generally lower than the free electron mass m_o. For electrons, the values of $\frac{m^*}{m_o}$ range from $\simeq 10^{-2}$ in solids such as Bi and InSb to $\simeq 1$ in most metals, for example Cu or Na. The holes also have similar effective masses but in a given solid electrons generally have lower effective masses than holes.

Plasma and cyclotron frequencies

The large range of densities and low masses have important consequences in the frequency of oscillation of the carriers when subjected to electromagnetic fields. The plasma frequency ω_p and the cyclotron frequency ω_c are the most important of the oscillations.

For typical semi-conductors, ω_p is of the order of 10^{12} sec^{-1} a frequency in the millimeter wave region of the electromagnetic spectra, while for metal ω_p is of the order of 10^{15} sec^{-1} within the visible region of the spectrum. Cyclotron frequencies in magnetic fields of 1000G range from 10^{10} sec^{-1} for metals to 10^{12} sec^{-1} for semi-conductors whose carriers have small m_e values.

Scattering frequencies

The scattering frequency ν for gases is often neglected compared to other frequencies since it can be very low for low density plasmas. But in solids because of ever present thermal vibrations of the lattice, scattering is very important. For solids the value of ν ranges from about 10^{10} to 10^{13} sec^{-1} as the temperature increases from that of liquid helium ($4.2^{\circ}K$) to room temperature ($300^{\circ}K$).

Lattice dielectric constant

Since the crystal lattice that contains the solid state plasma is itself polarizable, it contributes to the dielectric constant ϵ. In most semi-conductors the relative dielectric constant of the lattice $\epsilon_L = \frac{\epsilon}{\epsilon_o}$ is between 10 and 20. For semi-metals like Bi it can have values up to 100, which introduces a factor of 10 in the plasma frequency and the Debye screening length.

Dielectric relaxation frequency

Another important plasma parameter is ω_R, the dielectric relaxation frequency. It is defined by the relation

$$\omega_R = \frac{\omega_p^2 \epsilon_o}{\epsilon \nu} = \frac{\sigma}{\epsilon} \qquad (1)$$

where σ is the conductivity of the plasma. The reciprocal of ω_R is the dielectric relaxation time of a solid τ_R which ranges from $\simeq 10^{-18}$ sec for metals to 10^{-12} sec for many semi-conductors.

Distribution function

Metallic plasmas are governed by Fermi-Dirac statistics with a Fermi temperature of about 10^{4}°K. Most of the semi-conductor plasmas of interest will be non-degenerate so that the equilibrium distribution is assumed to be maxwellian. When external forces are applied, the effects of carrier drift and increased effective carrier temperature lead to a displaced maxwellian distribution.

Debye length

When the plasma has a finite temperature, another important parameter is λ_D, the Debye length. It is defined by the relation

$$\lambda_D = \frac{2\pi v_\theta}{\omega_p} \qquad (2)$$

where v_θ is the average thermal velocity of the carriers for a particular distribution function involved. For metals $\lambda_D \simeq 10^{-9}$m, while for semi-conductors it is $\simeq 10^{-6}$m. These values indicate the minimum linear dimensions that the solid can have in order that the plasma exhibits collective effects.

Diffusion effects

Scattering of charge carriers at a finite temperature in a solid results in diffusion. Most of the interesting interactions involve carrier bunching so that diffusion can play a critical role. It is characterized by the diffusion constant D, defined as

$$D = \frac{K_B T}{m\nu} = \frac{v_\theta^2}{2\nu} \qquad (3)$$

where v_θ is the average thermal velocity. For most solids, $v_\theta \simeq 10^6$m/sec

and $\nu \simeq 10^{13}$ sec^{-1} so that $D \simeq 10^{-1}$ m^2/sec. An important aspect of diffusion concerns the upper frequency limit that it imposes on any wave instability involving bunching. If v_ϕ is the phase velocity of the wave, the diffusion frequency ω_D is defined as

$$\omega_D = \frac{v_\phi^2}{D}$$

Then the wave frequency ω is limited by the inequality

$$\omega^2 < \omega_R \omega_D$$

where ω_R is the dielectric relaxation frequency.

2.2 Crystal structure

The crystallography of the II-VI compounds is somewhat complicated. The principal structure types are cubic zincblende (sphalerite) and hexagonal wurtzite in which the atoms are tetrahedrally bound in network arrangements related to those of the group VI semi-conductors. In addition, there are closely related polytypes which have tetrahedrally co-ordinated arrangements that are substantially derivative structures of zincblende and wurtzite.

Crystals encountered in practice are usually non-ideal and certain defects and imperfections which in many cases control the semi-conducting properties. Crystal imperfections are arbitrarily classified into point defects such as vacancies or impurity atoms, line or plane defects which result from the interaction or coalescence of elementary defects.

Description of crystal structure

The atomic arrangements in crystals result from geometric constraints associated with the sizes of the atoms, coulombic forces due to the charges on the atoms or ions and directional properties related to the nature of the chemical bonding. If electrostatic considerations prevail the

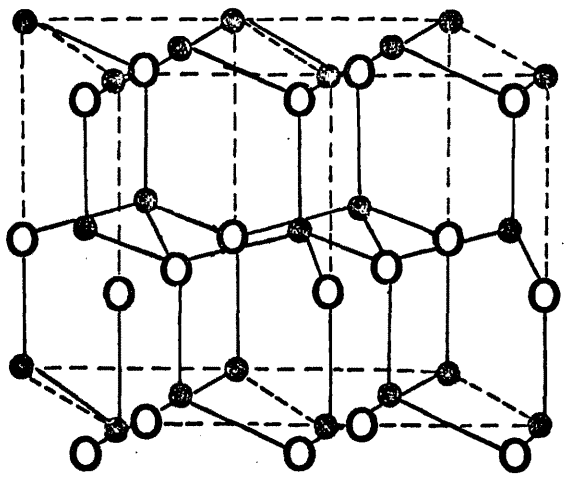

FIG.1 Wurtzite. The arrangement of metal atoms (small filled circles) and non-metal atoms (large open circles) in wurtzite, the hexagonal for ZnS. The arrangement adopted by CdS, CdSe. The dashed lines outline the orthohexagonal cell for which $a = \sqrt{3}\ a_{hex}$, $b = a_{hex}$; $c = c_{hex}$ and the cell edges are all at right angles to each other (after Pauling, 1960).

crystal is considered to be 'ionic' and distinguished from a 'covalent' crystal in which chemical or homopolar bonding seems important. Regarded from this point of view, the II-VI compounds crystallize in structures in which the binding varies from ionic to covalent and in most cases they exhibit characteristics intermediate to both extremes.

The majority of the II-VI compounds crystallize in structures which can be classified on the geometric basis of cations filling some of the interstitial positions in different sequences of close packed anions (Table 1). Equal sized spheres, packed together as closely as possible in a periodic structure, will be arranged in cubic close packing, hexagonal close packing or combinations of cubic and hexagonal close packed sequences. The close packed anion lattice has one octahedral site and two tetrahedral sites per anion, so that for the composition AB all the octahedral sites or half the tetrahedral sites are occupied by cations. Cubic zincblende structure is formed when cations occupy half the tetrahedral sites in a regular way, so alternate sites are vacant and hexagonal wurtzite when cations occupy half the tetrahedral sites in the hcp lattice. In a similar way, the numerous complex hexagonal and rhombohedral polytypes are formed when cations occupy half the tetrahedral sites in anion lattices with mixed cubic and hexagonal close packing.

Wurtzite structure

The II-VI compounds[9-11] apart from zincblende structure also crystallize in the wurtzite or zincite (zno) arrangements (Fig.1). The space group is C_6^4 - $P6_3mc$ and there are two molecules in the hexagonal unit cell with two Zn. Each Zn atom is bonded to four S atoms, approximately at the corners of a tetrahedron, one at the distance Uc and three at $\left[\frac{1}{3}a^2 + c^2(u - \frac{1}{2})^2\right]^{\frac{1}{2}}$. There are twelve next nearest neighbours; six at the corners of a hexagon in the same plane as the original atom at

Table 1

Classification of AB structures by anion packing

Packing	Interstitial sites occupied	
	All octahedral	½ tetrahedral
Cubic	Sodium chloride	Zincblende
Hexagonal	Nickle arsenide	Wurtzite
Cubic + hexagonal		Polytype

the distance a; the remaining six are at the corners of a trigonal prism at the distance $\left[1/3a^2 + \frac{1}{4}c^2\right]^{\frac{1}{2}}$. If $c/a = 2\sqrt{2}/\sqrt{3} = 1.6330$ and if $u = \frac{3}{8}$, the nearest neighbour co-ordination figure is precisely tetrahedral and the twelve next nearest neighbour distances are equal.

The distortion of compounds with the wurtzite structure has been discussed by Keffer and Portis[12] on the basis of a theory which assumes partial polar binding. The deformation results from long range forces due to postulated charges on each ion. When balanced against the elastic, piezoelectric and dielectric constants, these forces account for the magnitudes of the c/a ratios and the u parameters, all of which have the wurtzite structure.

The probable magnitude of the sub-lattice displacement can be estimated from the crystal distortion. If the bond stretching constants are large and the central atom moves to a position equidistant from the atoms on the distorted tetrahedron, then $u = \frac{1}{4} + 1/3(a/c)^2$. On the other hand, if the bond bending constants are large the central atom will move to maintain tetrahedral angles with the four neighbours and $u = \frac{1}{2} - (\frac{1}{24})^{\frac{1}{2}}a/c$. A relationship between the crystal distortion and sub-lattice displacement was found experimentally by Jeffrey et al[13] who observed for BeO and AlN that $\Delta_u = 2/3(a/c)^2 - \frac{1}{4}$. The sub-lattice displacement in these wurtzite structures appears to be twice the shift required to equalize the bond length.

Wurtzite does not have a centre of symmetry and there is a polar axis parallel to [0001]. As in zincblende, the II and VI ions of opposite polarity can be visualized as forming a network of permanent dipole moments. However, in wurtzite the moments do not balance but create a single polar axis. Consequently, in addition to being piezoelectric wurtzite crystals are pyroelectric and may develop potential differences of opposite signs on heating and cooling.

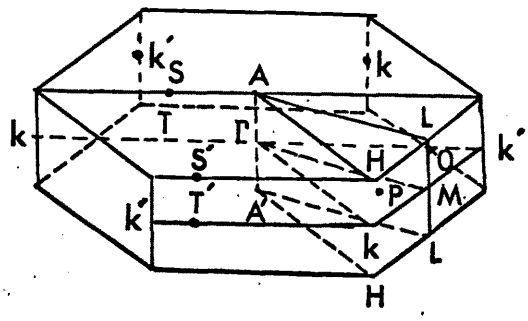

FIG.2 The Brillouin zone for wurtzite lattice with lines and points of special symmetry.

2.2.1 Band structure of the II-VI compounds

Wurtzite

In attempting to achieve an understanding of the properties of class II-VI semi-conducting compounds, it is necessary to relate them to the electronic structure of the material. We shall discuss briefly the wurtzite crystals.

The lattice of the wurtzite crystals consists of two inter-penetrating hexagonal close packed lattices, one containing the anions, the other cations. The translation vectors for this lattice are:-

$$\underline{a}_1 = \tfrac{1}{2}a(1,-\sqrt{3},0); \quad \underline{a}_2 = \tfrac{1}{2}a(1,\sqrt{3},0);$$
$$\underline{a}_3 = \underline{c}(0,0,1) \qquad (4)$$

where the vectors are given with respect to cartesian axes. The basis vector is $b = (0,0,\gamma)$ where $\gamma = \frac{3}{8}C$ for the "ideal" wurtzite structure and is within 1% of this value for the ZnS, CdS and CdSe. The reciprocal lattice is also hexagonal having the translation vectors:-

$$\underline{K}_1 = 2\pi a^{-1}(1, -(3)^{-\frac{1}{2}},0); \quad \underline{K}_2 = 2\pi a^{-1}(1,(3)^{-\frac{1}{2}},0)$$
$$\underline{K}_3 = 2\pi c^{-1}(0,0,1) \qquad (5)$$

The Brillouin zone which is the same as for the hexagonal close packed lattice is shown in Fig. 2. Several papers[14-16] have been published on the symmetry properties of the energy bands in wurtzite. To gain a first orientation in understanding of the electronic structure it is useful to note that to the extent that the lattice is "ideal", the arrangement of nearest neighbours is identical to that in the zincblende lattice and the next nearest neighbours are the same. Also the inter-atomic distances in both forms are quite comparable. This implies that the local environment and chemical bonding are nearly identical in both forms. As noted by BIRMAN[17] the essential difference between the

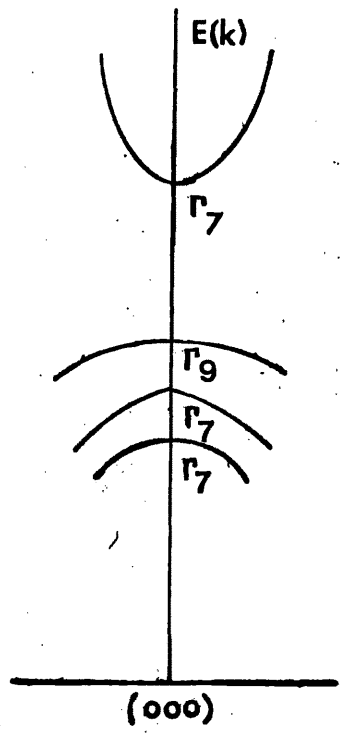

Fig.3 The conduction and valence band structure for wurtzite crystals around K = o. The irreducible representation indicated are those for the double group. The effects of small linear terms which can occur in Γ_7 bands are not shown in this drawing.

potential that an electron experiences in an ideal wurtzite lattice and that is a zincblende lattice is the relatively small difference in "crystal field" due to sites beyond the next neighbours.

It is clear from above that the conclusion drawn about the nature of the energy bands for the crystals with cubic form will be equally valid for those with the hexagonal form. The detailed differences in the band arise from the difference in the "crystal field" and from the difference in the Brillouin zones.

Because of the anticipated smallness of the difference in the "crystal field" it is possible to obtain the E(K) around Γ in terms of a simple perturbation of the corresponding bands in the corresponding cubic material. This is useful for the p-like valence bands which are depicted in Fig. 3. To obtain these $\underline{K} = o$ bands an interaction is introduced into the phenomenological valence band Hamiltonian for zincblende which, in the absence of the spin orbit interaction, splits the threefold $\Gamma_{15}(x,y,z)$ level into a $\Gamma_1(z)$ level and doubly degenerate $\Gamma_5(x,y)$ level (single group of $\underline{K} = o$ for wurtzite) which are separated by Δ_{cr}, the crystal field splitting. The result is known as the "quasi-cubic" model.[18]

Further insight into the wurtzite $E(\underline{K})$ is gained by recognising the correspondence of the c-axis, Γ-A-Γ', of the Jones (or "energy" or "double") zone for wurtzite (obtained by doubling the BZ in the c-axis direction) with the [1 1 1] axis from Γ to L in the zincblende Brillouin zone (BIRMAN,[17] 1959). By making the not unreasonable assumption that the energy shifts due to somewhat different boundary conditions in the two structures will be small, one would conclude that the $E(\underline{K})$ along Γ-Γ' will be reasonably close to those in zincblende from Γ to L. We note that there will be no energy discontinuity at the reduced BZ boundary,

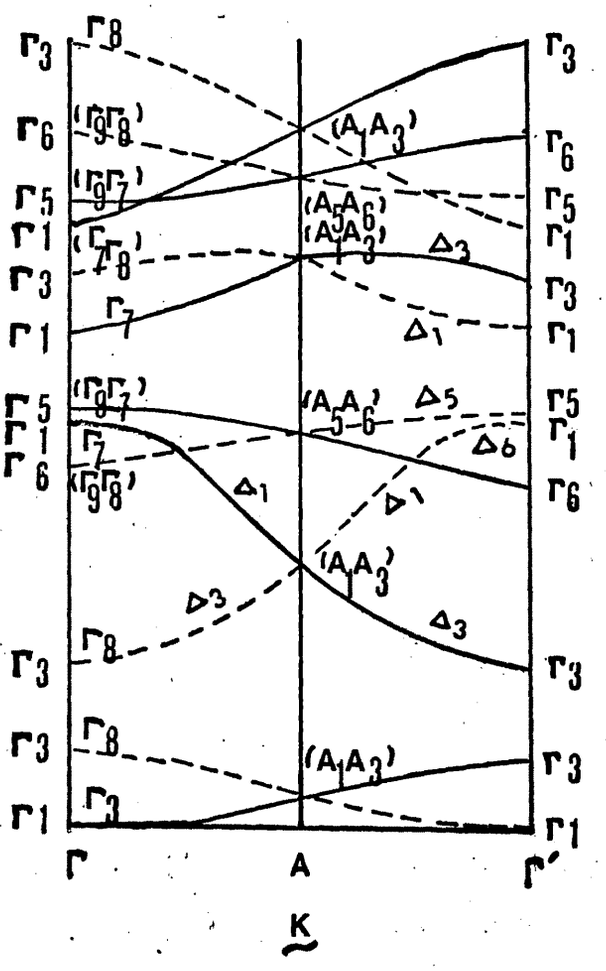

Fig.4 The energy bands for wurtzite along Γ -axis (i.e. c-axis) of the zone. The figure illustrates how E_μ ($\underline{K}$) for the wurtzite crystal in this direction are approximately related to those for zincblende crystal with the same constituents. The Γ -A-Γ' axis, which is the axis of Jones (or double) zone, corresponds to the Γ - L axis of the zincblende Brillouin zone. Except for a small crystal field splitting, Δ_{cr} and $\Delta_{cr'}$, the solid curves represent the $E(\underline{K})$ for the zincblende crystals.

the point A, because of the vanishing structure coefficient (e.g. see WILSON[19]). Across the boundary, the representation connect up according to $\Delta_1 \rightleftharpoons \Delta_3$, $\Delta_2 \rightleftharpoons \Delta_4$ and $\Delta_5 \rightleftharpoons \Delta_6$ with the above and the symmetries of the zone (which require that the bands be symmetric about A). One[20] can sketch the wurtzite bands in the c-axis direction from 'known' zincblende bands and the crystal field splittings Δ_{cr} and Δ_{cy}. Such a sketch is shown in Fig. 4. From this picture we see how the "extra" bands in wurtzite come about and roughly where they lie (e.g. the Γ_6 level is roughly 1 to 2eV below the Γ_5 level).

The principal band edges: wurtzite

Most of the detailed knowledge of the electron structure of these crystals come from the various studies of the exciton spectra. It is worthwhile to mention briefly important investigations made on CdS.

CdS: The first definitive determination of the band edges in a II-VI compound was made on CdS by THOMAS and HOPFIELD[21] in their studies of the exciton line spectra. From these studies they concluded that the absolute extrema associated with the line spectra are at the point in the BZ which is either at Γ or along the Γ - A axis, which has the same symmetry as Γ.

The value 0.22m $\pm$ 0.02m for the electron mass determined[22] by free carrier absorption and 0.21m $\pm$ 0.01m by Faraday rotation[23] is in substantial agreement with the 0.20m $\pm$ 0.01m value arrived at in the exciton Zeeman studies.[24]

The results of the galvanomagnetic measurements[25] on n-type samples are consistent with a single ($\underline{K}$ = o) conduction band minimum and an electron mass of about 0.20m. Cyclotron resonance of electrons has been observed by SWAWAMOTO[26] in 1963 and BAER and DEXTER[27] in 1964 and leads

to an effective mass of $m_{\perp} = 0.171m$ and $m_{\parallel} = 0.15m$ ($\perp$ and $\parallel$ are with respect to the c-axis). These values are lower by about 15 to 20% and are more anisotropic that the values obtained from the other experiments. Both of these differences have been attributed to "piezoelectric polaron" effects which manifest themselves in the cyclotron resonance measurements[28] and which are sizeable in CdS because of its relatively high piezoelectric coupling.

The near threshold absorption has also been measured in CdS by THOMAS et al[29] in 1960. The analysis of the absorption edge data showed that the data could be understood in terms of LO Phonon-assisted 'direct'-exciton creation. These results strongly indicate that the conduction and valence band extrema associated with the direct exciton are, in fact, the absolute extrema.

2.3 Phonons

Vibrations of the lattice are quantized with energy transitions which are multiples of h.f. values where f is the frequency of vibration. The quanta of vibrational energy is given the name 'phonon'.

The vector $\underline{U}q$ in the following equation when the lattice modes of crystal are excited and each atom is displaced from its ideal lattice site,

$$\begin{aligned} R_l &= l + U_l \\ &= l + \sum_q (\underline{U}q\, e^{i q.l} + \underline{U}q^{*} e^{-i q.l}) \end{aligned} \qquad (6)$$

where $\underline{U}q$ is the vector amplitude of the mode of wave vector q and complex conjugate term is included to make the displacement real, should contain a time factor $\exp(i\nu_q t)$, where ν_q is the frequency of the normal mode of wave vector $\underline{q}$. Indeed, $\underline{U}q$ is the sum of three such vectors, of different amplitudes, directions and frequencies, corresponding to three different acoustic modes of that wave vector. Take one of these at a time and

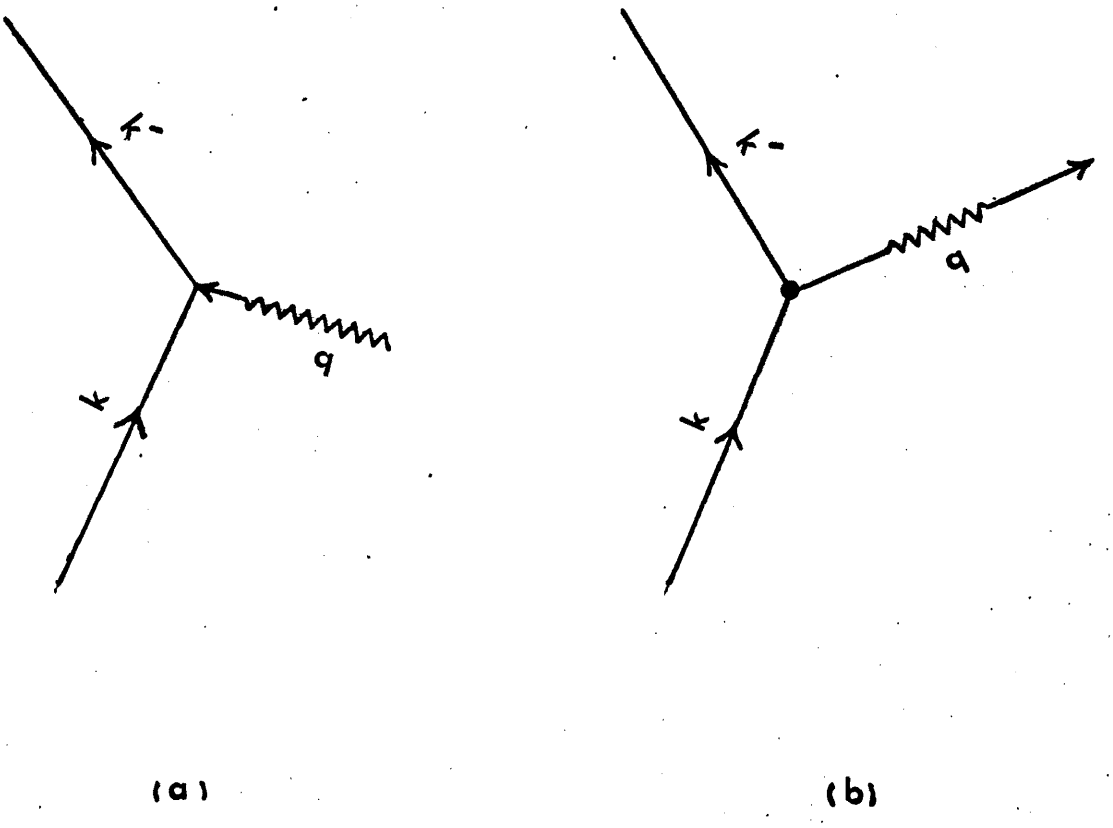

Fig.5 Electron scattering processes:

a) Phonon absorption;

b) Phonon emission.

remember that the states ψ_k and $\psi_{k'}$ of the incident and scattered beams must have energies $\mathcal{E}(k)$ and $\mathcal{E}(k')$ giving them time factors like $\exp\{i\mathcal{E}(\underline{K})t/\hbar\}$ and $\exp\{i\mathcal{E}(\underline{K}')t/\hbar\}$. When we average over time, we shall find integrals like

$$\int \exp\left[i\{\mathcal{E}(\underline{K}) - \mathcal{E}(\underline{K}') + \hbar\nu_q\}t/\hbar\right] dt$$

which must vanish unless

$$\mathcal{E}(\underline{K}) - \mathcal{E}(\underline{K}') + \hbar\nu_q = 0 \qquad (7)$$

In other words, the diffraction is inelastic; the beam has gained one quantum of the energy of the lattice mode with which it interacts.

In fact this is not complete, since the conjugate time dependence $\exp(-i\nu_q t)$ will also occur in the lattice vibration, giving a diffraction in which the frequency ν_q is lost by the electron. The two following conditions

$$\underline{q} = \underline{K}' - \underline{K} - \underline{g} \qquad (8)$$

$$\mathcal{E}(\underline{K}) - \mathcal{E}(\underline{K}') + \hbar\nu_q = 0 \qquad (9)$$

can be given a very graphic interpretation. We say that the incident electron (or X-ray or neutron) has interacted with the lattice to destroy (or create) a 'phonon', of wave vector $\underline{q}$ and energy $\hbar\nu_q$. This process can be represented by a diagram such as Fig. 5(a) or (b). The condition represented in Equation (9) is the rule for energy conservation in that process.

Looking at the equation as the following

$$\underline{q} = \underline{K}' - \underline{K} \qquad (10)$$

which holds for all values of $(\underline{K}' - \underline{K})$ in the first zone, we see it looks like a law of conservation of momentum. Multiply by $\hbar$ and we have

$$\hbar\underline{K}' = \hbar\underline{K} + \hbar\underline{q} \qquad (11)$$

The momentum of the electron has taken up the 'crystal momentum' $\hbar\underline{q}$ of the phonon which was destroyed.

In the general case the 'rule of conservation of momentum' does not hold; as we see in Equation (8) the electron can gain, or lose, momentum $\hbar \underline{g}$ in addition to the momentum of the phonon. We call such a process an Umklapp process or U-process. The extra momentum $\hbar \underline{g}$ is transferred to the crystal as a whole. An Umklapp process can be thought of as the creation (or destruction) of a phonon with, simultaneously, a Bragg reflection. The momentum is obviously transferred to the crystal as a whole.

The phenomena of inelastic diffraction is a valuable tool for the study of the lattice dynamics of crystals. The beam diffracted in a particular direction is associated with lattice modes having a definite wave vector $\underline{q}$. One can look at the change of energy of the diffracted particles and hence measure $\hbar \nu_q$. By looking into different directions and moving the crystal into different orientations, one can plot out the whole function ν_q. However, this experiment is only practicable with 'thermal' neutrons, whose wavelength is of the order of the lattice spacing at energies of the order of 0.1eV. The shift due to the phonon energy, which is of the order of KΘ or less - perhaps 0.01eV. - can easily be observed. For electrons and X-rays the beam energy must be much higher - tens or hundreds of electron volts - so that small change in energy in the diffraction process cannot be detected.

2.4 The amplification of ultrasonic waves in piezoelectric semi-conductors

Two basic properties of piezoelectric semi-conductors are of interest. Firstly, their conductivity can easily be tailored anywhere between that of an insulator and a conductor. Secondly, a most attractive property of this material is that of ultrasonic amplification within the bulk of the material. This is because of strong coupling between the carriers and the sound waves in piezoelectric semi-conductors. Therefore, comparing with metals, the low carrier density in a piezoelectric material makes it possible to attain a very high electron drift velocity at a reasonable power input to the crystal. The current oscillations and saturation in such material are due to the generation and amplification of acoustic flux within the semi-conductors.[33,35,36,41] HUTSON, McFEE and WHITE[33] discovered that the electronic attenuation could be reversed by the application of an electric field large enough to cause electrons to drift faster than the velocity of active sound wave within the crystal.

Many new phenomena were observed after the discovery of ultrasonic amplification which can be related to the ultrasonic properties of the semi-conductors. They are stated briefly and are the following:

(1) The current saturation resulting from an increase in the apparent resistance of the crystal above a critical electric field, which is associated with the build-up of ultrasonic flux.

(2) Under certain field conditions, the oscillations produced in the series current of piezoelectric semi-conductors.

(3) In piezoelectric semi-conductors the amplification of the acoustic flux was detected by SMITH[53] and has been related to the current saturation as mentioned in (1). The mechanism is briefly the transfer of energy from drifting carriers to acoustic waves (Appendix II) and occurs when the velocity of the drifting carriers exceeds the velocity of sound.[49] The condition for maximum gain is

$$\omega^2 = \omega_C \omega_D \quad \text{(Appendix II)}$$

(4) Harmonic generation of a travelling wave, where the harmonics of the primary wave are generated by a non-linear term in the electron response to the primary wave and subsequently amplified in the crystal.

(5) The so-called "anomalous sound propagation" in which sound waves are observed to travel at velocities lower than that of sound and are said to be associated with the interdependent propagation of a collection of sound waves as a single entity.

Many of the recently discovered phenomena are not completely understood and are still receiving considerable attention. Referring to (1) above, we require an understanding of this amplification process to start with. The experimental evidence of HUTSON, McFEE and WHITE verified semi-quantitatively the result of their derivation of the attenuation constant α.[33] A brief and simple description of α is given here, along the lines taken by WHITE.[50] A small signal analysis is used and to avoid unnecessary length, one dimensional case for n-type piezoelectric semi-conductors is considered.

The stress tensor T can be determined from the internal energy of the medium and for the ordinary solid is CS. But for the piezoelectric solid, however, there is additional contribution to the internal energy from the polarization fields, which accompany the lattice displacement. This additional energy is given by the product of the displacement and the electric field $\frac{1}{2}$ D.E. The stress tensor for the medium is then[45]

$$T = CS - eE \qquad (12)$$

Equation (12) follows from the Maxwell relation for the displacement field given by

$$D = eS + \epsilon E \qquad (13)$$

where,

C = elastic constant at constant electric field

e = piezoelectric constant

ϵ = intrinsic dielectric constant of the lattice

T = stress

S = strain

E = electric field

D = electric displacement

The strain may be written as:

$$S = \frac{\partial U}{\partial x} \qquad (14)$$

where,

U = lattice displacement

x = direction vector of propagation

The equation of motion of this mode is simply given by using the second low of motion:

$$\rho \left(\frac{\partial^2 U}{\partial t^2}\right) = \text{force/unit volume} = \frac{\partial T}{\partial x} \qquad (15)$$

where,

ρ = mass density of material

t = time

Therefore the equation of motion obtained from relations (12), (14) and (15) is:

$$\rho \left(\frac{\partial^2 U}{\partial t^2}\right) = C \left(\frac{\partial^2 U}{\partial x^2}\right) - e \left(\frac{\partial E}{\partial x}\right) \qquad (16)$$

The appearance of E on the right side of this equation plays an important role. Firstly, E may have contributions from "external" sources which act as inhomogeneous terms in the differential equation and hence to the generation of elastic waves from electric fields, set up as boundary

conditions of the crystal. Secondly, E may contain contributions from the lattice strain in the piezoelectric crystal through relation (13). Relation (16) is then the elastic wave equation in the presence of an electric field. To solve it, E must be determined in terms of particle displacement U.

In a one dimensional system, Gauss' equation is given by,

$$\frac{\partial D}{\partial x} = Q \tag{17}$$

and the charge continuity equation is

$$\frac{\partial J}{\partial x} = -\frac{\partial Q}{\partial t} \tag{18}$$

where,

J = electrical current density

Q = space charge

The space charge density may be given by,

$$Q = -qn_s \tag{19}$$

q = magnitude of the charge on an electron

n_s = number of electrons per unit volume required to produce the charge Q

If the collision frequency of electrons is very large compared to the frequency of the wave motion, the current density in n-type semi-conductors will be given as

$$J = q\mu n_c E + qDn\left(\frac{\partial n_c}{\partial x}\right) \tag{20}$$

where,

μ = electrons drift mobility

n_c = number of electrons in the conduction band

Dn = diffusion constant for electrons

In relation (20), the first term is due to the drift caused by the electric field and the second due to the diffusion caused by the

concentration gradient.

The density of electrons in the conduction band may be written as:

$$n_c = n_o + fn_s \tag{21}$$

n_o = equilibrium number of electrons which give electrical neutrality in the absence of an ultrasonic wave

The space charge qn_s is the deviation from equilibrium. However, some of this charge may be produced by immobile electrons trapped at states within the forbidden gap. These electrons do not contribute to the current. Only a fraction f of the space charge in the conduction band contribute to the current. In the absence of trapping f = 1 and all the space charge is due to conduction electrons. Trapping and its effects on wave propagation are dealt with in detail in references (31) and (51).

J, n_s and n_o can be eliminated from relations (17) to (21) as follows:

Equation (18) is,

$$\frac{\partial J}{\partial x} = -\frac{\partial Q}{\partial t}$$

$$\text{But} \quad Q = \frac{\partial D}{\partial x} \quad \text{from (17)}$$

Therefore relation (18) is written as,

$$\frac{\partial J}{\partial x} = \frac{\partial}{\partial t}\left(\frac{\partial D}{\partial x}\right) = -\frac{\partial Q}{\partial t}$$

$$\text{or} \quad \frac{\partial^2 D}{\partial x \partial t} = \frac{\partial Q}{\partial t} = -\frac{\partial J}{\partial x} \tag{22}$$

As equation (20) is,

$$J = q\mu n_c E + qDn\left(\frac{\partial n_c}{\partial x}\right)$$

$$\frac{\partial J}{\partial x} = q\mu\left\{n_c\left(\frac{\partial E}{\partial x}\right) + E\left(\frac{\partial n_c}{\partial x}\right)\right\} + qDn\left(\frac{\partial^2 n_c}{\partial x^2}\right) \tag{23}$$

Substituting for n_c from (21), in relation (22) we get,

$$\frac{\partial J}{\partial x} = q\mu\left\{(n_o + fn_s)\frac{\partial E}{\partial x} + E\left(\frac{\partial}{\partial x}(n_o + fn_s)\right)\right\}$$

$$+ qDn\left(\frac{\partial^2 (n_o + fn_s)}{\partial x^2}\right)$$

$$\text{So, } \frac{\partial J}{\partial x} = q\mu\left\{(n_o + fn_s)\frac{\partial E}{\partial x} + Ef\left(\frac{\partial n_s}{\partial x}\right)\right\} + qfDn\left(\frac{\partial^2 n_s}{\partial x^2}\right)$$

and putting $-\frac{\partial D}{\partial x}$ for qn_s from relations (17) and (19) gives,

$$\frac{\partial J}{\partial x} = q\mu n_o\left(\frac{\partial E}{\partial x}\right) - f\mu\left(\frac{\partial D}{\partial x}\right)\left(\frac{\partial E}{\partial x}\right) - f\mu E\left(\frac{\partial^2 D}{\partial x^2}\right) + fDn\left(\frac{\partial^3 D}{\partial x^3}\right)$$

Substituting this into relation (22) and simplifying gives:

$$-\frac{\partial^2 D}{\partial x \partial t} = \mu\frac{\partial}{\partial x}\left\{\left[qn_o - f\left(\frac{\partial D}{\partial x}\right)\right]E\right\} - fDn\frac{\partial^3 D}{\partial x^3} \qquad (24)$$

For a small signal case, the electric field may be given by:

$$E = E_o + E_1 e^{j(Kx - \omega t)} \qquad (25)$$

where,

E_o = applied d.c. field

E_1 = amplitude of sinusoidal field due to the untrasonic wave

K = is the propagation constant (given by $K = j\alpha + \omega/v_s$, α is defined as the attenuation constant in Np/cm and v_s the phase velocity of the wave)

ω = frequency of the wave

and the lattice displacement as

$$U(x,t) = Ue^{j(Kx - \omega t)} \qquad (26)$$

The elimination of D from relation (24) and (13) can be done as follows:

Relation (24) can be written as,

$$\frac{\partial^2 D}{\partial x \partial t} = -\mu qn_o\left(\frac{\partial E}{\partial x}\right) + f\mu\left(\frac{\partial D}{\partial x}\right)\left(\frac{\partial E}{\partial x}\right) + f\mu E\left(\frac{\partial^2 D}{\partial x^2}\right) + fD_n\left(\frac{\partial^3 D}{\partial x^3}\right)$$

Equation (13) is,

$$D = E + eS$$

$$D = E + e\left(\frac{\partial U}{\partial x}\right)$$

For small signal, it can be put,

$$E = E_o + E_1 e^{j(Kx - \omega t)}$$

$$U(x,t) = U e^{j(Kx - \omega t)}$$

Substituting for D and using the above relations and omitting d.c and second order terms in relation (24) gives,

$$j\omega(jK\epsilon E_1 - K^2 eU)_e^{j(Kx-\omega t)} = -j\mu q_o K E_{1e}^{j(Kx-\omega t)}$$

$$- f\mu E_o(jK^2\epsilon E + jK^3 eU)_e^{j(Kx-\omega t)}$$

$$+ fD_n(K^4 eU - jK^3\epsilon E_1)_e^{j(Kx-\omega t)}$$

Simplifying we get,

$$E_1 = -\frac{jKeU}{\epsilon}\left[1 + \frac{j\sigma}{\epsilon\omega}\left[1 + f\mu E_o\left(\frac{K}{\omega}\right) + jfD_n\omega\left(\frac{K}{\omega}\right)^2\right]^{-1}\right]^{-1} \qquad (27)$$

But $\sigma = qn_o$

= conductivity due to the equilibrium carriers

Substituting this in the wave equation (16) gives,

$$\rho\omega^2 = C'K^2 \qquad (28)$$

where C is the modified elastic constant given by,

$$C' = C\left(1 + \frac{e^2}{\epsilon C}\left[1 + j\frac{\sigma}{\epsilon\omega}\left[1 + f\mu\left(\frac{K}{\omega}\right)E_o + jD_n\omega f\left(\frac{K}{\omega}\right)^2\right]^{-1}\right]^{-1}\right) \qquad (29)$$

The solution of $k = j\alpha + \left(\frac{\omega}{V_s}\right)$, the propagation constant, is a fourth order equation with complex coefficients.

But if the attenuation is small, i.e. $|\alpha| \ll \frac{\omega}{V_s}$, then the above expression can be simplified by putting $K = \frac{\omega}{V_s}$ in (29). For further simplification of (29) we can put,

$\omega_C = \frac{\sigma}{\epsilon}$ = dielectric relaxation frequency

$\omega_D = \frac{V_s^2}{fD_n}$ = diffusion frequency and

$\gamma = 1 - \frac{f\mu E_o}{V_s}$ = which is the measure of the ratio of the electron drift velocity (μE_o) to the velocity of sound.

$$K^2 \approx \frac{K^2}{1-K^2} = \frac{e^2}{C\epsilon} \quad (\text{since } K^2 \ll 1)$$

This quantity $\frac{e^2}{C\epsilon}$ is approximately equal to the square of the electro-mechanical coupling, a quantity used to measure piezoelectric activity. This gives,

$$C' = C\left[1 + K^2 \frac{\gamma + j\frac{\omega}{\omega_D}}{\gamma + j(\frac{\omega_C}{\omega} + \frac{\omega}{\omega_D})}\right] \tag{30}$$

From which we obtain the approximate solutions. Calculation of the attenuation constant α and the phase velocity V, can be derived as follows:

Since,

$$\alpha = I_m K$$

From relation (28)

$$K = \omega (\frac{\rho}{C'})^{\frac{1}{2}}$$

As, $$V_s = (\frac{C}{\rho})^{\frac{1}{2}}$$

Therefore, we have

$$\alpha = \frac{\omega}{V_s} C^{\frac{1}{2}} I_m C'^{-\frac{1}{2}} \tag{31}$$

Equation (30), therefore, gives

$$C' = C\left[1 + K^2 \frac{\gamma^2 + \frac{\omega}{\omega_D}(\frac{\omega_C}{\omega} + \frac{\omega}{\omega_D}) - j\gamma\frac{\omega_C}{\omega}}{\gamma^2 + (\frac{\omega_C}{\omega} + \frac{\omega}{\omega_D})^2}\right]$$

Since $K^2 \ll 1$, by using the binomial expansion and omitting non-linear terms to obtain

$$I_m C'^{-\frac{1}{2}} = C^{-\frac{1}{2}} \left(\frac{\gamma \frac{\omega_C}{\omega}}{\left(\gamma^2 + \frac{\omega_C^2}{\omega^2}(1 + \frac{\omega^2}{\omega_C \omega_D})^2\right)}\right) \frac{K^2}{2}$$

Putting this value in (31), we get

$$\alpha = \frac{K^2}{2}\frac{\omega_c}{V_s\gamma}\left[1 + \frac{\omega_c^2}{\gamma^2\omega^2}\left(1 + \frac{\omega^2}{\omega_c\omega_D}\right)^2\right]^{-1} \tag{32}$$

The phase velocity is given by,

$$V = \mathrm{Re}\sqrt{\frac{C'}{\rho}} = V_s C^{-\frac{1}{2}}\,\mathrm{Re}C'^{\frac{1}{2}}\omega_c \tag{33}$$

$$\mathrm{Re}C'^{\frac{1}{2}} = C^{\frac{1}{2}}\left[1 + \frac{K^2}{2}\,\frac{1 + \frac{\omega_c}{\omega_D\gamma^2} + \frac{\omega^2}{\omega_D^2\gamma^2}}{1 + \frac{\omega_c^2}{\omega^2\gamma^2}\left(1 + \frac{\omega^2}{\omega_c\omega_D}\right)^2}\right]$$

and hence, the phase velocity

$$V = V_s\left[1 + \frac{K^2}{2}\,\frac{1 + \frac{\omega_c}{\omega_D\gamma^2} + \frac{\omega^2}{\omega_D^2\gamma^2}}{1 + \frac{\omega_c^2}{\gamma^2\omega^2}\left(1 + \frac{\omega^2}{\omega_c\omega_D}\right)^2}\right] \tag{34}$$

Since all the terms within the square brackets in relation (32) will always be positive, we see that γ will be negative, when α is negative. In other words, we would expect amplification when γ is negative.

The drift velocity may be defined as,

$$V_d = -f\mu E_o$$

then

$$\gamma = 1 - \frac{V_d}{V_s}, \text{ which is going to be negative}$$

when $V_d > V_s$. If there is trapping, the conductivity modulation is reduced by a factor f. In this case d.c field required for amplification is higher when trapping occurs. If the electric field is reversed, we have

$$\gamma = 1 + (f\mu E_o/V_s) \quad \text{or}$$

$$= 1 + \frac{V_d}{V_s}$$

Thus, simply reversing the electric field produces a new velocity of sound and the magnitude of gain and loss is also changed, i.e. the material is non-reciprocal.

3. Review of previous work

3.1 Introduction

Current oscillation and saturation in semi-insulating cadmium sulphide was first reported by Smith[53] and McFee,[56] an effect which they ascribed to the acoustoelectric current accompanying an ultrasonic flux.

When a high voltage pulse is applied to certain semi-conductors, whose crystal axis has been orientated either parallel or perpendicular to the c-axis, with respect to the sound wave, it is found that above a certain critical electric field the current is not related to the applied voltage by Ohm's law, but is a more complex manner. In CdS it has been observed that below the threshold voltage for current oscillation the current is at all times proportional to the applied field (see Figure 6). Above the threshold voltage the current remains ohmic for an incubation time of the order of 1μsec., which decreases with increasing field. Subsequently the current drops to about its value at the threshold and remains more or less constant for a short period before rising once more to the ohmic value. The cycle repeats for as long as the voltage pulse is applied, with a period which is the time for transverse or longitudinal acoustic waves to travel from one end of the crystal to the other.

These acoustoelectric instabilities arise from the strong interaction between a drifted electron distribution and the phonon spectrum in piezo-electrically active semi-conductors. Intense phonon beams are created as the electrons amplify a selected portion of the phonon spectrum propagating in a relatively narrow cone. The transfer of drift momentum from the electrons to the phonons in this process alters the current and the electric field distribution in the material

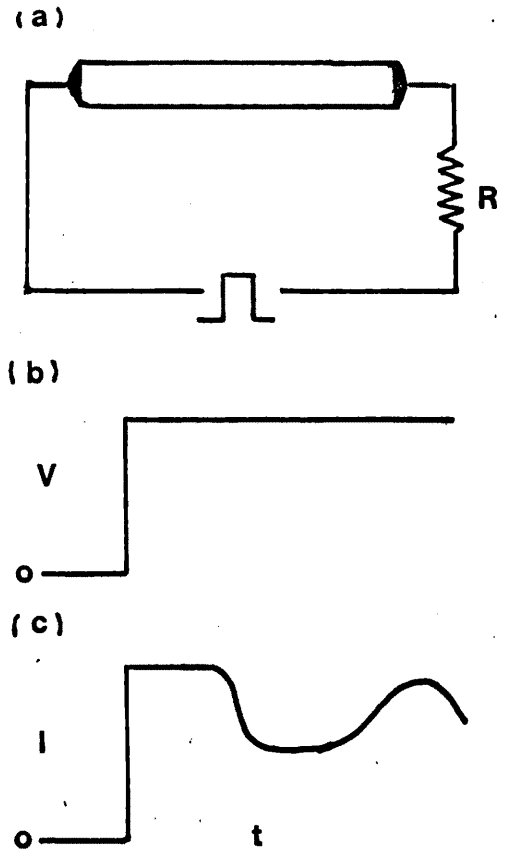

Fig.6 Continuous current oscillations due to an acoustoelectric domain:

a) Specimen with series resistance for measuring current with pulse generator,

b) voltage pulse,

c) current wave form.

which may in turn alter the acoustoelectric gain. Such instabilities are most readily observed in the resistance of the sample, in the apatial distribution of the amplified acoustic flux and in the associated electric field. These perturbations become concentrated in stationary and propagating domains. More subtle forms of the instability are revealed from studies of the frequency spectrum of the amplified flux, which show a very complex evolution during the transition from weak to strong acoustic flux. In the high field regions of the domains, hot carrier instabilities may become apparent.

It will be seen that the type of illumination distribution is important since it produces a non-uniform conductivity along the length of the specimen. It is worthwhile to examine the effects observed in semi-insulating materials and then explain the phenomena observed in semi-conducting crystals, because the oscillations obtained in semi-conducting material are less complex.

3.2 Current oscillations

The phenomena of current oscillations and saturation are caused by the presence of amplified acoustic flux. An acoustic flux is generated spontaneously in a specimen with no input by (a) the thermal equilibrium phonon distribution or (b) the shock produced by an applied voltage pulse. Acoustic waves may be generated at regions of discontinuity or high electric field gradient and at regions of piezo-electric irregularity by a time varying electric field.[41,65,66] Both electrodes introduce field discontinuities and in non-uniformly illuminated specimens high field gradients occur at the boundaries between the two regions of differing conductivity. The thermal generation of the

acoustic flux is supposed to be uniform throughout the specimen and continuous in time. Shock excitation produces a localised gradient in the piezo-electric stress, occurring during changes in local field. Piezo-electric irregularities also occur at inhomogeneities of the crystal structure and the application of a high voltage pulse may cause sufficient excitation of these regions to generate acoustic waves.

There are two types of current oscillations to be considered, i.e. (1) damped and (2) continuous oscillations. Damped current oscillations shall be considered in detail under current saturation. These damped oscillations have been associated with the build-up of acoustic flux. The dependence of this build-up time on the applied field, conductivity and crystal length has been dealt with by Ishida et al[51] for semi-insulating CdS.

In the next two sections, conditions for oscillations in semi-insulating and then semi-conducting material will be discussed.

3.2.1 Semi-insulating crystals

Acoustoelectric oscillations are possible in semi-insulating CdS, provided it is illuminated so that the optimum carrier density for amplification can be set up. It has been found that these crystals show only damped oscillations leading to current saturation as discussed by McFee et al[55] and others,[81] if the illumination is either uniform or stronger near the anode electrode.[82] On the other hand, samples of semi-insulating materials normally require a non-uniformity of conductivity along their length to give continuous oscillations. This non-uniformity of conductivity may be obtained by non-uniform illumination and a sufficiently large drift field is applied. The following types

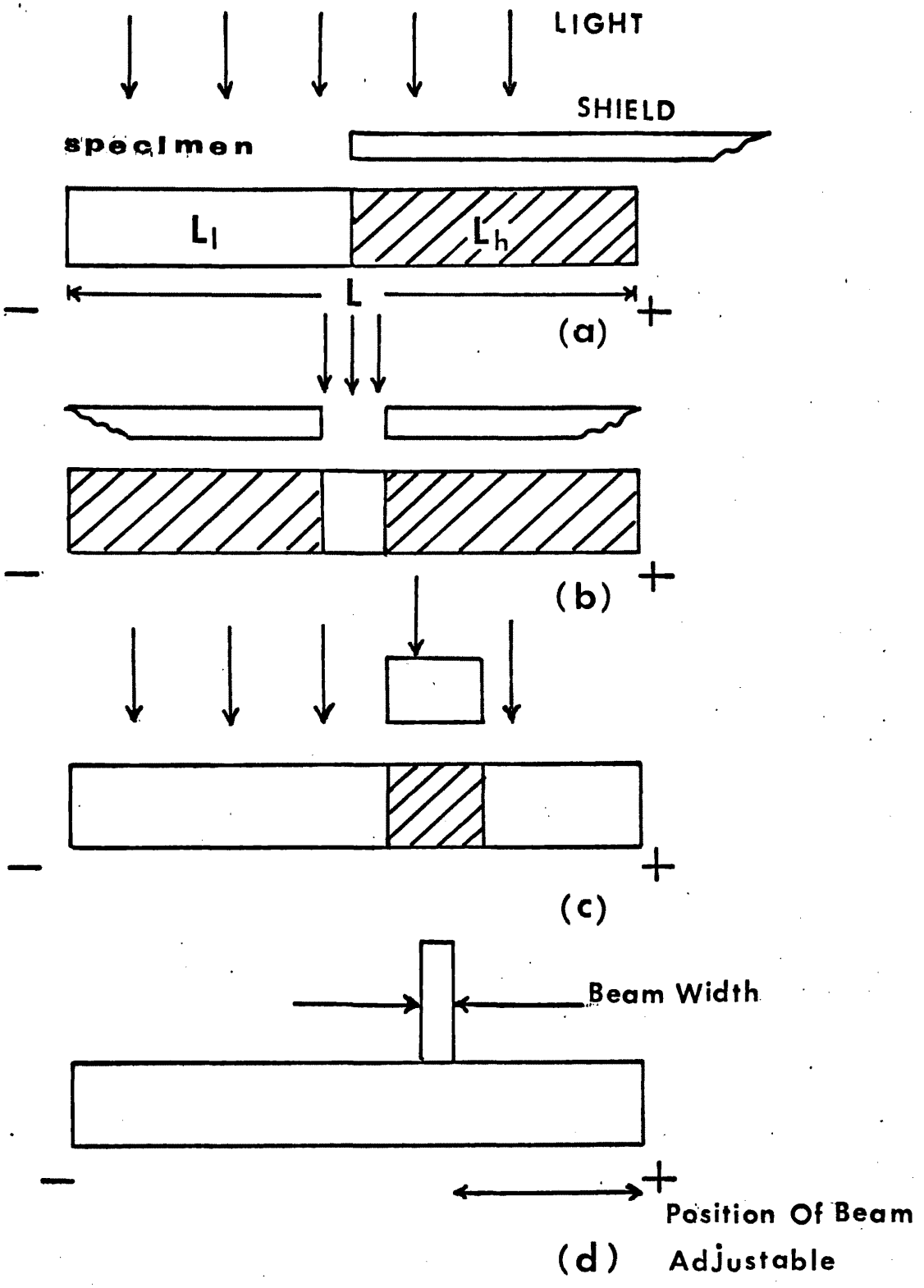

FIG. 7 . METHODS OF NON UNIFORM ILLUMINATION

of illumination distribution have been reported (see Fig. 7):

a) A length beginning from the positive end is shaded.[35,36,58]

b) A fine, narrow, transverse strip of the specimen is illuminated at a point along its length.[37,57]

c) The specimen is totally illuminated and a strip of ceramic positioned at some distance from the anode end obscuring a strip of the crystal perpendicular to the crystal axis.[49]

No continuous oscillations have been observed with the negative end shaded.[36,58]

d) Under highly localised illumination with intense red light 6328°A.[80]

With the illumination as in a) oscillations begin to appear when the field in L_1 exceeds a threshold value.[35,58]

(L_1 = low resistivity region)

(L_h = high resistivity region)

At this moment, the current flowing exceeds the saturation current of high resistivity region L_h. These oscillations appear at voltages just above the threshold voltage. They are damped, but the damping diminishes as the applied voltage is raised and the oscillations become continuous at a critical voltage V_c. Further raising of the voltage merely increases the amplitude of the oscillations. The amplitude of continuous oscillations as shown in Fig. 8 is between a minimum, which is the saturated current of L_h, and a maximum which is near the ohmic current of the sample.

i.e. $$I_{max} \approx \frac{\text{Applied voltage}}{\text{ohmic resistance of } L_1 + \text{ohmic resistance of } L_h}$$

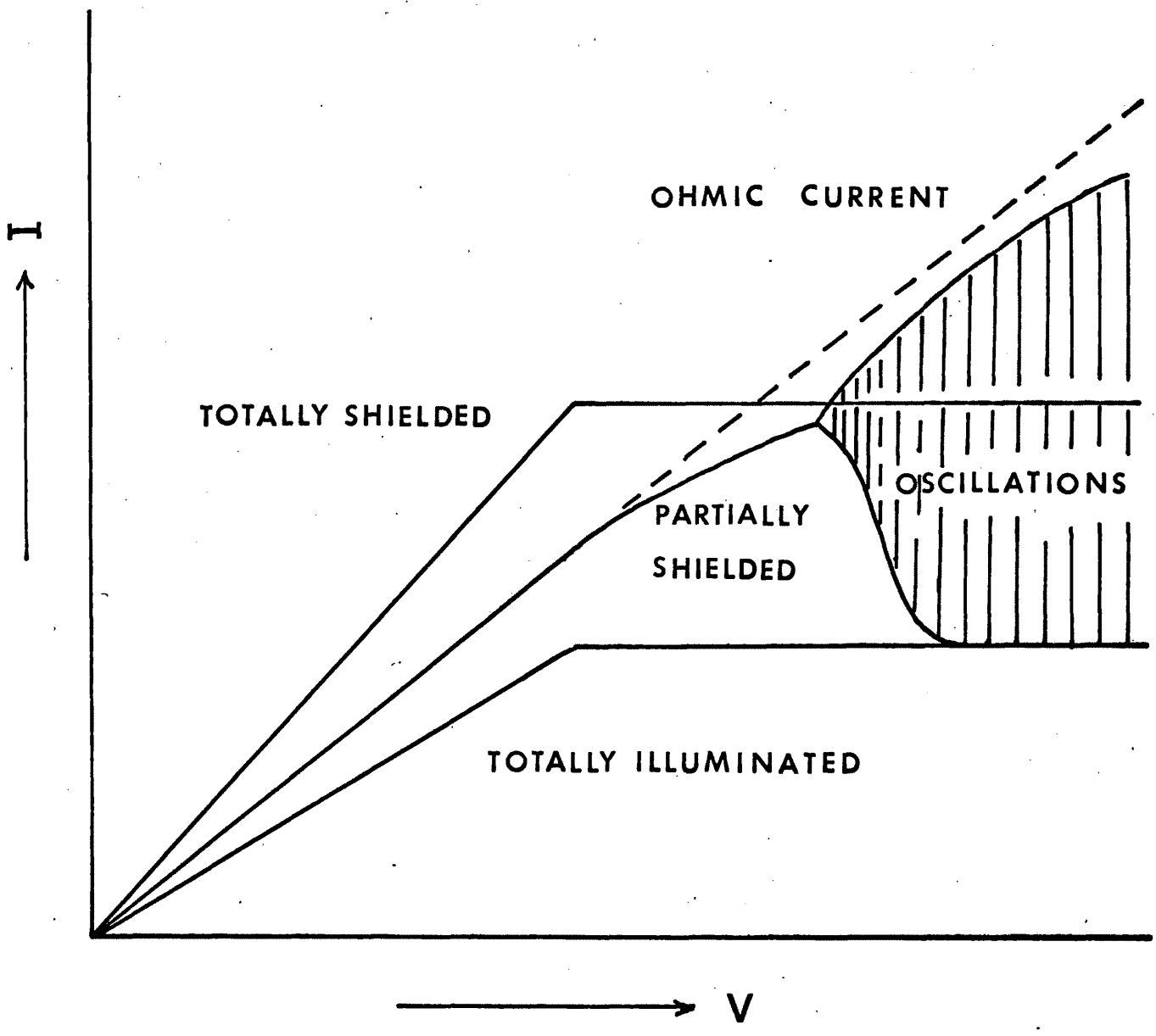

FIG. 8 SCHEMATIC I-V CURVE

This maximum current may exceed the saturation current for L_1 at high enough voltages.

A range of oscillation frequencies have been observed with this type of illumination. Yamamoto[58] reported that the frequency of oscillations depended on the length of the specimen L, the length of high resistivity region L_h and slightly on the applied voltage. Okada[35] reported that the oscillation frequency corresponds to a single or double transit time for a sound wave to travel the length of the crystal. W.C. Wang[36] in 1965 observed that the frequency of oscillations is inversely proportional to the length of the high resistivity region L_h.

Banduin and Buchy[46] used a specimen of varying cross section to achieve a non-uniform field without changing the carrier density and with a narrow end at the cathode. With the same kind of illumination as a) they obtained damped oscillations with periods increasing linearly with L_h. Beyond a certain length of Lh, the oscillations were continuous and the periods decreased with increasing L_h. In all cases no continuous oscillations occur when L_h exceeds a certain length (usually about half the sample length).

With the illumination system of b) Kikuchi[57] observed discrete frequencies for different positions of the light spot in samples of CdSe. The threshold voltage for oscillations varied for the different positions of the light spot. The frequencies in a particular specimen varied by a factor of about two, and corresponded to the single and double transit times for a sound wave to travel the distance between the electrodes. The frequency transition occurred when the light spot was moved from one point on the specimen to a point about half a millimetre away. At intermediate positions of the light spot mixing of the two frequencies occurred.

These oscillations described above were similar to the one observed by Gay and Hartnagel,[48,49] using the illumination system c). They found that frequency varied in steps after changing the position of the shielding strip. A number of oscillatory modes in the specimen were observed depending on the position of the ceramic strip. For certain values of the distance of the strip from the anode, two frequencies are observed simultaneously. Between the frequency changeover, a beating effect was often observed which involved the two neighbouring frequencies. These effects depended very sensitively on the position of the narrow mask and on the background illumination of the masked strip. These oscillations become damped and disappear when the distance of the ceramic strip from the anode lies between $\frac{L}{3}$ and $\frac{L}{2}$. They expected high fields near the positive edge of the narrow mask, under amplifying conditions, and explained[48,49] the phenomena as described below.

Acoustic flux is generated by applying a voltage pulse V_s during the rise time T_g. Then flux packets of width $V_s T_g$ propagate along the specimen. Above a threshold voltage[33] for current saturation or oscillations the acoustic waves travelling along the specimen will grow. An acoustic electric current of density J_{ae}, associated with the amplified flux (Appendix I) causes the field in their vicinity to be higher than the average field in the specimen. This may be shown by the relation (derived in Appendix I):

$$J = q\mu_z n(z)\, E(z) + J_{ae}(z)$$

(neglecting the diffusion current which is small) where,

J = current density through the specimen

z = direction of carrier drift

(z = 0 at the cathode)

The current density is constant throughout the specimen and $J_{ae}(z)$ is

negative for growing acoustic flux. If it is so, then $E(z)$ should increase. It is then possible that the domains of high energy acoustic flux may thus be detected as high field domains in the specimen.

Thermal acoustic noise may be envisaged as acoustic waves generated continuously by sources uniformly distributed through the specimen. Under the amplifying conditions a continuous stream of flux from each of these sources would be amplified as they propagate towards the anode and attenuated as they propagate in the opposite direction. After a period $\frac{L}{V_s}$ has elapsed from the time amplifying conditions were imposed, one would expect the amount of flux at the anode to be the sum of the amplified flux from all the generating sites along the specimen. Therefore, this would cause the electric field in the specimen to rise exponentially towards the anode. Deviations from pure exponential rise of the field may be due to the losses at the end of the sample. This equilibrium condition can be maintained by the continuous stream of acoustic flux and then it is possible to have a stationary high field domain near the anode.[55]

Considering the effects of electric field distribution and the reflection of flux at the anode, it is seen from the curves of $\alpha V_s \gamma$ (derived in Appendix II) that the acoustic waves[30] are undergoing less attenuation by travelling against the drift electrons than the gain experienced by a wave travelling in the direction of the electrons at the high fields, i.e.

$$|\alpha| \text{ is larger for } \gamma = 1 - \frac{V_d}{V_s} \text{ than for } \gamma = 1 + \frac{V_d}{V_s}$$

If it is so, then there is every possibility that the waves grow indefinitely by repeated reflections, provided there is no redistribution of the field. Weinreich's[1] relation (Appendix I) shows that the acousto-

electric current produced by the attenuation of reflected acoustic flux also opposes the current through the specimen and causes a rise in the local field. It has been shown by many workers that under the condition of acoustic gain the ultrasonic flux in the transient state (current oscillations) is concentrated in domains originating at one electrode and amplified as they propagate with the sound velocity in the direction of carrier drift. Since the applied voltage V, across the specimen is constant there has to be redistribution of field along the specimen when these high field domains grow. The applied voltage is given by:

$$V = \int_0^L E_{(z)} dz$$

The redistribution of field results in the saturation or oscillation of current through the specimen.

Ellis and Cornwell,[80] using the type d) illumination, observed continuous current oscillations in semi-insulating CdS at frequencies from 100-700KHz, depending on the illuminated regions of the specimen. They failed, however, to observe any relationship with distance of these illuminated spots from the electrodes.

3.2.2 Semi-conducting crystals

The acoustoelectric current oscillations described so far are those observed in semi-insulating materials but results of a different type occur in semi-conducting CdS. This type occurs in CdS crystals of about 1Ω-cm resistivity and does not rely on any carrier generation by illumination. With semi-conducting material the oscillations observed are less complex than in semi-insulating CdS. The semi-conducting specimens do not require an initial non-uniform conductivity distribution. These oscillations are caused by the production of clearly defined travelling high field domains

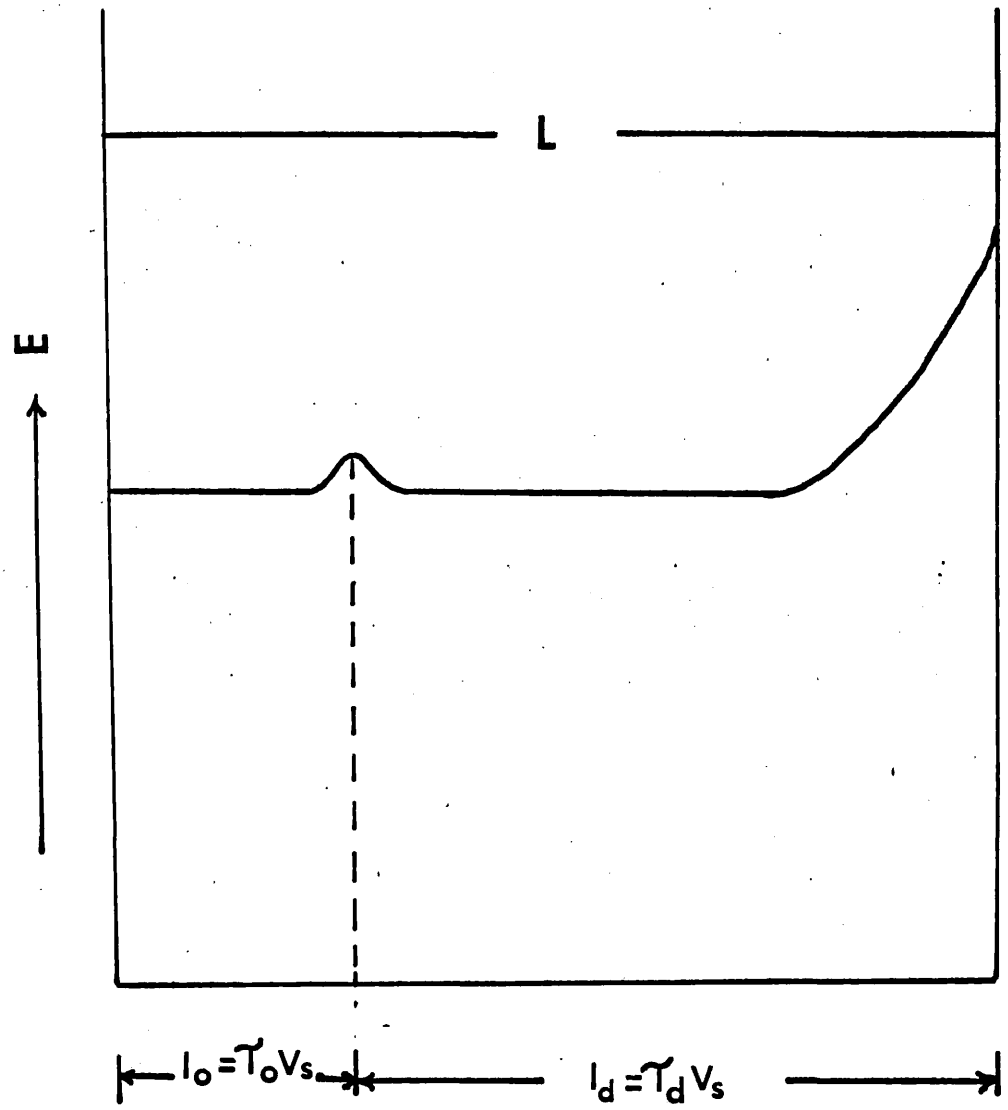

FIG. 9 DOMAIN'S NUCLEATION IN SEMICONDUCTING cds

which are very similar to the domains of the Gunn effect.[82] These growing high field domains travel across the crystal with the velocity of sound. The period of oscillations is made up of two parts; an "incubation" period τ_o, and a period τ_d, where a domain is detectable. Ishida et al[59] found that τ_d corresponded closely to the sonic transit time, and that τ_o depended on the applied field, decreasing as the field increased. Many workers[41,60,63] found that the total period, $\tau = \tau_o + \tau_d$ corresponded to the sonic transit time. Again τ_o decreased with increasing field. Haydl and Quate[60] observed that on the application of a pulse of sufficiently high voltage, the current remained ohmic for a time τ_o before a domain begain to grow from a point a distance $l_o = \tau_o V_s$ from the cathode (Fig. 9). This domain grows as it travels to the anode and depletes the field outside it to E_{th} (threshold field for oscillations). It decays rapidly on reaching the anode and after a time τ_o from its arrival and extinction at the anode another domain grows at l_o. This implies that the domains originate at the cathode and take a time τ_o to grow to a detectable level.

This effect can be understood as a negative resistance phenomenon produced by the fact that an incremental increase in the acoustoelectric field can be greater than the incremental increase in the applied field. This will cause the total current through the sample to be a decreasing function of applied field so that the current voltage curve becomes negative. It is not necessary to have the acoustic flux being reflected and returned to the cathode so that a loop gain in excess of unity is obtained. As soon as one domain has reached the anode and has been extinguished, a new one is formed at some nucleating centre near the cathode electrode. Before a domain is nucleated the I-V relation is ohmic. A domain will cause current saturation during its transit. The

current oscillation occurs, therefore, between a high current value, which is given by the low field resistance of the crystal, and a saturated current value.

Silva and Bray[41] detected the domains described above by double probe measurements of the pulsed voltage distribution along the sample length in p-type GaSb and attributed the flux generation to simple time variation of the electric field. It has been noted that acoustic flux may be generated at regions of strong electric field gradient or discontinuities in piezo-electric materials in a time varying field.[65,66] The anode in the p-type materials was the region of a field discontinuity and the onset of the pulse provided the time variation of the acoustic flux generation. When the first domain decayed at the cathode, the current in the sample rose and caused a field change which generated another domain. It is then possible to have more than one generating site along the length of the specimen. These generating sites become active if strong field gradients[41] or material discontinuities exist. Haydl and Quate[60] verified experimentally that acoustic transducers on short voltage pulses could inject several domains into a specimen at a time. The width of the domain is of the same order as the rise time of the voltage pulse.

Haydl,[61] considered the possibility of these domains, originating from thermal acoustic noise, which is always present in the specimen. He applied a voltage pulse just below that required for oscillations to a specimen of semi-conducting CdS. At some time during the pulse he increased the applied voltage above the threshold for oscillations. A domain was then found located at the anode after a fraction of a sonic transit time in the specimen. A domain initiated by shock excitation at the cathode could not have arrived at the anode so quickly so that it was

proposed that domains form and grow at a threshold of acoustic energy, i.e. the moment the energy level of acoustic flux at some point in the specimen reaches this threshold value, a domain will form at that point. By applying a voltage above the threshold voltage for current oscillations but below that for oscillations, a steady state is achieved with a distribution of flux energy higher at the anode end. From the expected distribution of flux, Haydl showed that the domain would form quite near the anode.

Stanley[63] proposed a mechanism for domains in semi-conducting CdS which had also been proposed by many others[35,36,58] for the oscillations in non-uniformly illuminated semi-insulating CdS. This model depends on the distribution of potential along the specimen preventing amplification at the cathode, where the field is lower, while a domain exists. He maintained that as the domain reaches the anode and disappears, the field in the rest of the specimen should rise again, until amplifying conditions would prevail at the cathode end and a new domain form. By raising the applied voltage to a certain high value, it was shown that oscillations ceased. This was because the field in the cathode region could not fall below E_{th} (threshold field for oscillations), and thus amplifying conditions existed throughout the specimen at all times, and a steady state saturation condition was established.

It has been observed[60] that domains in semi-conducting CdS are greater in amplitude but narrower in width than those in semi-insulating CdS. Typical domain fields are more than 3×10^4 V/cm, the domain width is more than 150μ, whereas the domain fields in semi-insulating CdS are between 10^3-10^4 V/cm and have domain width of the order of the length of the specimen but obviously a little shorter. Domains have been studied

by probe contacts along the crystal,[82] by Brillouin scattering by a moving domain giving its phonon intensity[83] and by microwave transmission measurements.[84,85] By the optical method[64] a frequency range of 100-1500MHz was detected and no change of this frequency range occurred between room temperature and 77°K. This frequency range falls considerably below that expected from the maximum gain condition

$$\omega^2 = \omega_c \omega_D$$

S. Zemon et al[86] also investigated the frequency spectrum of the acoustic waves in domains generated in semi-insulating CdS, by using Brillouin scattering of 6328A° He-Ne laser beam. A frequency range from 150-375MHz was detected at room temperature. They also showed that the frequency of maximum acoustic intensity varied as the square root of carrier concentration.

Impact ionization occurs in CdS at fields higher than 2.1×10^3 V/cm, as determined by the measurement of the Hall voltage and conductivity.[87] This phenomenon will therefore occur inside the travelling domain with its high field value.

These electroacoustic domains have not only been studied in semi-conducting CdS, but also in GaAs and in InSb. Hervonet[88] has shown theoretically that a transverse magnetic field increases the piezo-electric amplification and Ishida and Inuishi[89] measured a differential negative resistance in semi-conducting CdS with travelling domains.

Microwave emission has also been observed under oscillatory conditions. In GaAs, Hiyakawa et al[40] observed emission between 4.2 GHz to 6 GHz. In CdS, Haydl and Quate[67] observed microwaves emitted in the frequency range of 2 to 4 GHz.

3.3 Current saturation

There is a large amount of information about the saturation of current in a piezo-electric semi-conductor in a strong electric field. R.W. Smith[53] tried to relate the current saturation in piezo-electric semi-conductors to the generation and amplification of acoustic flux. Earlier on amplified acoustic flux had been observed at the output of a CdS acoustic amplifier when no input was applied.[53] The mechanism of energy transfer from drifting carriers to acoustic waves is discussed in Appendix I. This transfer occurs when the velocity of drifting carriers exceeds the velocity of sound.[47] The dark current in semi-conducting CdS of conductivity 0.1 mhocm^{-1} saturates at an applied field of approximately 1600V/cm. Since the mobility of electrons in the material is 300 cm^2 volt^{-1} sec^{-1}, their drift velocity in this field is comparable with the velocity of sound in the crystal. Using voltage pulses of nanoseconds rise time, Smith[53] found that for the first 50-100 nanoseconds the current remained constant at its ohmic value and then decayed to the final saturation value. It[54] was observed that the time required for the onset of current saturation after the application of the field pulse depended upon the conductivity of the material, the smaller the conductivity the larger the onset time.

In 1956 Weinreich[30] pointed out the possibility that the interaction between acoustic waves and conduction electrons would be increased if electrons were made to drift near the velocity of sound. He also explained that the electrons would amplify acoustic waves if their drift velocity exceeded the sound velocity. The piezo-electric coupling in wurtzite was measured by Hutson et al[31] after Nine[90] had reported on the strong attenuation of sound waves by free carriers in semi-insulating CdS. Hutson and White[31] worked out the theory of the

attenuating properties of free carriers. Amplification was first observed in CdS at 45MHz,[33] when it was realized that piezo-electric semi-conductors would be an ideal material for an acoustic wave amplifier. This work has served to point out the significant features of the travelling wave interaction. The origin of the acoustic flux, which is to be amplified, has not yet been established conclusively.

R.W. Smith[53] from the condition of maximum gain

$$\omega = (\omega_C \omega_D)^{\frac{1}{2}}$$

expected the most amplified acoustic waves to be between at frequencies of 10 and 10^3GHz. He used conductivities from 0.01 to 3mhocm^{-1} but failed to detect these hypersonic waves or electromagnetic waves, which should accompany the bunching of electrons. By using tuned transducers, in 1963 McFee[56] detected a continuous range of acoustic frequencies between 15 and 400MHz. He also managed to find a relationship between the maxima of the transit oscillations of acoustic flux energy as it built up to the minima of the damped current oscillations which observed. However, these frequencies detected were of much lower values than that expected from the maximum gain condition.

Microwave emission of 850 to 2000MHz has been observed from CdS crystals under saturated current conditions.[44] It is thought to originate from piezo-electric coupling between conduction electrons and acoustical phonons in the crystal.[50]

In semi-insulating crystals the current saturation will occur when a certain degree of illumination is applied.[42,53] The degree of saturation is definitely higher for higher conductivities. Under non-uniform illumination the threshold field for saturation seems to occur when the field in the region of lowest resistivity is at the threshold

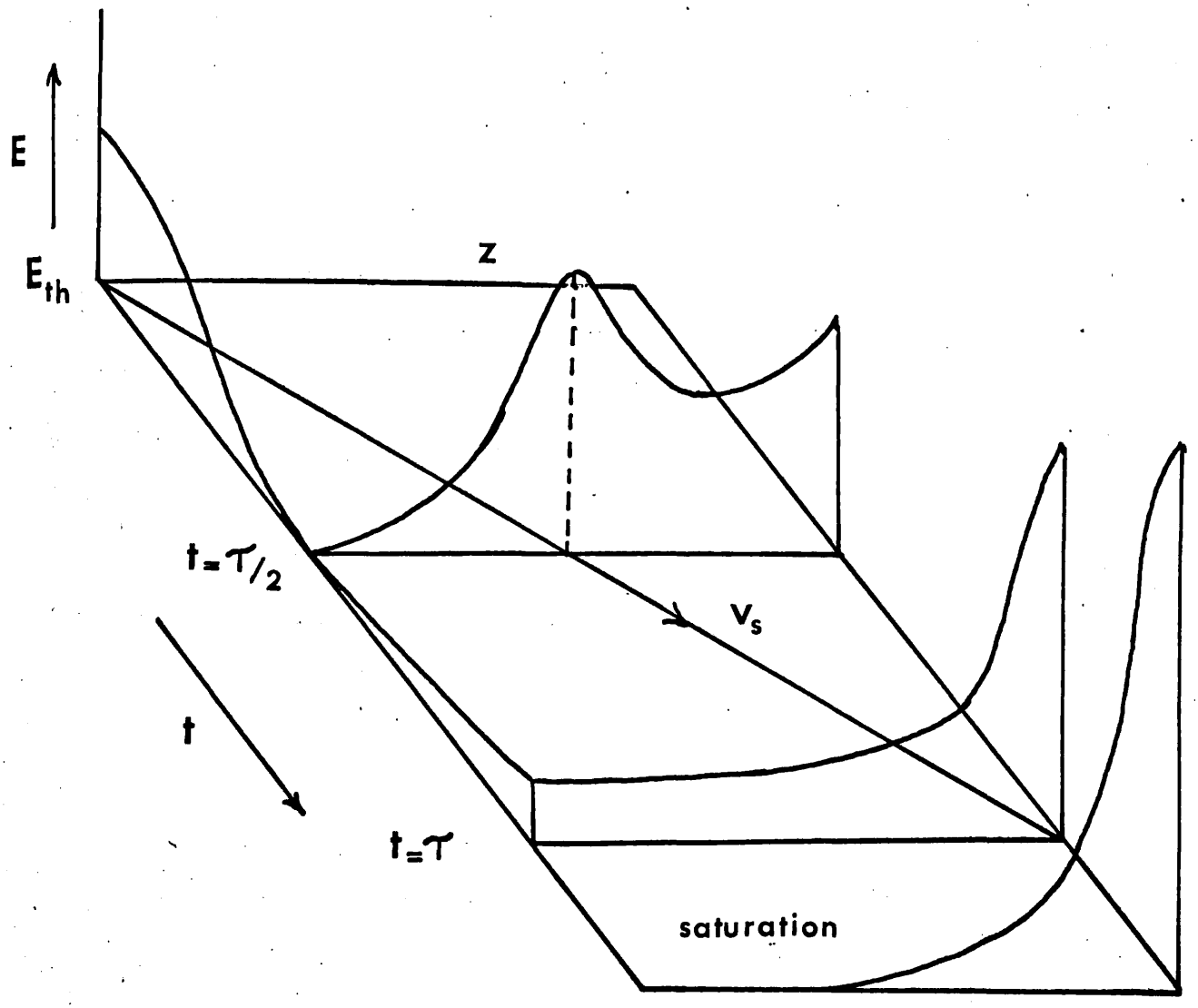

FIG. 10 DAMPED CURRENT OSCILLATIONS

field for saturation under uniform illumination.[58]

The current voltage characteristics of CdS crystals displayed current saturation after a few damped oscillations under uniform illumination. This has been closely related to the acoustoelectric interaction. It has been studied theoretically[92-95] and experimentally.[55,96,97] Saturation[54] in current occurs under the condition

$$V_d = \mu E_{th} = V_s$$

where μ, E_{th} and V_s are the electron drift mobility, threshold drift field and the sound velocity respectively. Considering a homogeneous sample then the only sources of acoustic flux from shock excitation are the electrodes. When a high voltage is applied to a specimen, a domain is generated at the cathode and grows as it travels towards the anode. Because of the growth of the domain and the thermal flux, the field near the cathode is reduced and hence the current falls (Fig. 10). When the amplified domain reaches the anode, it is partially reflected and the remainder of the domain extinguished as the acoustic flux leaves the specimen.

Considering the reflection coefficient, if it is small then most of the domain is extinguished and the field at the cathode end rises to compensate for this. But it will not rise to its initial state, however, because of the growth of the stationary domain of thermal acoustic flux near the anode. The increase of field at the cathode end causes a rise in current and initiates another domain. This second domain will not grow as large as the first because of the reduced gain conditions.[30] Its extinction on reaching the anode end forms another domain which should coincide with the reflected part of its first domain. The gain conditions reduce as the stationary domain at the anode grows further. This cycle is repeated until eventually the stationary domain causes the

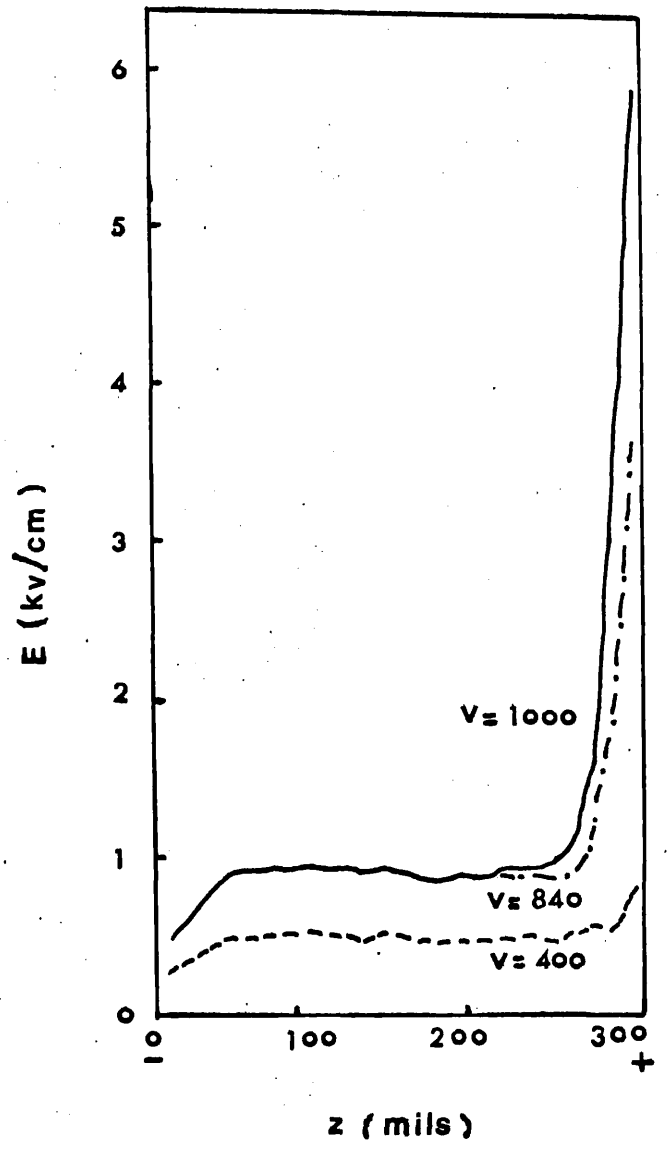

Fig.11 Steady-state electric field distribution in CdS under uniform illumination (after McFee and Tien[55]).

field at the cathode to be at E_{th} and no more variation of current occurs.

If the reflection coefficient at the anode is large then only a small portion of the domain is extinguished. This causes a small increase in field at the cathode, which may not be sufficient to initiate another domain. The first domain is amplified after its second reflection but damps out eventually.

For[54] low reflection of flux from the electrodes the period of damped oscillations is then $\frac{L}{V_s}$ and, for highly reflective electrodes, the period of oscillations may be given by $\frac{2L}{V_s}$, where L is the length of the specimen and V_s is the velocity of sound in CdS. When the damped oscillations are damped out, the so-called stationary domain may continue to grow in height and become narrower, leaving a greater part of the filament with a field of E_{th}. After some time an equilibrium is reached when the base of the domain reaches a point where field does not fall below E_{th}. The spatial distribution of electric field in CdS is measured under the condition of current saturation.[55,62,63] McFee and Tien[55] however, found that at low voltages the field was reasonably even in a homogeneous sample of semi-insulating CdS. At a voltage above the saturation voltage, a narrow high field region appeared at the anode, leaving the field in the rest of the sample at the threshold field E_{th} (Fig. 11). Increasing this voltage only increases the field in the high field domain and the field in the rest of the specimen still remains at E_{th}. Similar phenomena have been observed in current saturated semi-conducting CdS.[61,62] When a high voltage, above threshold for saturation, is applied, a domain forms at the cathode and is amplified as it propagates with the velocity of sound in the direction of carrier drift towards the anode, where a part of it moves out leaving a residual field.

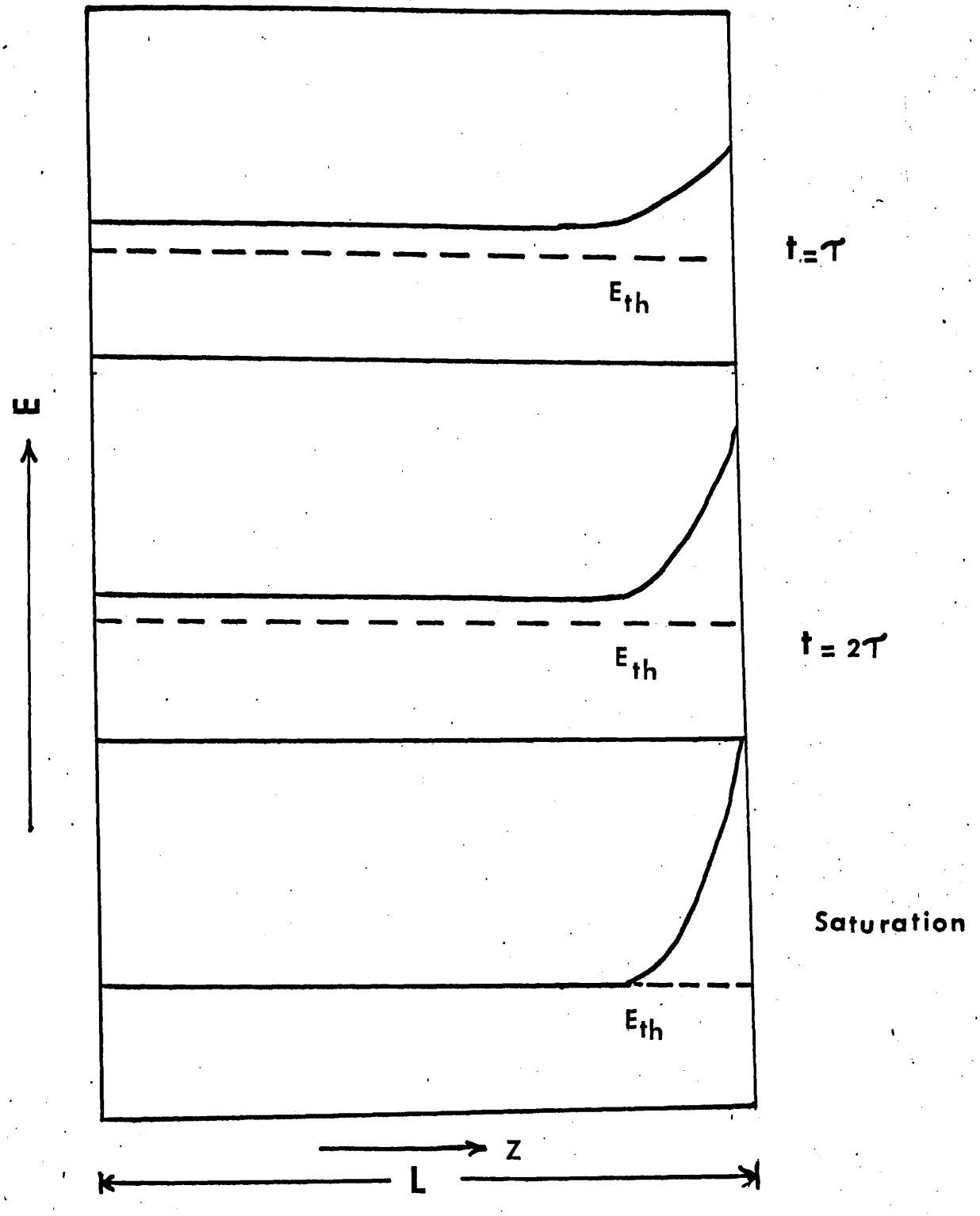

FIG. 12 STATIONARY DOMAIN'S GROWTH AT ANODE

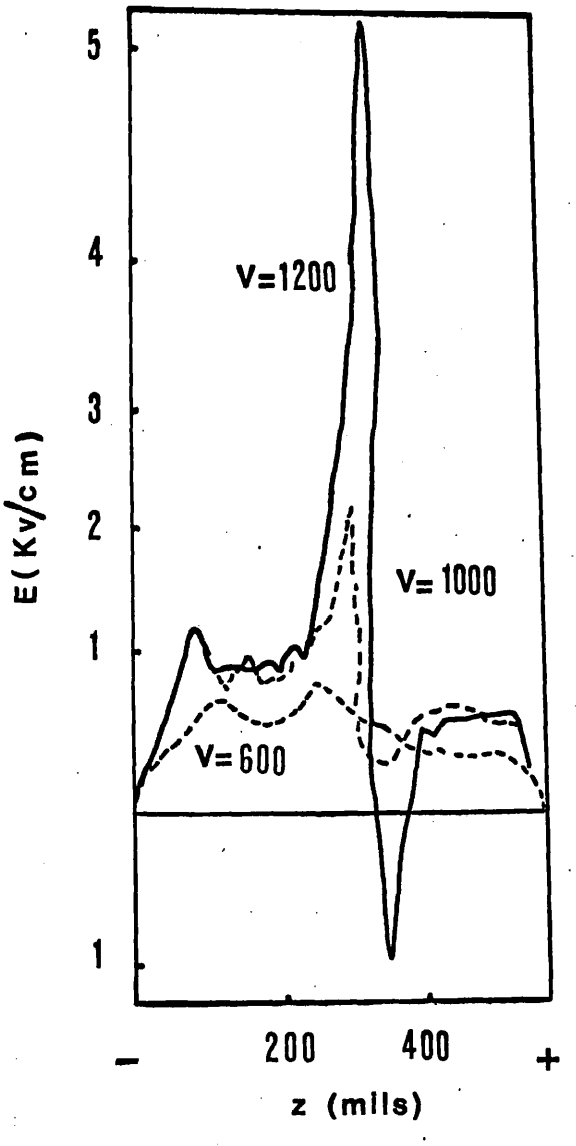

FIG.13 AFTER McFee et Tien

Steady-state electric field distribution in CdS under non-uniform illumination (cathode half of sample slightly masked).

In the meantime, a subsequent domain is formed and travels towards the anode. This process is repeated until a stationary domain grows at the anode and reaches its full size (Fig. 12). The field in the remainder of the specimen is then above E_{th} and travelling domains no longer nucleate.

In an inhomogeneous sample, where the low field resistance was slightly higher at the cathode than at the anode end, McFee and Tien[55] found that a stationary domain formed at the point where the resistivity changed. In such cases the high resistivity region L_h behaves as an amplifier and growth of a domain decreases the field in low resistivity region L_l. L_l then will behave as an attenuator when the field falls below E_{th}. The attenuation of flux further decreases the field (Weinreich's relation[30]) and it is possible for the field to become negative[55] in this region, as shown in Fig. 13. This could be simulated in homogeneous samples by slightly shading the cathode half. These high field domains are the regions of high energy acoustic flux.

Rannestad[78] has shown that one can obtain current saturation by acoustoelectric amplification either with the transverse or the longitudinal acoustic waves, and that the gain in the transverse mode is usually larger than the gain in the longitudinal mode.

3.3.1 Two step current saturation

Ishiguro and Uchida[72] observed that the wave form of the current pulse obtained when a high electric field is applied to semi-insulating CdS specimens has two steps at different times. Both steps occur in the saturation region of the pulse current, the first at a time t_1 which is necessary to build up the ultrasonic flux,[53,56] and the second step at a time t_2 when the applied voltage is much higher than that for current

saturation. Ishiguro and Uchida[72] associated the first step to bunching of the electrons and the second to quantum mechanical interaction between drifting electrons and acoustic phonons.

Autin et al[73] observed that the width of the steps was a function of the crystal conductivity or the illumination intensity, and was also related to the field applied to the electrodes. They also observed small amplitude oscillations as the current was falling to its final value.

Large amplitude steps were seen by P. Das and A.J. Steckl[77] in cadmium sulphide specimen when the ends of the specimen were optically polished and made parallel to one another up to 10-sec accuracy. These steps appeared only when a very large electric field was applied and when the conductivity of the crystal varied by illumination. There appeared to be two distinct current saturation levels accompanying these steps of long time duration. The starting time of these two levels decreased as the conductivity was increased from low value, but reached a steady state value for larger conductivity with the appearance of some smaller steps before the first current saturation level. They proposed the possibility of two different sound velocities being responsible for the two step saturation of the current.

Rannestad[78] observed and explained the two step process on the basis that low voltage saturation was due to the transverse mode and high voltage saturation may be caused due to the longitudinal mode.

Autin et al[73] found that a voltage much above the two step saturation voltage, a non-uniform distribution of field exists, along the length of the specimen. Voltage probe measurements showed that in two step saturation region a definite maximum appears near the cathode but Autin et al[73] were uncertain about the existence of a second maximum existing near the positive contact.

3.4 Trapping and capture

Fig. 14 pictures trapping and thermal release of electrons in electron traps (transition 5 and 5′) and trapping and thermal release of holes in hole traps (transit 4 and 4′); also capture of an electron (transition 7) and of a hole (transition 6) in recombination centres.

A centre with an energy level lying near to the band edges will be more likely to act as a trap than a recombination centre (and vice versa for centres with levels lying near the middle of the forbidden gap), the distinction between traps and recombination centres being a distinction drawn on the basis of the relative probability of the thermal ejection versus recombination, i.e. on kinetic conditions, and not on the basis of the intrinsic nature of the centres themselves. If capture processes connected with transitions 6 and 7 involve the radiation of the electronic energy lost as photons, luminescence emission is observed of the type indicated in Fig. 15.

3.4.1 Detection of traps

The following measurements are useful in obtaining information about trapping:

a) Growth of luminescence emission intensity or of photo-conductivity after the beginning of excitation.

b) Decay of luminescence emission intensity.

c) Thermally stimulated trap emptying.

d) Optically stimulated trap emptying.

e) Space charge limited current dependence on voltage.

f) Photodielectric effect.

Two of these methods are discussed briefly as they have been used by the author of this thesis to detect traps in semi-insulating CdS crystals.

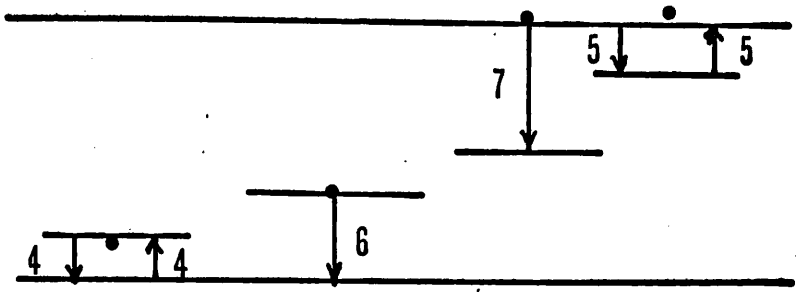

FIG.14 Trapping and Capture

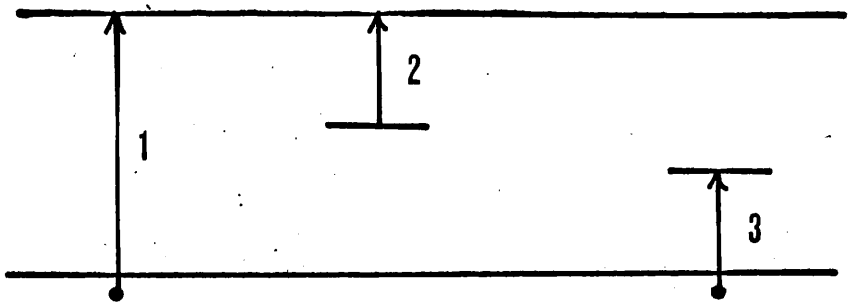

(a)

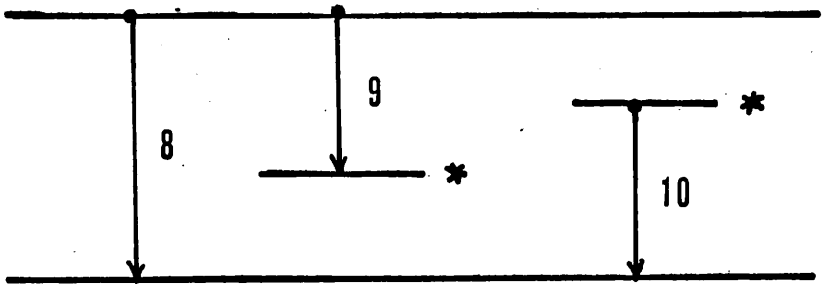

(b)

FIG.15 Electronic Transistions
(a) Absorption and Excitation
(b) Recombination

1) Optically stimulated trap emptying

Filled traps may be emptied by the absorption of optical energy, or by utilization of thermal energy. The trap depth may be obtained from the stimulation spectrum of either luminescence or photoconductivity.

2) Space charge limited current dependence on voltage

Measurements of the variation of space charge limited current injected into a crystal through an ohmic contact as a function of electric field applied to the crystal can be used to give an indication of the total trap density, trap distribution with energy and hence the actual location of fairly monoenergetic trapping levels.

3.5 Traps and effects of trapping

Trapping is a fundamental process for energy storage in almost all semi-conductors. This energy storage is accomplished by spatial localization of an excited electron or hole in such a way that the electron or hole is prohibited from moving freely through the crystal, unless supplied with thermal or optical energy. When the trapped electron or hole is released it is free to move until captured by a recombination centre or by another trap. These regions of the crystal which are able to capture electrons and holes and detain them in a restricted volume are called 'traps'. The names, traps and trapping, are associated with centres and processes which are determined by thermal equilibrium exchange with the nearest allowed band. It is used to distinguish between "trapping centres", the occupancy of which is determined by thermal equilibrium processes and "recombination centres", the occupation of which is determined by recombination kinetics. Because of this type of definition, there is always an inherent vagueness in determining what types of centres are traps. Any centre can be a trap under one condition

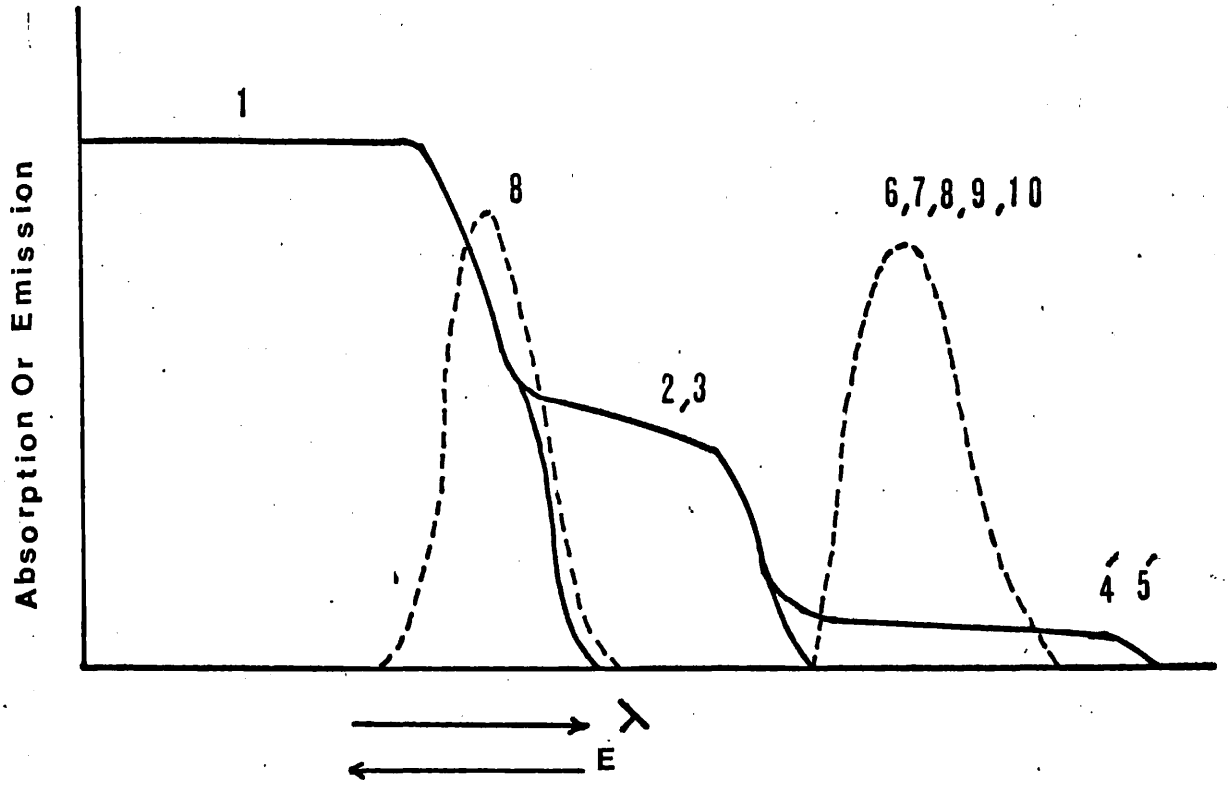

FIG. 16 Representative Absorption Spectra (solid lines) and Emission Spectra (dashed lines)

of light intensity or temperature and a recombination centre under another condition.

3.5.1 Electronic transitions

Some of the electric transitions commonly found in photoconductors are shown schematically in the energy band diagram of Fig. 15. These may conveniently be divided into three types:

1) Absorption and excitation Fig. 15a.

2) Trapping and capture Fig. 14.

3) Recombination Fig. 15b.

Absorption and excitation

There are three types of absorption resulting in photoconductivity.

Transition 1 corresponds to absorption by the atoms of the crystal itself, producing a free electron and hole for each photon absorbed.

Transition 2 corresponds to absorption at localised imperfections in the crystal, producing a free electron and a hole bound in the neighbourhood of the imperfection for each photon absorbed.

Transition 3 corresponds to absorption, raising an electron from the valence band to an unoccupied imperfection level, producing a free hole and an electron bound in the neighbourhood of the imperfection for each photon absorbed.

The transition a) resulting in exciton formation,

b) between ground state and excited state of an imperfection, and

c) within allowed bands,

may be omitted because these do not directly produce free carriers. Idealized absorption spectra illustrating these transitions are given in Fig. 16. There is a cut-off of absorption at the minimum energy required for the transition; this minimum energy corresponds to the

band gap for transition 1, and the corresponding wavelength is called the absorption edge. For light of greater density than the minimum absorption is continuous and fairly constant (depending on the density of states and the transition probabilities involved) up to a certain maximum energy, which would mark a transition from the bottom of the valence band to the top of the conduction band. In most real crystals the conduction band overlaps higher allowed bands and the maximum energy for absorption is not found. To a first approximation, the photoconductivity has the same dependence on wavelength as the absorption.

Trapping and capture

This probability has already been discussed in section 3.4.

Recombination

Three types of recombination transitions are illustrated in Fig. 15b. The free electron may combine directly with a free hole according to transition 8; the probability of this transition is usually rather small. Frequently transitions of type 8 are radiative, i.e. the lost energy is emitted as a photon with approximately the energy of the band gap. Such emission is called edge emission.

Recombination may also occur as is the more usual case through recombination centres; either an electron being captured by an excited centre containing a hole (transition 9) or a hole being captured by an excited centre containing an electron (transition 10). Transitions 9 and 10 may also be radiative.

3.6 Effects of space charge limited currents injected by high fields

A number of investigators have shown that it is possible to increase the rate of decay of photoconductivity by the application of a

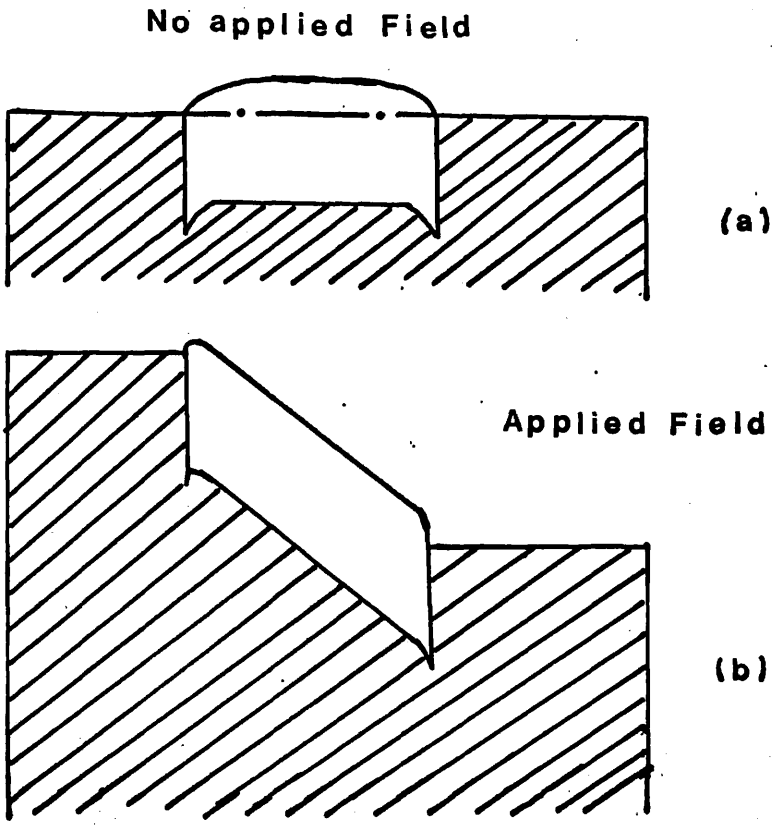

FIG.17. Energy Level Diagrams

Energy level diagrams for a material with ohmic contacts, (a) in the absence of an applied field; (b) in the presence of an applied field.

high electric field.[98-100] Most of the data presented by Boër and Kümmel[98,100] indicates that the application of high fields has the effect of freeing electrons from traps but could also be interpreted in terms of the effect of space charge limited current injected by the high fields. Kallmann and Mark[100] interpret their data as indicating that the effect of the high fields is to reduce considerably the probability of retrapping rather than to empty traps directly by a field ionization effect.

Fig. 17 shows typical diagrams for an insulator or semi-conductor with ohmic contacts. When an external field is applied, a virtual cathode is formed, a reservoir of electrons being present in the material, available for use as needed to replenish charge. If, however, the field is large enough electrons will be injected into the bulk of the material to form a current which will be limited by space charge considerations. But the fact that large space charge limited currents are seldom found in practice can be attributed to the effects of traps on the space charge limited conduction process.[101]

It may be helpful to consider briefly the analogy between space charge limited current in a thermionic diode and such currents in a solid. In a thermionic diode, the space charge limited density is given by:

$$I = 2.3 \times 10^{-6} \frac{V^{3/2}}{d^3} \text{ amp/cm}^2 \qquad (35)$$

whereas, Mott and Gurney derived the expression

$$I = 10^{-13} V^2 \mu k/d^3 \text{ amp/cm}^2 \qquad (36)$$

for the space charge current through a slab of insulator a centimeter thick, and a voltage v applied across a cathode-anode space of d. μ is the mobility of the charge carriers and k is the dielectric constant.

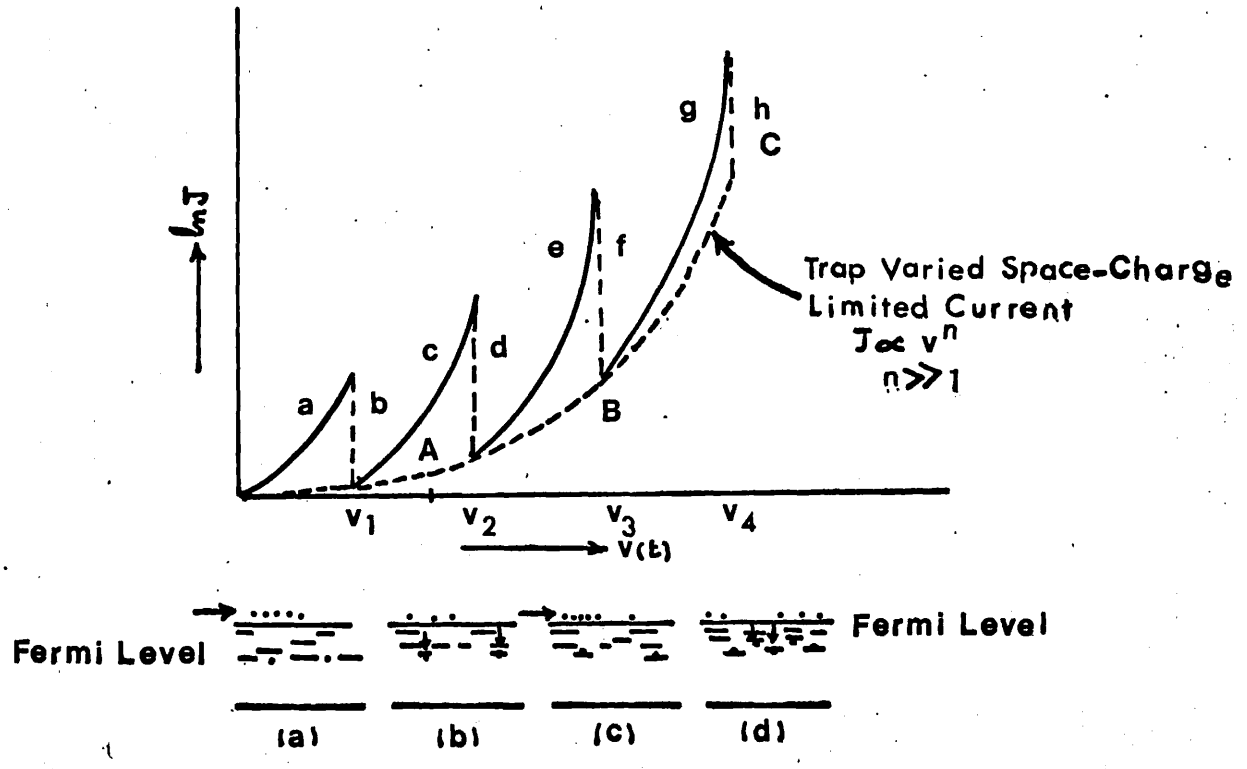

Fig. 18 Field dependence of current on applied voltage for measurements in the space charge limited range for a crystal like CdS, illustrating the transient effects obtained with sudden increases in voltage followed by periods of steady voltage.
The low energy-level diagrams picture the injection and trapping of charge, as occurring in the corresponding lettered portions of the log JV_sV plot.

Smith and Rose[102] have taken advantage of the existence of ohmic contacts when I_n electrodes are used on CdS to investigate the existence of such space charge limited currents. By applying low electric fields, of the order of 10^3 volt/cm, to insulating CdS crystals they were able to measure currents which increased as a high power of the applied voltage; these currents were interpreted as space charge limited currents, and the variation of current with voltage according to a power greater or equal to 2 was attributed to the effects of traps.

Fig. 18 shows a typical dependence of current on voltage for measurements in the space charge limited range for a crystal like CdS. If the applied voltage is raised from zero to a value V_1, the current increases along a curve of type a, the steepness of the curve increasing directly with the rate at which the voltage is increased to V_1. If now the voltage is held at V_1, the current decreases along curve b to a much smaller value. If the voltage is again raised to V_2 the current increases along curve c and then settles back along curve d if the voltage is held at V_2. The equilibrium value of current at each voltage is the space charge limited current to be compared with Equation (36). It is found that the current increases with between the fourth and tenth power of voltage, and that the absolute values of current are much smaller than those predicted by Equation (36). The small energy level diagrams in Fig. 18 (lettered to correspond to the pertinent segments of the current voltage curve) show how the interaction between traps and the space charge limited currents produces the observed transient effects and the deviations from Equation (36). Whenever the voltage is increased there is a sudden increase in the density of free electrons injected from the cathode. In time, however, most of these electrons are captured in traps. Finally, a steady state is set up so that the rate of thermal

excitation of electrons out of traps is equal to the rate of capture of free electrons by traps, i.e. the Fermi level is raised to a new position consistent with a higher density of free electrons. Most of the injected electrons are trapped, thus making the observed space charge limited currents much smaller than they would be in a trap free solid. For every K_T that the Fermi level is raised, the density of free carriers increases by a factor of e, so that a rapid dependence of current on voltage is expected.

According to Lampert[70] the I-V characteristics (Fig. 17) can be characterized by three distinct regions; a low level linear region A, in which the current is mainly due to electrons existing in thermal equilibrium, a square law region B in which injected charge dominates over the thermal equilibrium current and a rapidly rising region results from the filling of the discrete set of traps. The density of the trapping centres and their energy level can be calculated from such curves.

If[101] $V_{ft}(j-1)$ is the voltage corresponding to the filled traps at energy level $E_C - E_{t(j-1)}$ and $V_{ft(j)}$ that for the traps at $E_C - E_{t(j)}$, then

$$V_{ft(j)} - V_{ft(j-1)} = \frac{L^2}{2\epsilon} N_{t(j)} \qquad (37)$$

In any square law region corresponding to particular θ_j, this is given by:

$$\theta_j = \frac{N_C}{2N_{t(j)}} \exp\left(-\frac{E_C - E_{t(j)}}{K_T}\right) \qquad (38)$$

where N_C is the density of conduction band states within K_T of the bottom of the band E_C. θ_j is the ratio of the measured current at an appropriate voltage in the region considered to the Childs' law current at that voltage. Having obtained the trap density $N_{t(j)}$ from Equation (36), Equation (37) gives the energy depth $E_C - E_{t(j)}$. The possibility exists that a shallow

trapping level with a relatively low density $N_{t(k)}$ will be masked by a shallower level of density $N_{t(j)}$. The condition for this is,

$$\frac{N_{t(j)}}{N_{t(k)}} > \exp\left(\frac{E_{t(j)} - E_{t(k)}}{K_T}\right) \qquad (39)$$

Injections from ohmic contacts has also been involved in the investigation of low-field electroluminescence in insulating CdS crystals by Smith.[103] Electrons injected from an ohmic I_n contact recombine in the crystal with holes injected from a field formed contact of I_n, to produce luminescence emission, mainly with an energy equal to the band gap of CdS.

4. Experimental techniques

4.1 Preparation of samples

4.1.1 Material

The material on which these experiments were performed was single semi-insulating CdS crystals, obtained from G.E.C. and also very kindly supplied by Prof. J. Anderson of Imperial College, London. The specimens cut from G.E.C. and Imperial College materials are shown in Table 2, and measured dark conductivities are also given.

4.1.2 Making of ohmic contacts

Rectangular bars of CdS were cut from the boule with a diamond saw, charged with 'Aquagrind 80'. After cutting the specimens were degreased and given a thorough wash in absolute alcohol. They were then dried in a desiccator. The surfaces of the specimens were then polished to $^1/_4$ micron flatness with Alumina powder type A (0.3 micron) and Alumina powder type B (0.05 micron) with a polishing machine using lap made of Swedish pitch and beeswax. These bars of CdS were etched in an etching solution comprised of two parts of HCl and five parts of absolute alcohol (C_2H_5OH). The specimens were then given a final rinse and kept in alcohol to minimise contamination.

These specimens were ready then for making electrical contacts. For the measurements to be reported later, electrical contacts were required, which in the presence of strong electric field should be linear, regular and of low resistance. It was desirable otherwise to produce contacts which should have given the minimum potential drop during current flow. The voltage-current characteristics of such contacts should be

linear and non-rectifying, i.e. symmetrical about the origin. Such contacts will be referred to as ohmic contacts. These contacts do represent an ideal type which is never realized in practice, but which may be approached by suitable techniques. However, the question of contacts is particularly difficult and important in the case of our material of wide gap near insulating crystals, where the contact properties are largely, if not fully, determined by the nature of the contact.

In order to achieve this a thin layer of indium was then evaporated in a vacuum of 10^{-5} torr on to each end surface of each bar. The thickness of the film was determined by observing the transparency of a glass slide, placed adjacent to the jig carrying specimen while held in a vacuum chamber. The evaporation of indium was stopped when glass slide became quite opaque. The specimens were mounted in end-on positions in the jig with the help of dental wax. The other end of the bar could easily be coated just by reversing the position of the jig in the vacuum chamber as they were mounted along end-on positions. To remove the wax the specimens were rinsed in warm carbon tetrachloride and later washed in absolute alcohol. Although the melting point of dental wax ($70^{\circ}C$) was far below that of indium ($156^{\circ}C$) care had to be taken while mounting and removing specimens. The best procedure adopted was to remove the jig from the hot-plate as soon as the dental wax was fluid enough to flow. This ensured that the temperature of the jig would not rise too much while specimens were being mounted or removed.

The thin film of indium on the end surfaces was then diffused slightly into the specimen by short heat treatment. This heat treatment was achieved by heating the specimens lying on their sides in an inert

Table 2 Specimen Characteristics

Specimen Number	Source	Length mm	Dimensions cross-section mm^2	Orientation	Conductivity (dark) ohm cm^{-1}	Illumination intensity with tungsten lamp watt cm^{-2}	Conductivity ohm cm^{-1}	Conductivity with laser (2mW) ohm cm^{-1}
TRS_1	G.E.C.	3.28	0.74 x 0.88	$\perp$ to c-axis	1.32×10^{-7}	3.9×10^{-2}	3.8×10^{-4}	
TRS_2	G.E.C.	2.32	0.39 x 0.80	$\perp$ to c-axis	1.07×10^{-7}	3.9×10^{-2}	3.7×10^{-4}	
TRS_3	G.E.C.	2.31	0.33 x 0.80	$\perp$ to c-axis	2.6×10^{-7}	3.9×10^{-2}	3.03×10^{-4}	
TRS_4	Imperial College	4.58	0.80 x 0.98	$\parallel$ to c-axis	2.92×10^{-6}	3.9×10^{-2}	4.7×10^{-4}	
TRS_5	Imperial College	4.59	0.96 x 0.88	$\parallel$ to c-axis	3.0×10^{-6}	9.1×10^{-2}	5.6×10^{-3}	
TRS_6	Imperial College	4.57	0.97 x 0.89	$\parallel$ to c-axis	2.8×10^{-6}	2.3×10^{-3}	4.8×10^{-4}	
TRS_7	Imperial College	3.0	0.92 x 0.5	$\perp$ to c-axis	2.78×10^{-6}	2.5×10^{-3}	1.9×10^{-4}	
TRS_8	G.E.C.	2.82	1.15 x 2.27	$\perp$ to c-axis	3.8×10^{-7}	8.3×10^{-2}	2.9×10^{-5}	4.9×10^{-5}
TRS_9	G.E.C.	2.30	0.27 x 0.58	$\perp$ to c-axis	2.8×10^{-7}	7.9×10^{-2}	4.1×10^{-5}	6.3×10^{-5}

Contd/

Table 2 Specimen Characteristics (Cont'd)

Specimen Number	Source	Length mm	Dimensions cross-section mm^2	Orientation	Conductivity (dark) $(ohm\ cm)^{-1}$	Illumination intensity with tungsten lamp watt cm^{-2}	Conductivity $(ohm\ cm)^{-1}$	Conductivity with laser (2mW) $(ohm\ cm)^{-1}$
TRS_{10}	G.E.C.	2.33	0.39 x 1.77	$\perp$ to c-axis	1.95×10^{-7}	8.1×10^{-2}	6.2×10^{-5}	4.8×10^{-5}
TRS_{11}	Imperial College	4.58	0.8 x 0.98	$\parallel$ to c-axis	2.92×10^{-6}	2.4×10^{-3}	2.27×10^{-4}	
TRS_{12}	Imperial College	4.55	1.09 x 0.69	$\parallel$ to c-axis	8.0×10^{-3}	2.4×10^{-4}	1.7×10^{-1}	
TRS_{13}	Imperial College	3.0	0.92 x 0.51	$\perp$ to c-axis	9.3×10^{-3}	2.1×10^{-4}	2.0×10^{-1}	

atmosphere (100% Argon). The diffusion of indium was carried out at 460°C at atmospheric pressure for 3 to 5 minutes. During the process of diffusion, a constant check was made at the ends of the specimen and as soon as the layers of indium disappeared into the specimen at both ends, the heating was stopped.

Another layer of indium was evaporated onto the ends to give more even contact surfaces as small globules could be seen with the aid of a high power microscope to form during the diffusion process. For the second layer of indium the evaporation was stopped, when the glass slide had just turned opaque.

The dark conductivities of the specimens varied somewhat (see Table 2) although they came from single CdS boules. There is a likelihood that this variability may have been caused by the heat treatment and diffusion process as crystals were seen to undergo slight colour changes.

It was quite possible to achieve ohmic contacts without the diffusion process if sufficient care was taken to ensure that the end surfaces were perfectly clean and flat. These contacts would be mechanically weaker and more easily rubbed off during experiments.

4.1.3 Preparation of ohmic contacts of equal area along the surface of the specimen for determination of the field distribution

The field distribution along the specimen was determined by measuring the potential at several points when a known voltage was applied to the ends of the crystal. To reduce the surface potential drop, small contacts of metal were evaporated on to the crystal surface at equal distances of a few mm. Because of the small lengths and high resistivities of the photoconductive specimens, it was quite difficult

to make evaporated contacts of equal area along the surfaces of the crystals. Moreover, it was essential to know the field distribution along the sample length as a function of distance and time. The following procedure was adopted and proved successful. Pieces out of fine and thin mica sheet were cut according to the size of each specimen. Under a microscope holes of equal areas were carefully punched in each mica piece at equal distances. The number of holes depended upon the length of specimens (maximum up to seven). The surface of the crystal where evaporation was to be made was cleaned thoroughly and then was mounted lengthwise in the jig. The mica sheet was then mounted carefully above the surface where the evaporated contacts were to be made. The jig was then put in the vacuum chamber for evaporating a thin layer of indium as described before. Evaporation was stopped as soon as the adjacent glass slide had turned opaque. In order to avoid the rubbing of the indium during experiment another coating of indium was made. Each evaporated contact was tested and all proved to be quite ohmic.

4.2 Preparation of electrical probes for electric field distribution

In order to measure the domain motion and field distribution along the sample, etched tungsten probes were used. They made direct contact with the evaporated areas along the surface of the specimen. Their response time was reported[67] to be of the order of 10 to 50 n sec. These probes were made of pure tungsten wire 0.012" in diameter. Two inches long electrical probes were cut out of the above mentioned tungsten wire. They were then etched on the principle of electroplating in a solution comprised of 1 part caustic soda and four parts of distilled

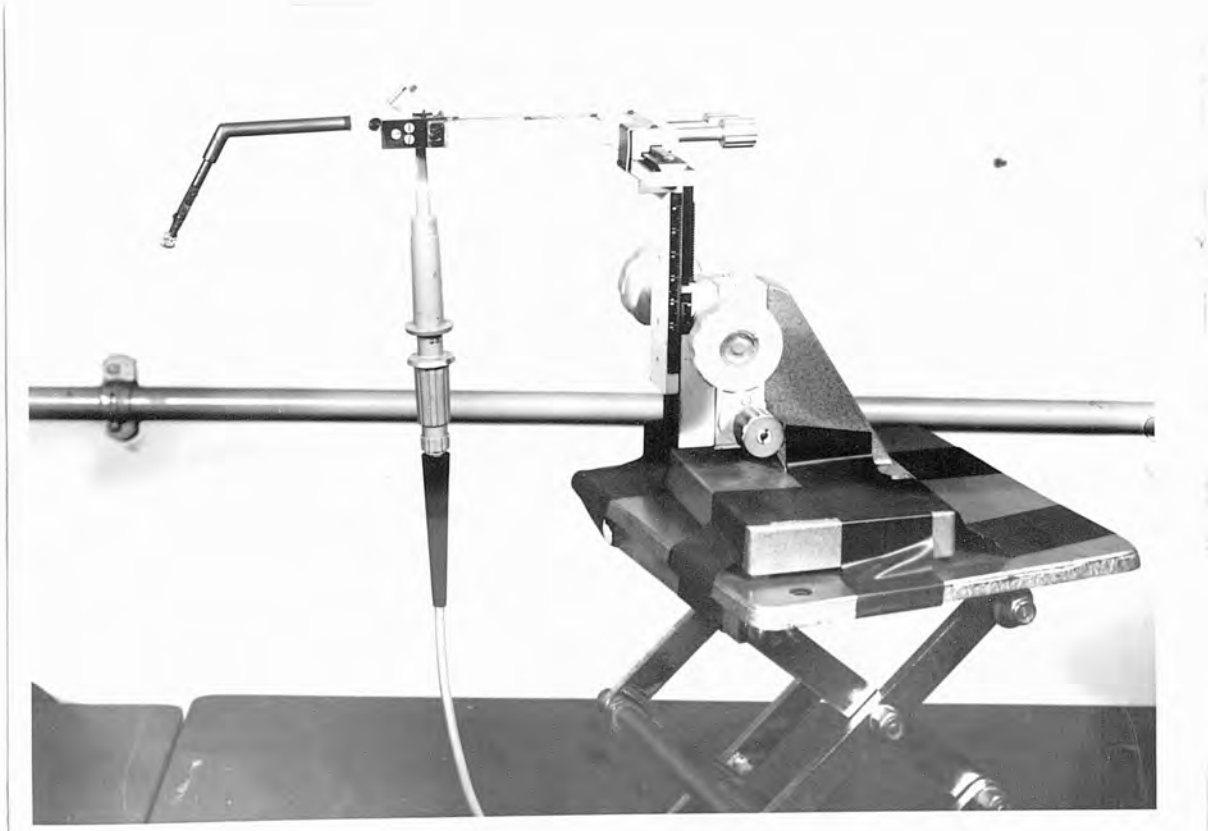

FIG.19 ELECTRICAL PROBE APPARTUS

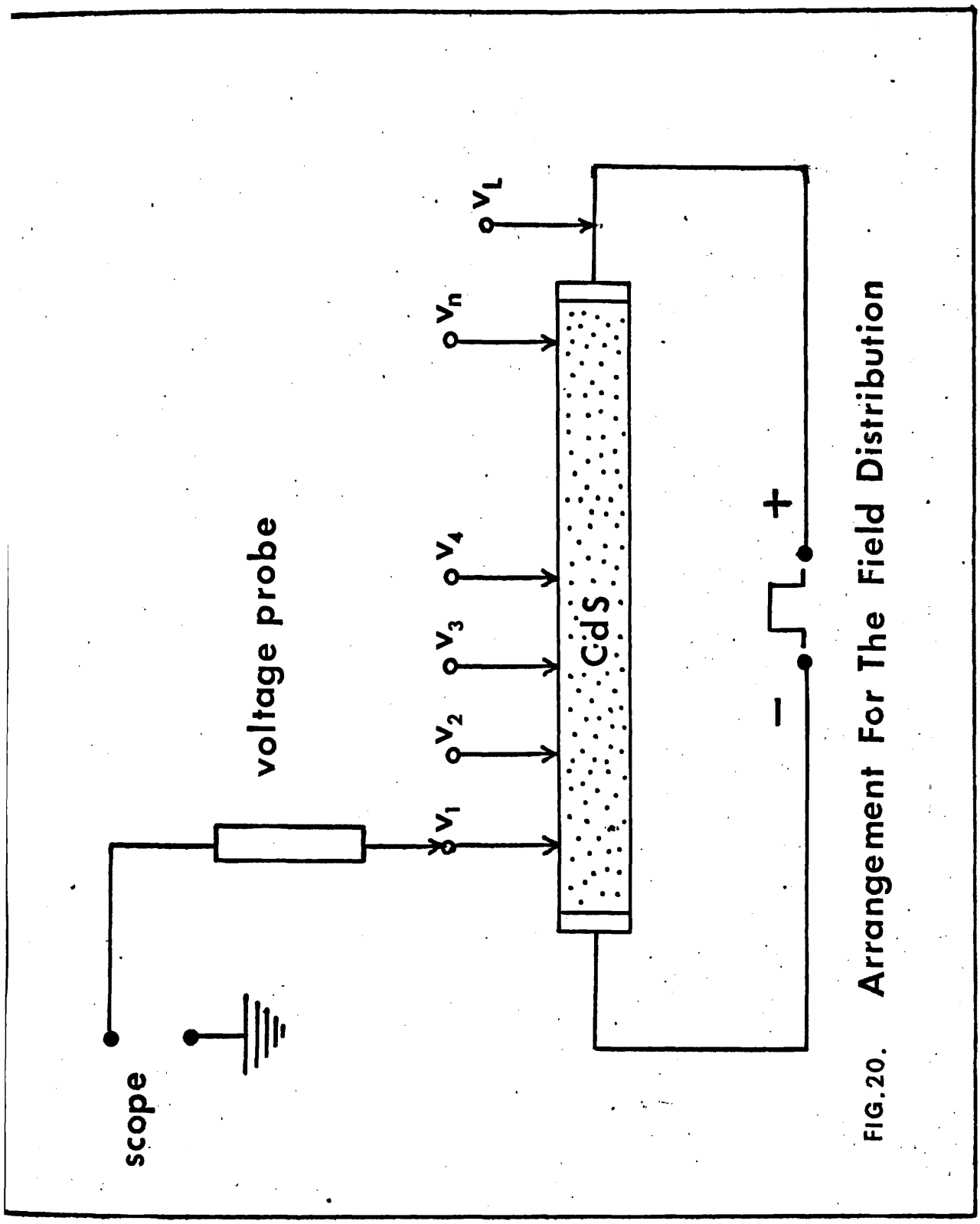

FIG.20. Arrangement For The Field Distribution

water. The etching of probes was done for about 2 to 3 minutes. These probes were then thoroughly washed with absolute alcohol and kept in a desiccator. This electrical probe was then soldered to the end of a brass arm, being fixed to a micromanipulator (see Fig. 19). The basic experimental arrangement with the monitoring probe is also shown in Fig. 20.

4.3 Illumination arrangements

Specimens were placed between a mount consisting of a copper plate (negative electrode) and a copper head attached to an adjustable spring loaded plunger (positive electrode, see Fig. 21). All experiments were performed at room temperature and in a perfectly dark room to exclude the effects of light from unrelated sources. Illumination from a high intensity light source provided with a variable transformer was obtained through a small aperture. Light shields of varying sizes were used for shading the left end (positive electrode) or right end (negative electrode) of the specimen as and when required. These light shields were made of ceramic rods about 6cms long. About 1cm of one end of these rods were grounded as shown in Fig. 21 to one of the following thicknesses: 0.5mm; 0.6mm; 0.71mm or 1.0mm. These ground ends were placed immediately in front of the specimen (see Fig. 22) and would cast shadows of their respective thicknesses on it. The other end of the shield was clamped to a moveable metal arm, attached to a micromanipulator. This enabled the movement of the shield to be measured as shown in Fig. 21c.

In early experiments, localised intense illumination of 6328^{o}A red light was obtained through an adjustable slit placed in front of a helium neon laser (computer system model No.G3) and finally focused the

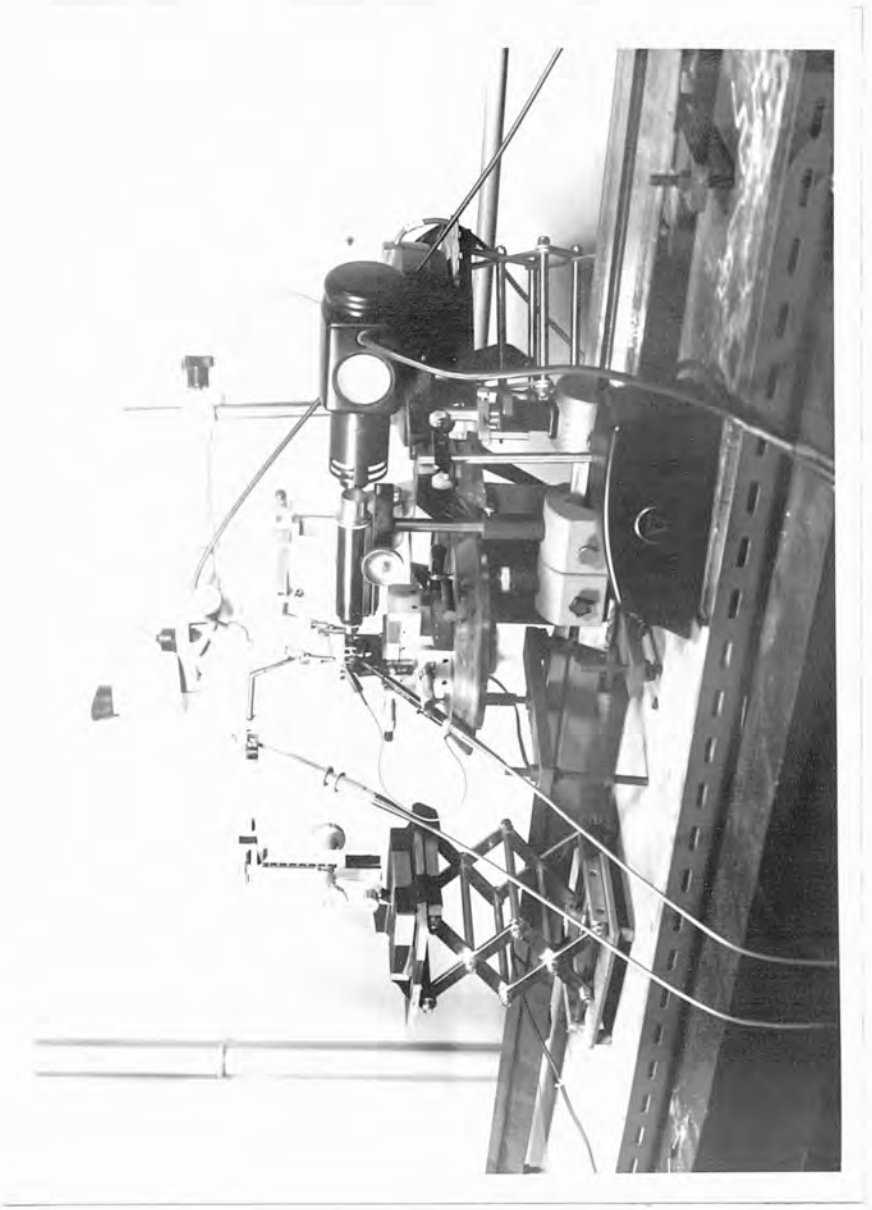

FIG. 21a EXPERIMENTAL ARRANGEMENT

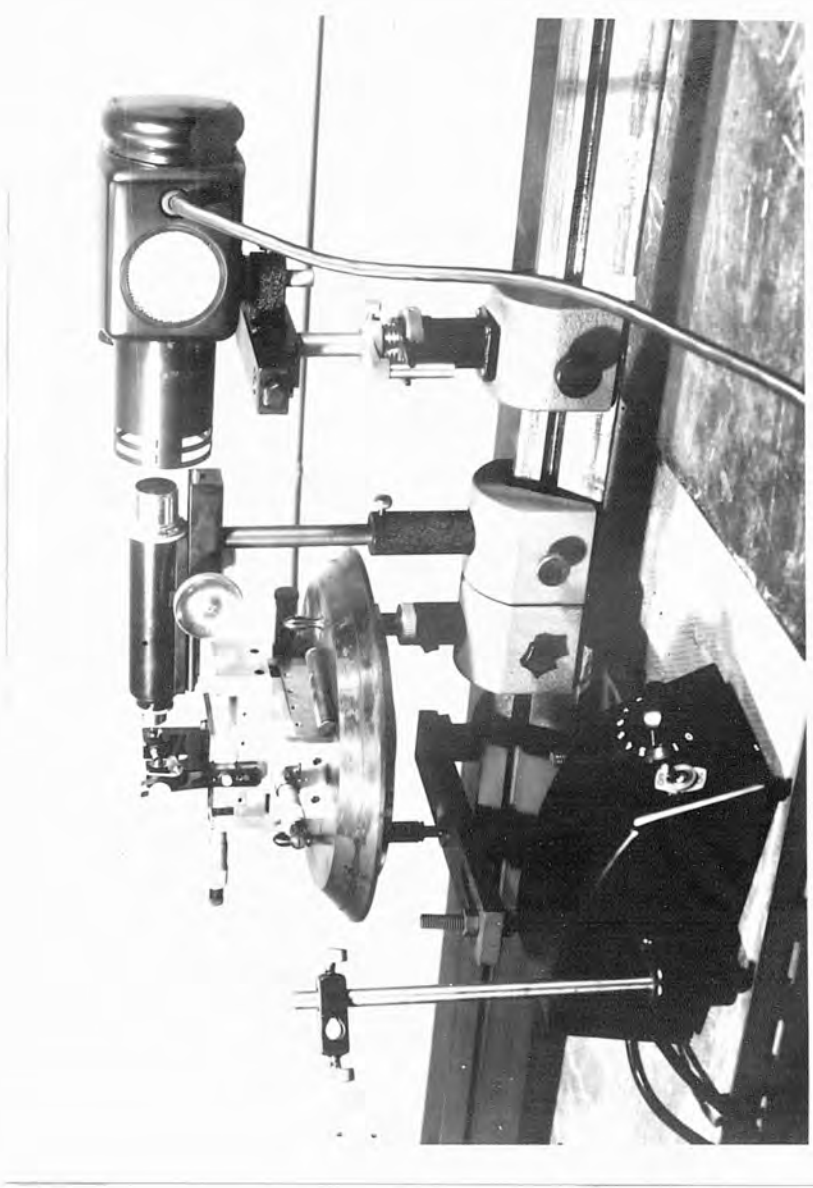

FIG. 21b SPECIMEN ILLUMINATED

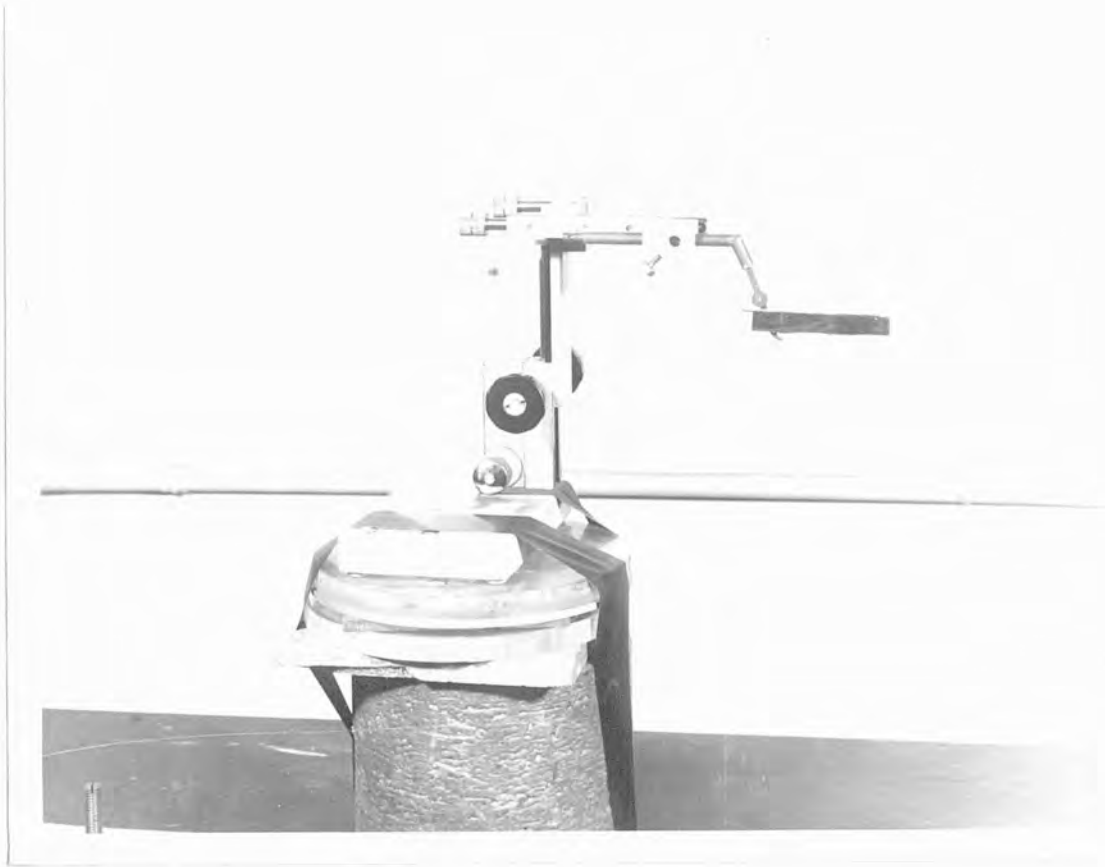

FIG. 21c SHIELDING APPARTUS

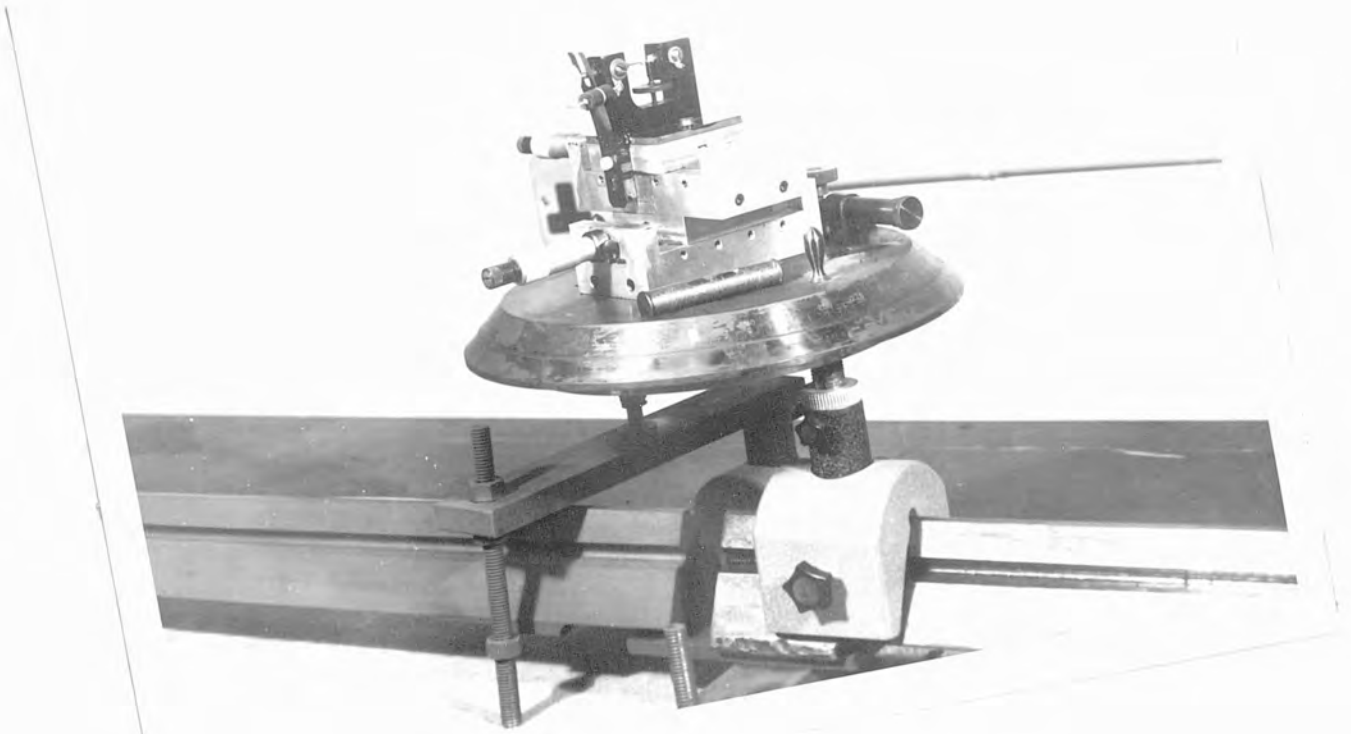

FIG. 21d JIG FOR HOLDING SPECIMEN

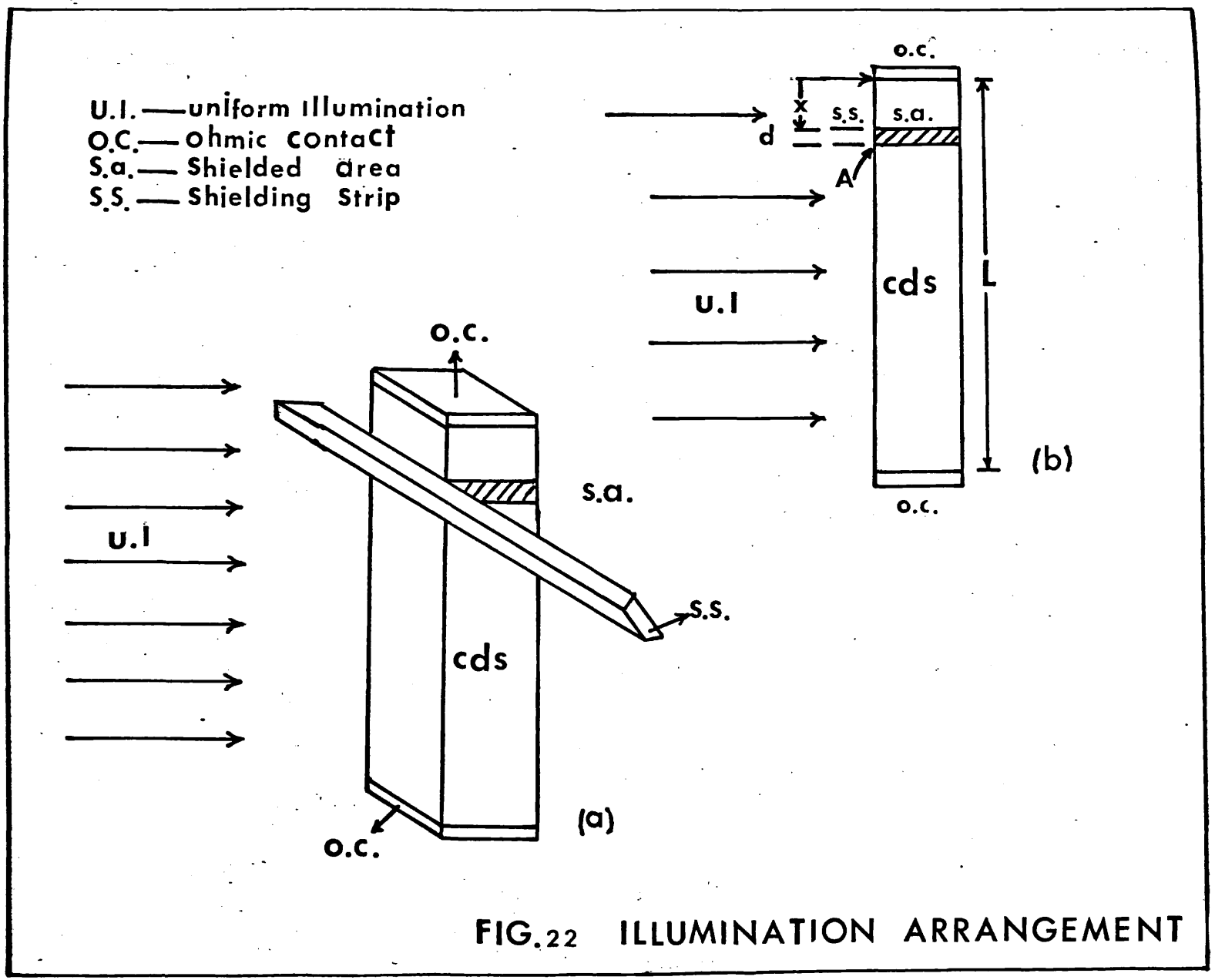

FIG. 22 ILLUMINATION ARRANGEMENT

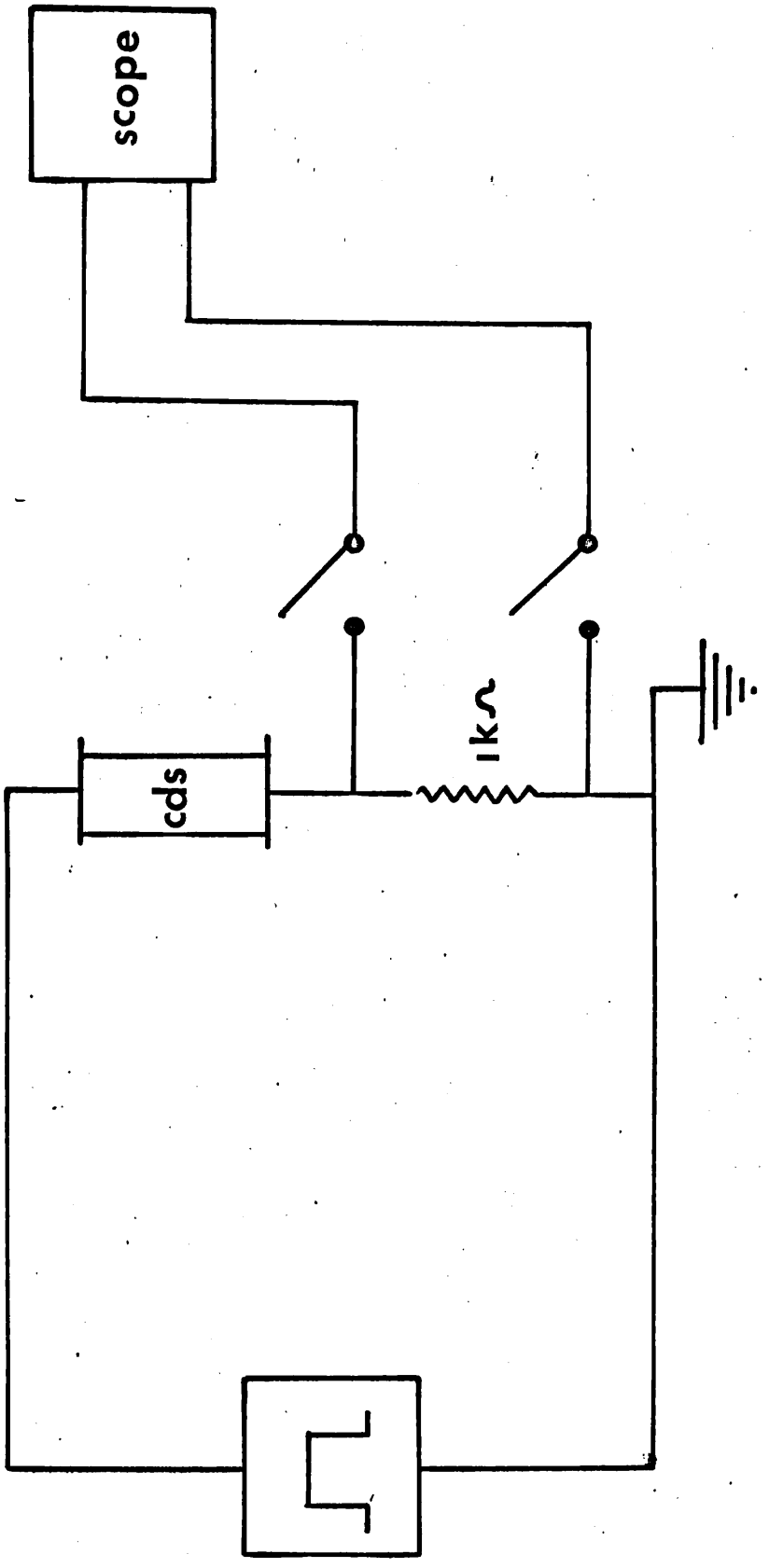

Fig.23 ELECTRICAL CIRCUIT

beam with a convex lense of 8mm focal length on the polished surface of the specimen. The scanning of crystal by the laser beam was obtained by mounting the jig carrying the specimen on a special moveable table, which itself was resting on a rotating table, to be moved along in a horizontal or vertical direction with the help of micrometer screws attached to them (see Fig. 21d).

4.4 Electrical circuit

A block diagram of the circuit is shown in Fig. 23. The low impedence pulse generator was designed and built in the laboratory to give pulses of 10μsec., and μ100 sec., duration. The repetition rate for 10μsec., was 15-20 pulses per second, whereas for 100μsec., pulse it was about 10-15 pulses per second. The low repetition rate (the minimum achieved with the present design) employed was to avoid excessive heating of the specimens. The rise time varied from 0.4μsec. for 10μsec., pulses to 0.6μsec., for 100μsec., pulses. Positive pulses of up to 1.4Kv (max. current 50m amps) are obtainable.

The potential along the surface of the specimen and the current wave forms were observed on a Model 544 Tektronix oscilloscope. A 100Ω or 1000Ω resistor (comparable with the sample resistance) was placed in series with the specimen to obtain the current wave form. A high voltage Tektronix probe was used for measuring the field distribution along the samples.

Table 3 Classification of Experiments

No.	Type of Illumination Distribution	Source of Illumination	Current Pulse: Oscillations	Current Pulse: Saturation	Specimen Number	Reference to previous work	Page Number
1	None (darkness)	NIL	Yes, H.F. Sinusodial	Yes	TRS_{12}-TRS_{13}	None	92
2	a) Uniform	Tungsten Lamp	No	Yes	TRS_1 -TRS_7	53,54,55,59	156
	b) Uniform	Tungsten Lamp	Yes, H.F. Non-sinusodial	No	TRS_8 -TRS_{10}	None	98
3	a) Non-uniform illumination i.e. masking anode end	Tungsten Lamp	Yes, M.F. Sinusodial	Non-ohmic behaviour after threshold voltage	TRS_1 -TRS_4	35,36,58	105
	b) To obscure a strip of sample with ceramic strips	Tungsten Lamp	Yes, M.F. Sinusodial	Non-ohmic behaviour after threshold voltage	TRS_5 -TRS_7	48,49	117
	c) To obscure a strip of specimen with light strip	Tungsten Lamp	Yes, M.F. Sinusodial	Double-saturation	TRS_{11}	None	142
4	Localised Illumination	He-Ne laser (2mW)	Yes, H.F. Non-sinusodial	No	TRS_8 -TRS_{10}	None	149

5. Experimental results and discussion of the results

5.1 Introduction

The techniques described in Chapter 4 were used to investigate the response of specimens of cadmium sulphide to a high voltage pulse. The aim of this investigation was to study the instabilities in current under the various types of illumination described in Chapter 3. Investigations were carried out of: a) current saturation phenomena, b) sinusodial and non-sinusodial current oscillations, c) field distributions under oscillatory and steady state conditions, d) conductivities of specimen at various times and under different illumination intensities and e) variation in the resistance of the sample at different positions of the shielded strip.

A wide range of physical phenomena were produced by different experimental conditions, as already mentioned. It was found that the material was very variable. Characteristics of the specimens used in these experiments have already been described in Table 2, in Chapter 4.

5.2 Classification of experiments

In the course of investigation some completely new phenomena have been observed and some work has been compared with the results of other workers. The results of the investigation are anticipated and the phenomena classified in Table 3. Modulation means amplitude modulation. In this chapter, experimental results are described and an attempt is made to explain the phenomena observed.

All observations were carried out at room temperature.

5.3 Continuous oscillations

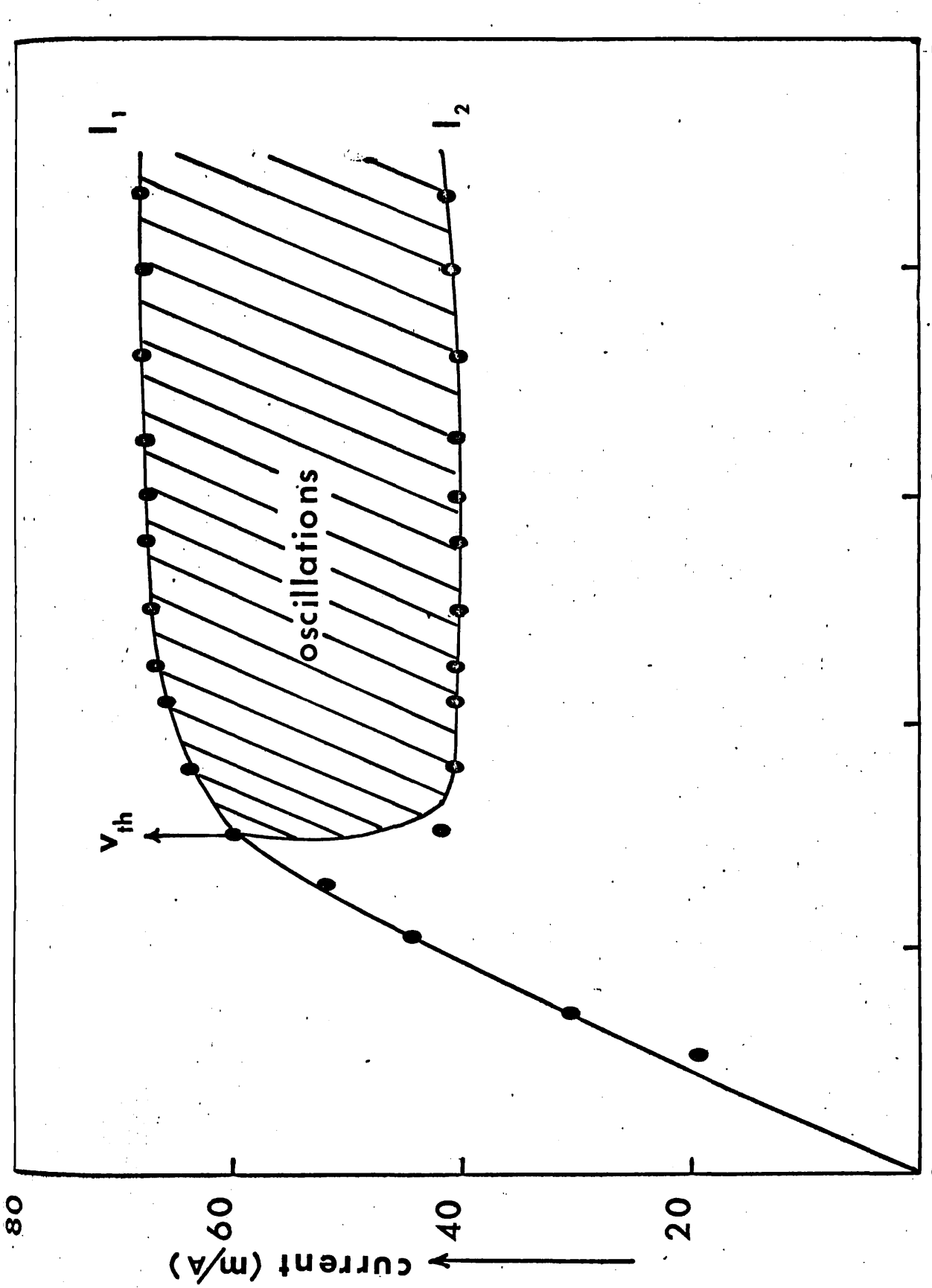

Fig.24 I-V Characteristics (SPECIMEN TRS12)

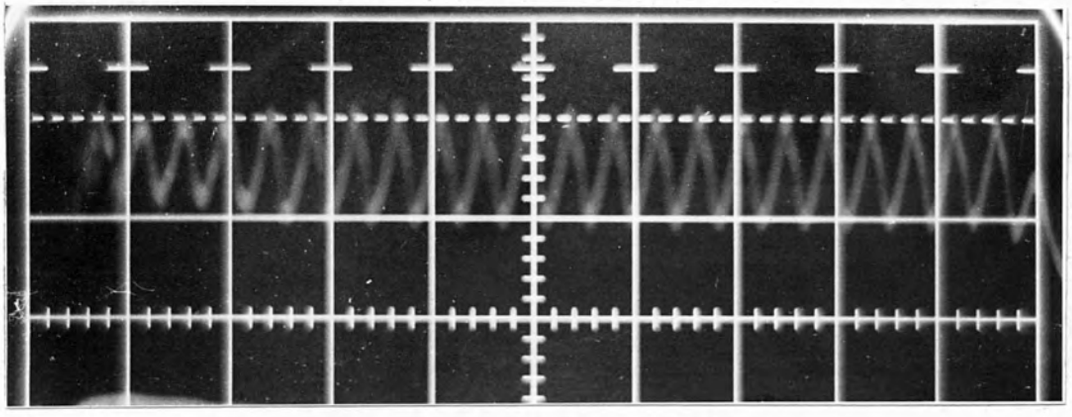

Fig.25 Wave form of the current oscillations for CdS specimen TRS_{12} in complete darkness at an applied voltage of 1100 volts.

Horizontal scale = 1 μ sec/div.

Vertical scale = 20 mA/div.

5.3.1 Oscillations in complete darkness

It was seen that two specimens TRS_{12} and TRS_{13} cut from a single CdS crystal oscillated continuously when a high voltage pulse was applied in total darkness; an effect that has not been reported before. Considerable care was taken to ensure the complete absence of light in the room and careful inspection of the specimen revealed no luminous discharge occurring at the electrodes or in the bulk of the material. All instrument lamps were properly covered and oscilloscope was screened by a hood.

The magnitude of the current pulses in darkness is shown in Fig. 24 for various applied voltages. The relationship between I and V is ohmic, but becomes non-linear as the current begins to oscillate at higher fields. Above the threshold voltage V_{th}, the current oscillates between two values I_1 and I_2, where I_1 is the saturation current and I_2 results from a negative incremental resistance.

Fig. 25 represents a typical trace of the current pulses generated in specimen TRS_{12}. It is seen that the current rises to the saturation level I_1 in about 0.8μsec and then decreases to I_2 in about 0.2μsec, rising again to I_1 after a further 0.2μsec.

The field distributions shown in Fig. 26 were measured under oscillatory conditions. A probe shows that the period of oscillation is approximately equal to the time taken by the sound wave to travel between the position of the high field and the anode end of the specimen and not related to the transit time between cathode and anode.

Current saturation and oscillation occur independent of the field direction (II or $\perp$ to c-axis). The current saturation observed in Fig. 24 at an applied voltage of 480 volts can be attributed to the formation of a stationary high field domain as described in Chapter 3.

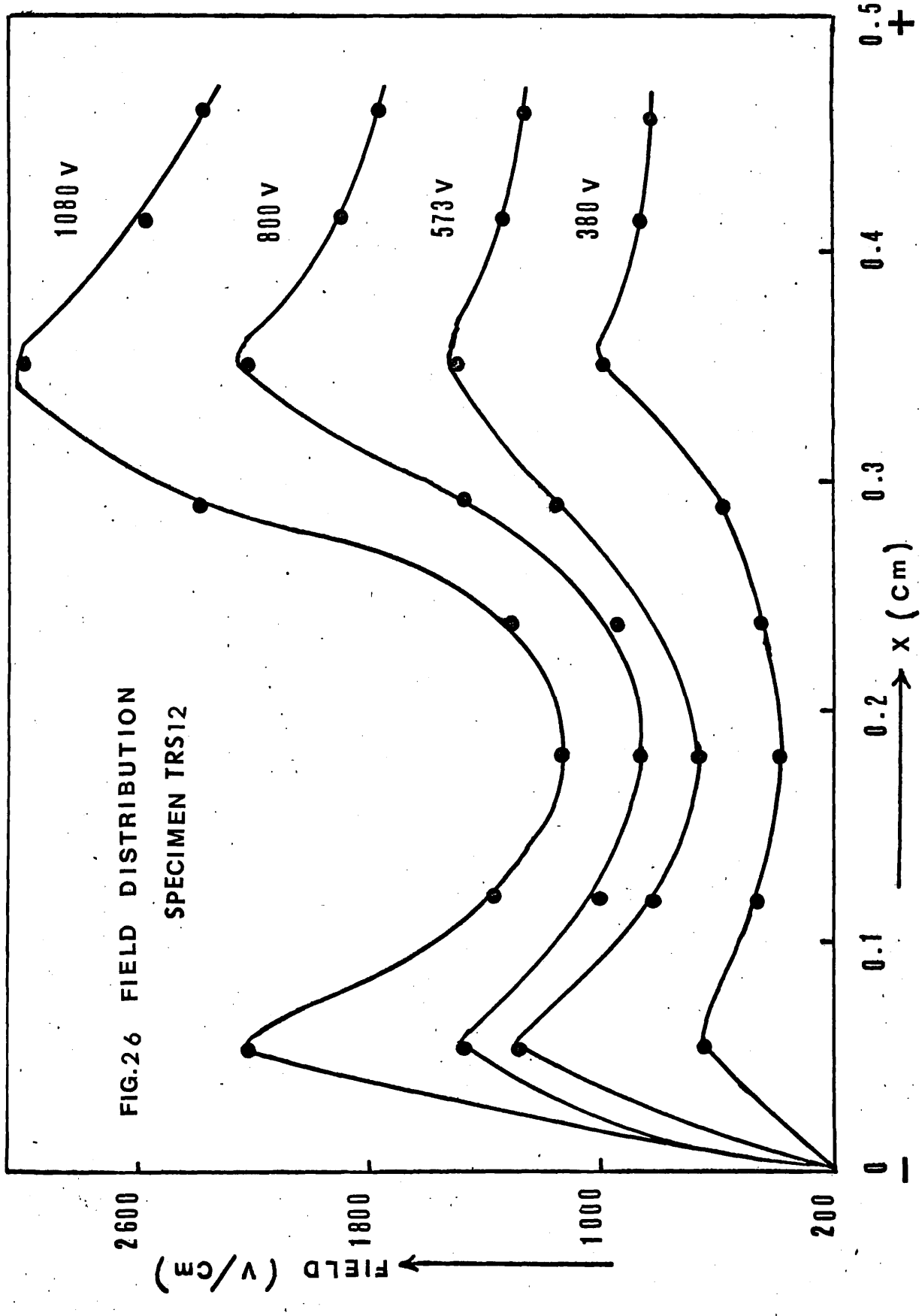

FIG.26 FIELD DISTRIBUTION
SPECIMEN TRS12

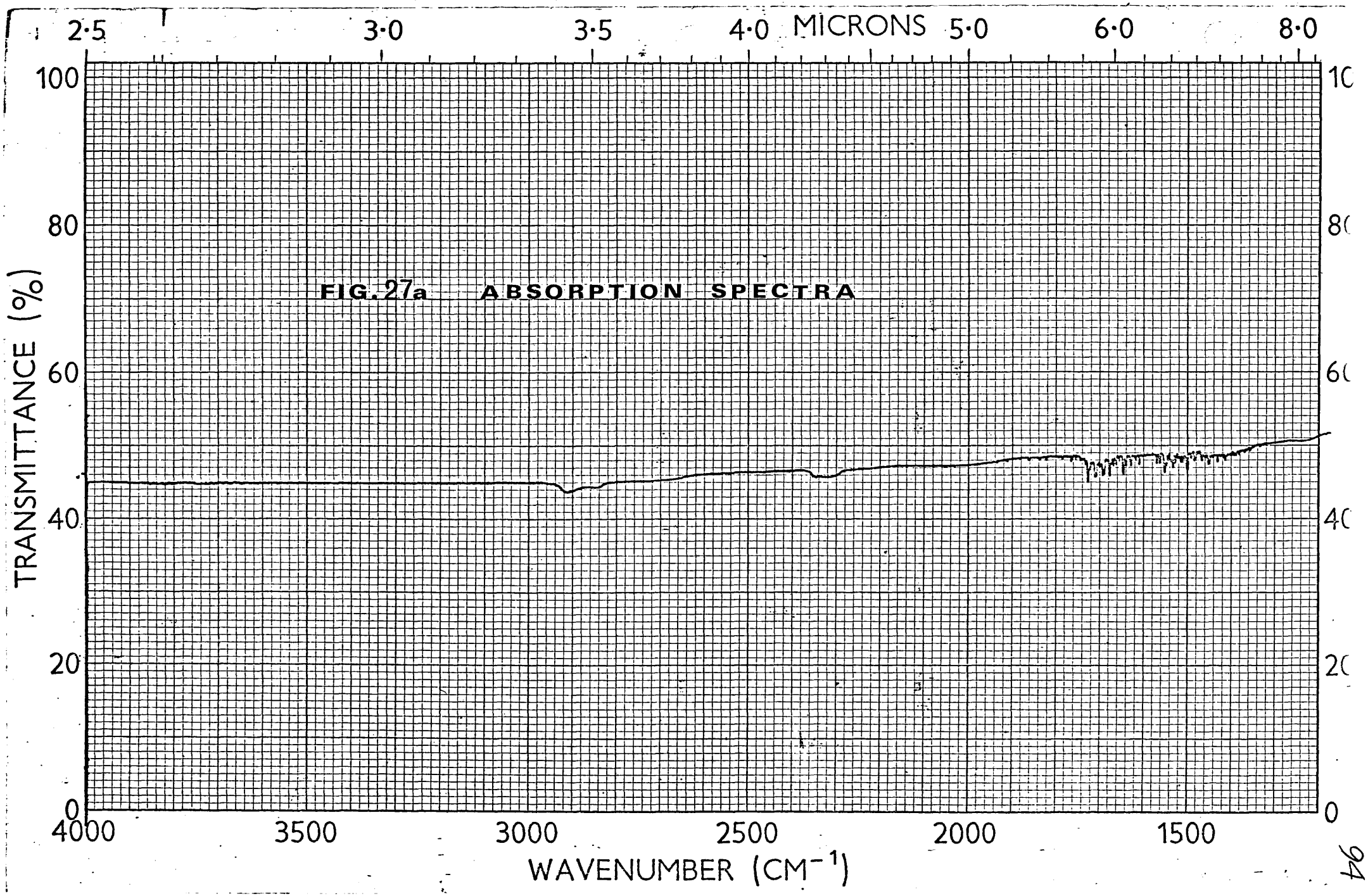

FIG. 27a ABSORPTION SPECTRA

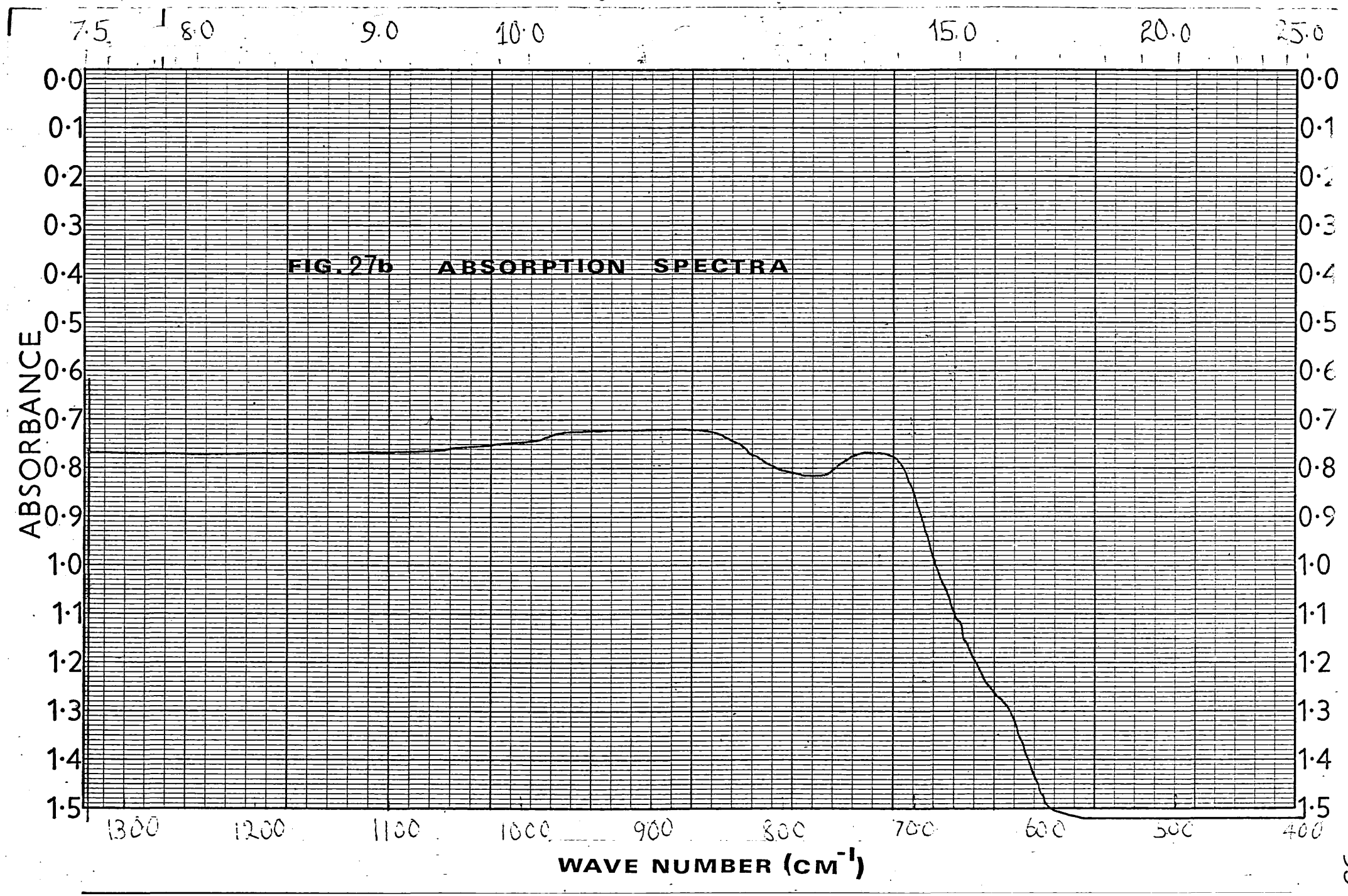

FIG. 27b ABSORPTION SPECTRA

The absorption spectra of the material has revealed bands which could be attributed to electron traps, as shown in Fig. 27(a,b), and having energies as low as 0.08eV. It is believed that one of these levels plays an important role in the phenomena observed.

The occurrence of dark current oscillations poses the problem of explaining the origin of the extra charge carriers. According to Chynoweth,[71] the field required to field ionize the 0.08eV centre is about 10^4-10^5V/cm. This is 100 times more than the field used in the experiment, so the field ionization of these centres can be easily ruled out. On the other hand, a donor ionization energy of 0.08eV would seem to require a drift velocity of 10^6 to 10^7cm/sec., in order to ionize by collisions. The drift velocities calculated are comparable with the velocity of sound in the material $\sim 10^5$cm/sec. It appears that the ionization of low energy centres has occurred at the velocity of sound, a phenomenon well known at low temperatures in CdS. It is quite possible that during the growth of crystal the appropriate, easily ionized impurity has entered the material. The relatively slow ionization rate evidenced by the rather slow rise of current with field may be explained if the majority carriers, travelling just at the sound velocity, never take part in ionization. Most additional carriers created by the few fast electrons are also velocity limited and the ionization rate is reduced by the ratio of the velocities of fast electrons to that of sound limited electrons.

It is, however, suggested that in CdS a possible mode of interaction between acoustic flux packets and the trapping rate may result from the high field regions which have been shown to be associated with acoustic flux build-up.

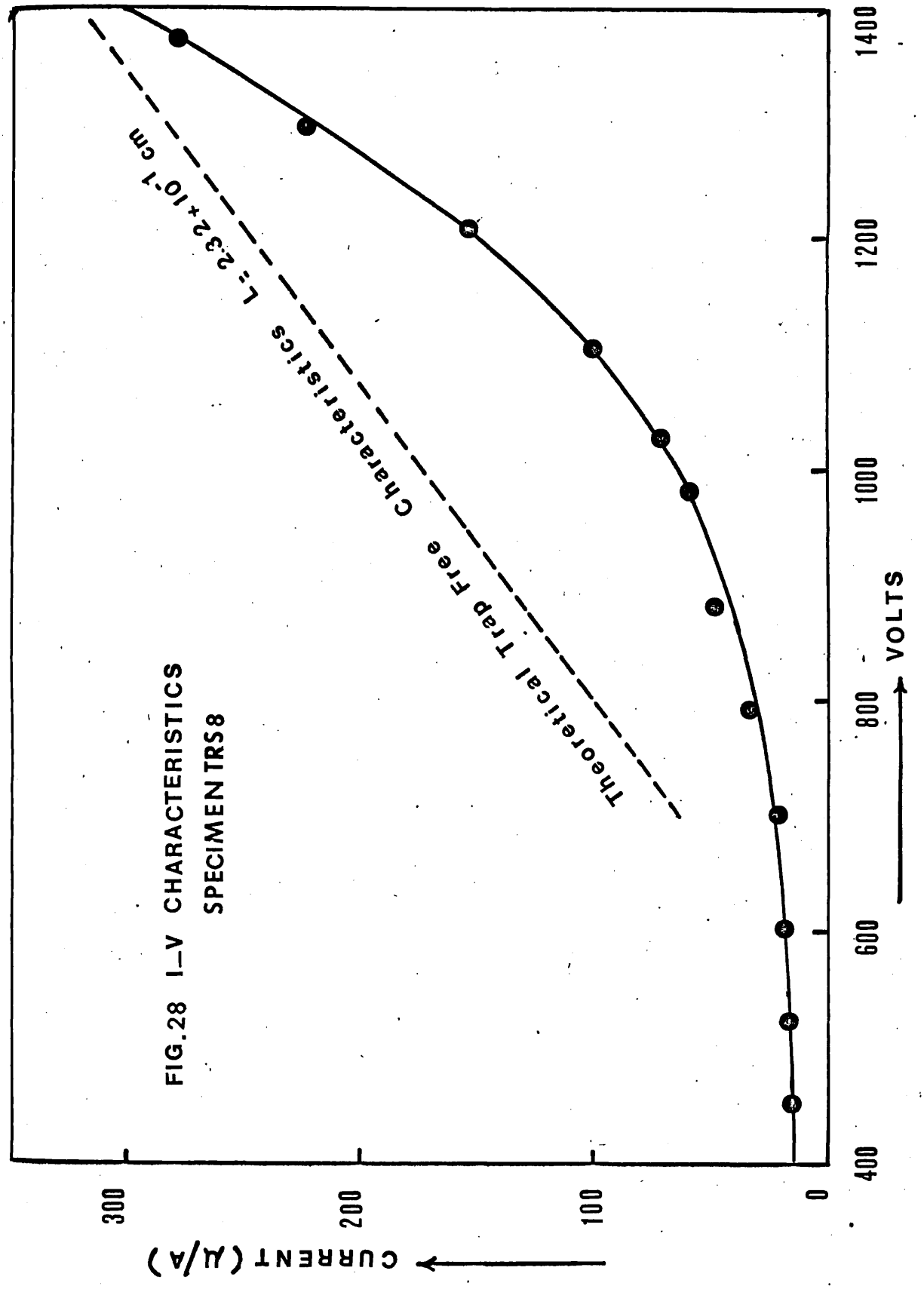

FIG.28 I–V CHARACTERISTICS
SPECIMEN TRS8

5.3.2 Non-sinusodial oscillations with uniform illumination

Semi-insulating CdS material normally requires a non-uniform conductivity along the length to give continuous oscillations, but it was found that some CdS specimens oscillated under uniform illumination. These were relaxation oscillations of high frequency and have not been reported before. The specimens chosen for this experiment had the dimensions and conductivities under the illumination intensities given in Table 2.

Fig. 28 represents the dependence of the current on the voltage applied to the specimen TRS8. The I-V characteristics are of complex form. It is seen that at low voltages the current voltage characteristics fall below the linear ohmic relation. This[70] sub-linear part is gradually replaced by a region in stronger electric fields with a dependence of $I \propto V^2$. This type of relationship between current and voltage has often been shown for the injection of electrons in the dark into insulating cadmium sulphide crystal platelets ($\sigma = 10^{-6}-10^{-7}\Omega^{-1}cm^{-1}$). No report has so far been found of the dependence of current on applied voltage for bulk material. The full I-V curve shows the features of the Lampert theory for a single discrete trapping level. From the resulting I-V characteristics and using equations 37, 38 the trap densities and energy levels are calculated. Fig. 28 also shows the Child's law relationship for the specimen, which was calculated by assuming a dielectric constant of 10 and an experimentally measured drift mobility of 300 $cm^2V^{-1}sec^{-1}$ at room temperature. The trap filled limit voltage V_{TF} and θ (ratio of the measured current to the Child's law current at V_{TF}) for the curve give a trap density of $1.66 \times 10^{-14} cm^{-3}$ at an energy of 0.21eV below the bottom of the conduction band. The cross section S_t of the traps into which these electrons decay was calculated

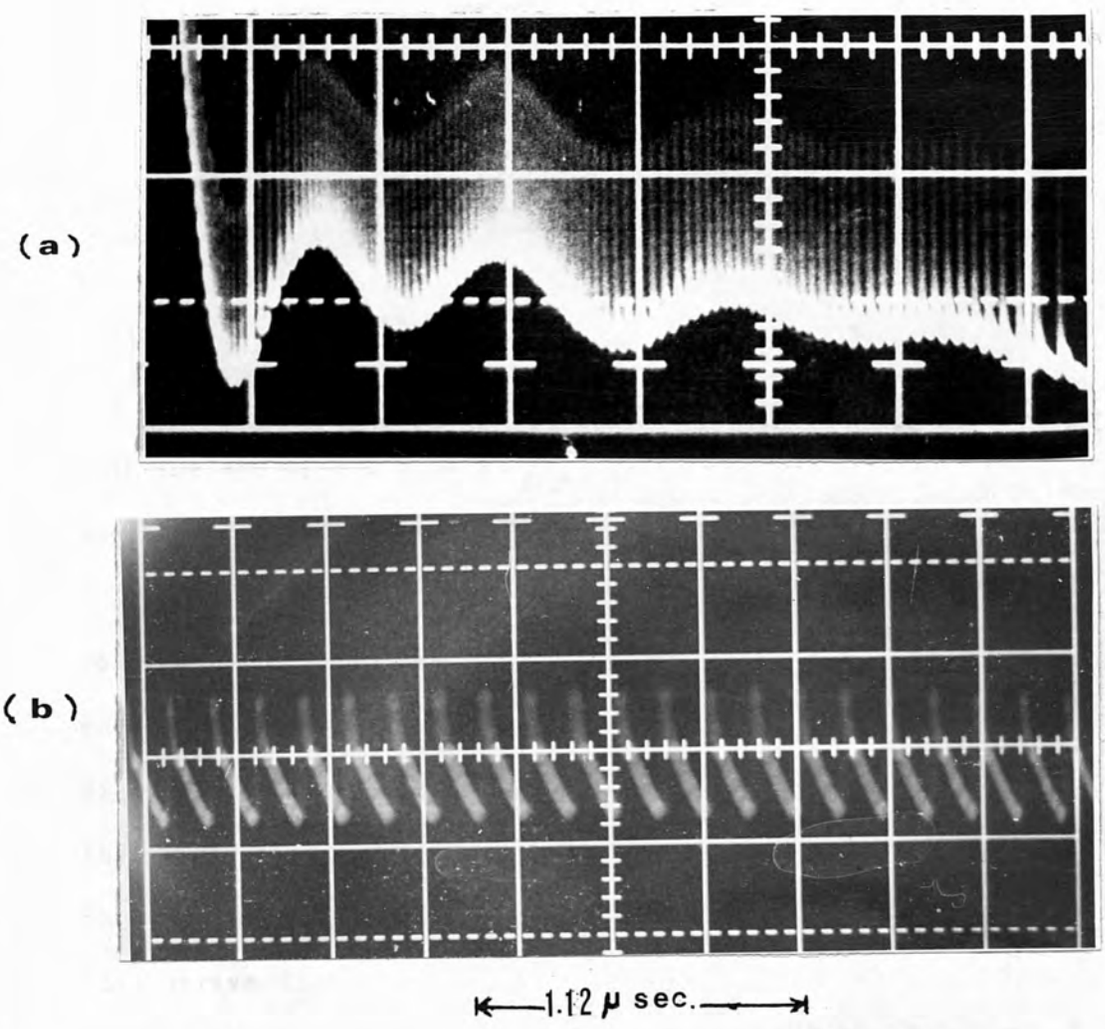

Fig.29 Non-sinusodial continuous current oscillations in CdS specimen TRS_8 when interelectrode area is uniformly illuminated.

(a) Horizontal scale = 10 μsec./div.
Vertical scale = 20 μA/div.

(b) Horizontal scale = 0.3 μsec./div.
Vertical scale = 25 μA/div.

from the relation $S_t = (\tau v n)^{-1} cm^2$, where τ is the decay of the current; v thermal velocity of the electrons and n is the number density. The calculated cross section for this set of traps was $S_t = 1.4 \times 10^{-15} cm^2$. Absorption spectra of these specimens obtained by means of a Perkin Elmer 337 grating spectrometer showed an active band of energies ranging from 0.21eV to 0.19eV, in the range 2.5 to 25 micron as shown in Fig. 27. The trap energy calculated from the I-V characteristics nearly coincided with the absorption peak at λ = 6.23 micron. It is clear from these measurements that active traps are present in the material.

Fig. 29 shows (a) the current oscillations obtained when a 1000 volts pulse of 100μsec duration is applied to specimen TRS8 and (b) its wave form. From the shape of the generated current pulses as shown in Fig. 29b, it is seen that rise time of the pulse is very fast compared to its decay time. It is also noted that the pulse rise time which is in the range of 10^{-9}sec remains the same for all the specimens, but decay time varies from specimen to specimen. The results for this type of uniform illumination have been summarised in Table 4.

The resulting complex current voltage characteristics can be explained on the basis of the charge formed in the CdS crystal when electric current flows through it. The negative charge increases with increase in the applied voltage to the specimen. This means that the cathode injects into the crystal more electrons than the number lost at the cathode. If the excessive negative charge of the crystal is partly or completely localised in the bound state (at traps) then these bound states may act as additional scattering centres. Thus, when the voltage is increased, the number of charge traps acting as effective scattering centres increases and the mobility of the free carriers decreases. This effect keeps the current in the sub-linear part of I-V characteristics. The

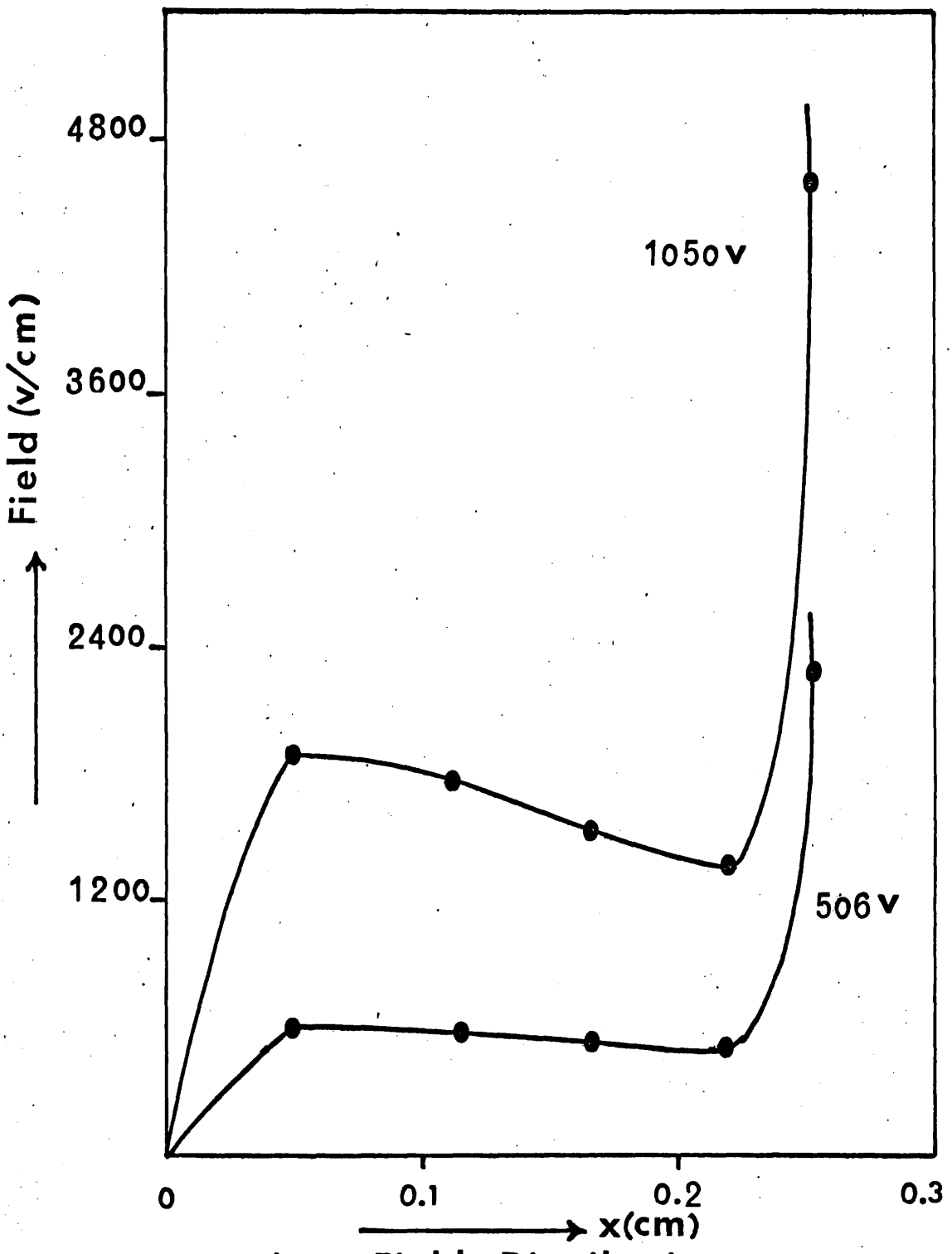

Fig. 30 Field Distribution
SPECIMEN TRS 8

subsequent rise of the current at a voltage of 800 volts as the current instability develops requires the assumption that the processes leading to multiplication of free carriers by the electric field takes place. Such processes may be the emptying of shallow traps by the electric field, or by the impact ionization of these traps by fast electrons.

The field distribution along the length of the sample for various applied voltages is shown in Fig. 30. The results indicated that at voltages (0-800 volts) corresponding to the sub-linear region of the I-V characteristics, the distribution of field along the length of the specimen was uniform, but at voltages (800-1400 volts) corresponding to the rapidly rising part of the characteristics, a high field region was formed near the positive end of the crystal. Such presence of non-uniformity of electric field can result in electric oscillations.

It is seen from volt-ampere characteristics (Fig. 28) that initially the current increases with increase in applied voltage. Only the application of a voltage difference from $I \infty V^2$ region of I-V characteristics to the illuminated crystal leads to a discontinuous increase in the current followed by a fall off (Fig. 29b). This indicates that the process of electron capture by traps plays a decisive role in the observed phenomenon. Obviously, with an increase of the applied voltage, the density of injected charge increases and the quasi-Fermi level at the cathode is displaced into the conduction band. This non-equilibrium charge is partially captured at traps which thereby change their charge state and become effective scattering centres for conduction electrons. Thus the appearance of relaxation type of oscillations in CdS crystal can be explained by occupation and emptying of trap states. Indeed, the occupation of states leads to a decrease of

the electrical conductivity of the material as a result of charge in the mobility of free carriers. One of the possible consequences of a decrease in the mobility could be the field liberation of electrons from traps. The increase in the resistance of the contact part of the crystal leads to a redistribution of the potential over the length of the sample. Thus the occupied traps are in an electric field of increased intensity which increases the probability of their being emptied. The avalanche-type liberation of electrons from the traps leads to an instantaneous increase in the current flowing through the sample after which occupation and a decrease of the mobility of free carriers recommences.

The relaxation oscillation of the current in CdS can exist as long as the traps are occupied by injected charge and their liberation as a result of field ionization. The conditions to observe such oscillations can be created by the choice of temperature, illumination and field intensity at which the crystal operates.

Table 4 Tabulation of results when the specimen is uniformly illuminated

Specimen Number	Applied Voltage (volts)	Oscillation Frequency (MHz)	Period of Oscillation (μsec.)	Amplitude of Oscillation (μA)
TRS_8	1000	7	0.14	20
TRS_9	1100	6	0.16	15
TRS_{10}	1000	6.3	0.15	20

5.3.3 Oscillations with the high resistivity near the anode end (Fig.7)

Continuous current oscillations in CdS crystal occur if there exists in the specimen a non-uniform distribution of electrons due either to non-uniform illumination or to non-uniformities in the crystal itself. Such instabilities were first observed by Smith[53] and McFee.[56] This non-ohmic behaviour was interpreted as the result of energy transfer from electrons to acoustic waves travelling in the direction of drifting carriers. Since then several investigators[41,67] have inferred from their measurements that the current oscillations were accompanied by non-uniform distribution of electric field within the crystal.

Using the non-uniform illumination shown in Fig. 7 the author has observed oscillations of large amplitude in CdS crystal and inferred from field measurements that nucleation of a high electric field domain takes place, where the resistivity of the specimen changes from low to high resistivity. It is also observed that the high field domain does not move, contrary to the case of dark conductive crystals. The specimens chosen for this experiment had the dimensions and conductivities under the illumination intensities given in Table 2. The experiments were mainly performed for the crystal with electric field perpendicular to c-axes of the specimens since it was difficult to observe continuous oscillations when the voltage was applied parallel to the c-axes. Only one sample TRS_4 gave oscillations when voltage was applied parallel to the c-axis.

The current voltage characteristics of the specimen TRS_1 are shown in Fig. 31 when it has been divided into a high resistivity region L_h and a low resistivity region L_l. It has been observed that for continuous oscillations the length of the low resistivity region L_l should always be greater than that of high resistivity region L_h. It

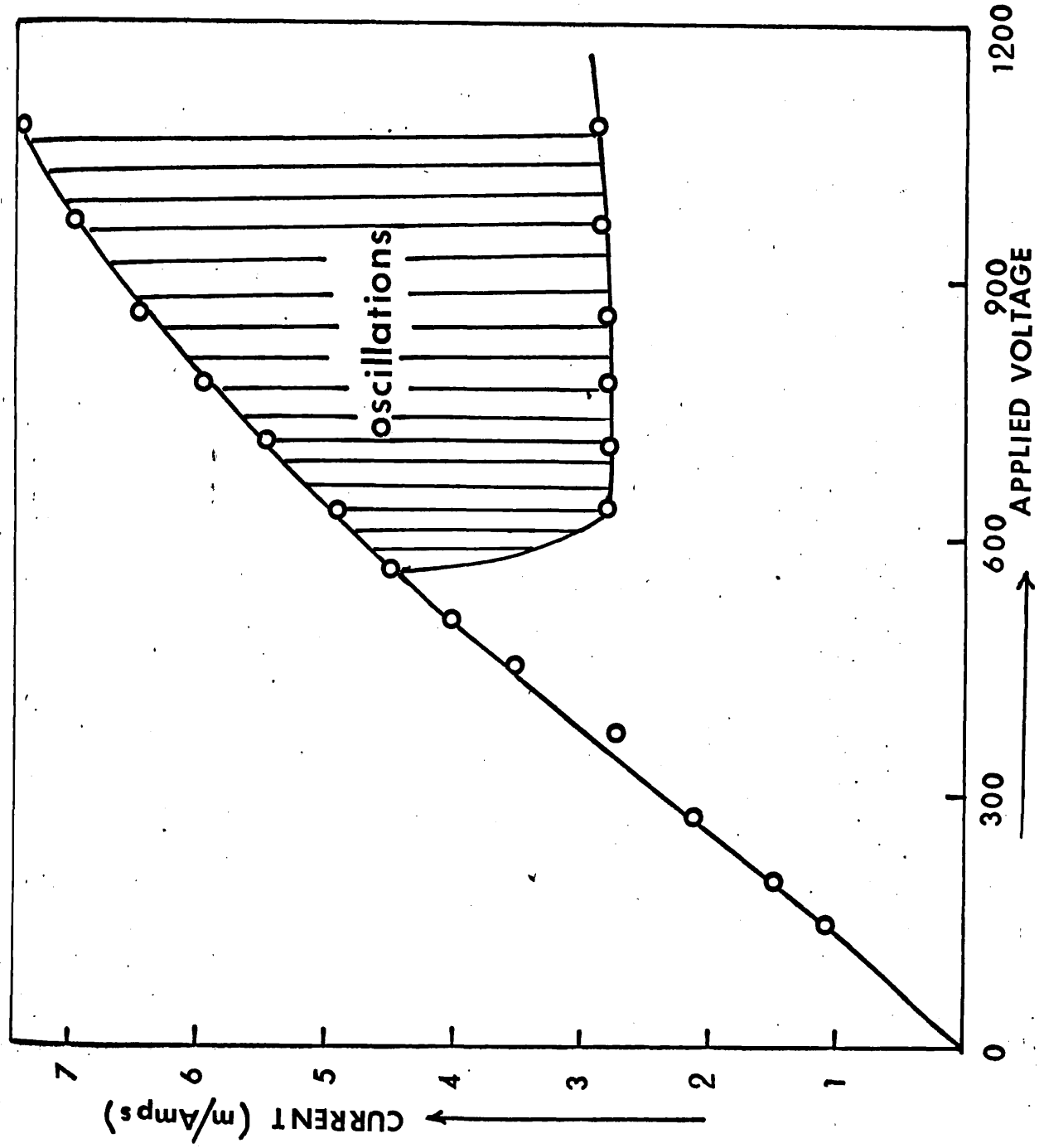

FIG. 31 I-V CHARACTERISTICS SPECIMEN TRS1.

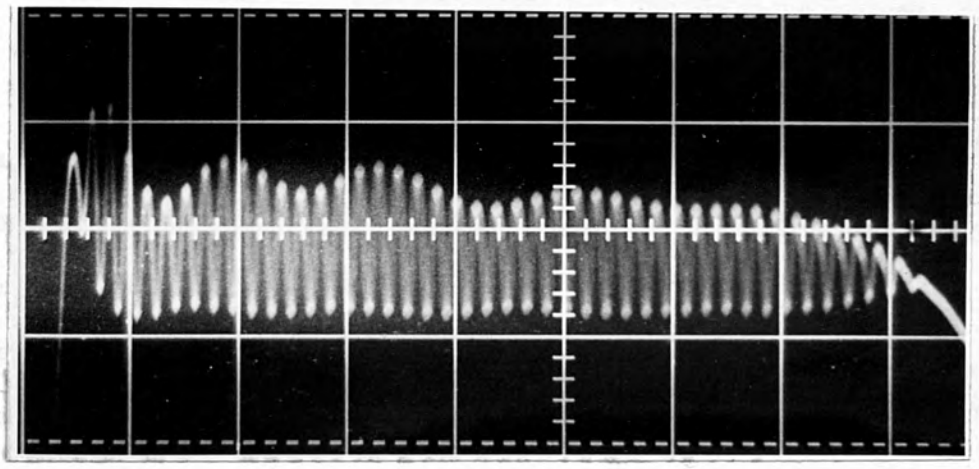

Fig.32 Continuous oscillating current recorded when CdS specimen TRS_1 was illuminated, but a strip of 0.48mm shielded the anode end.

Horizontal scale = 10μsec./div.
Vertical scale = 2 mA/div.

is seen from Fig. 31 that ohms law is obeyed at voltages up to 560V, but deviations occur above this value and the current oscillates. This oscillating current is apt to damp out at a voltage just greater than critical 560V, but continuous oscillations can be maintained by a further rise in voltage. If the applied voltage is reversed the current ceases to oscillate and increases ohmically with voltage. Frequency measurements reveal the kind of period associated with forward transit of acoustic waves between the electrodes.

Fig. 32 shows the wave form of the current oscillations at the voltage of 1000 volts. The amplitude of oscillation is 3mA with a frequency of 550KHz, corresponding to a period of oscillation τ = 1.8μsec. The results for this type of illumination distribution have been summarised in Table 5. It is seen that the period of oscillation for specimens with direction along the sample length is perpendicular to c-axis is approximately equal to the transit time τ_s of the shear waves through the sample.[56] However, in specimen TRS_4, with direction along sample length parallel to c-axis, it is seen that the period depends also on the L_h region. It is observed that the period of oscillation increases as the length of L_h region becomes larger.[36] The variation in the period of oscillation recorded is from 1.2μsec to 1.4μsec, by using different width of ceramic strips.

Figs.33(a,b) show the field distribution measured in specimens TRS_1 and TRS_4. It is seen that on raising the applied voltage above the threshold for current oscillation, a high electric field domain appears near the anode end of the sample. Also, comparison of these curves shows that on raising the applied voltage higher than required for oscillation increases the field in the high field region. It is also noted that voltages picked along the sample oscillate with current. In particular the electric field of the L_1 region oscillates about the

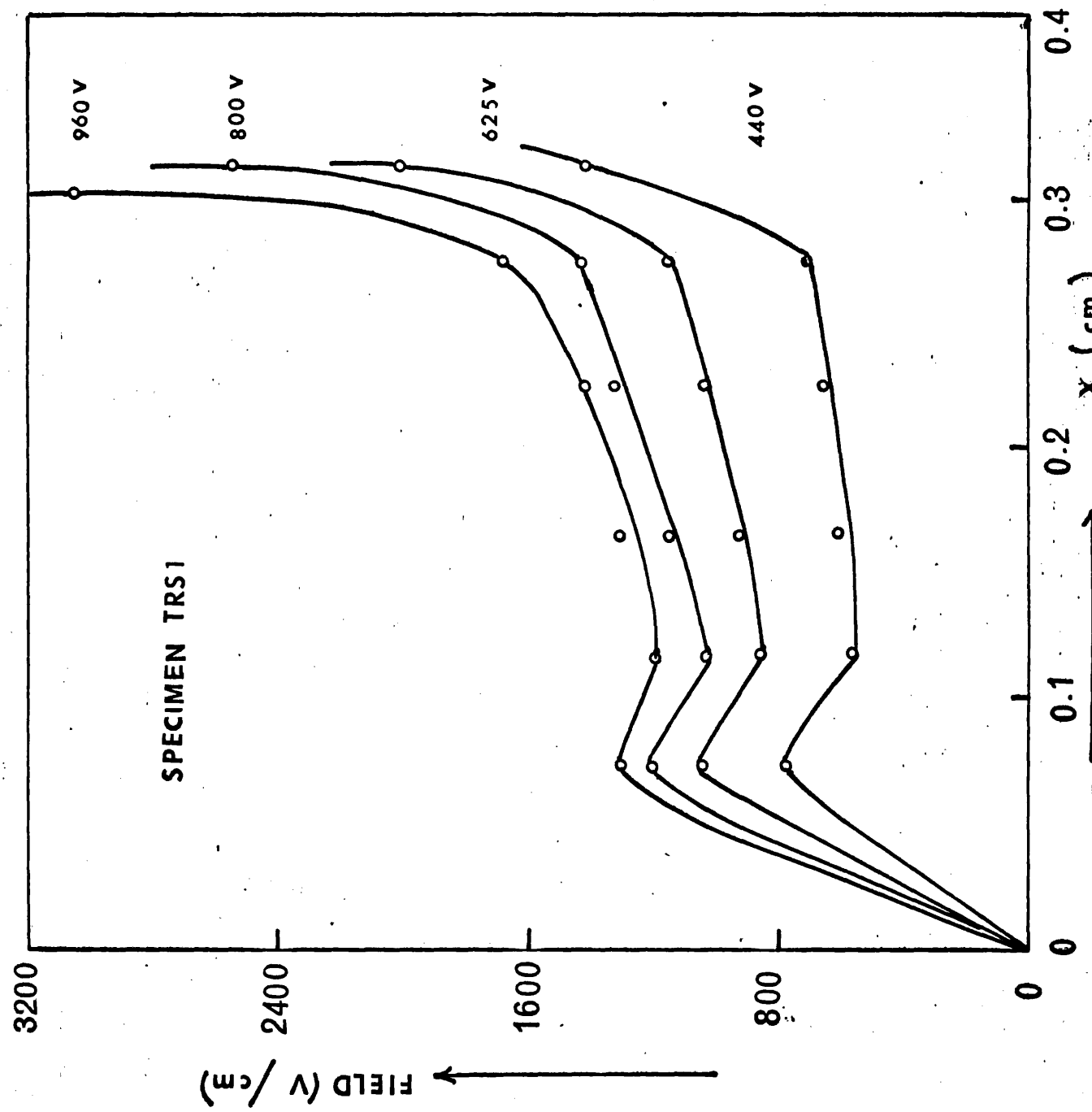

FIG.33a FIELD DISTRIBUTION

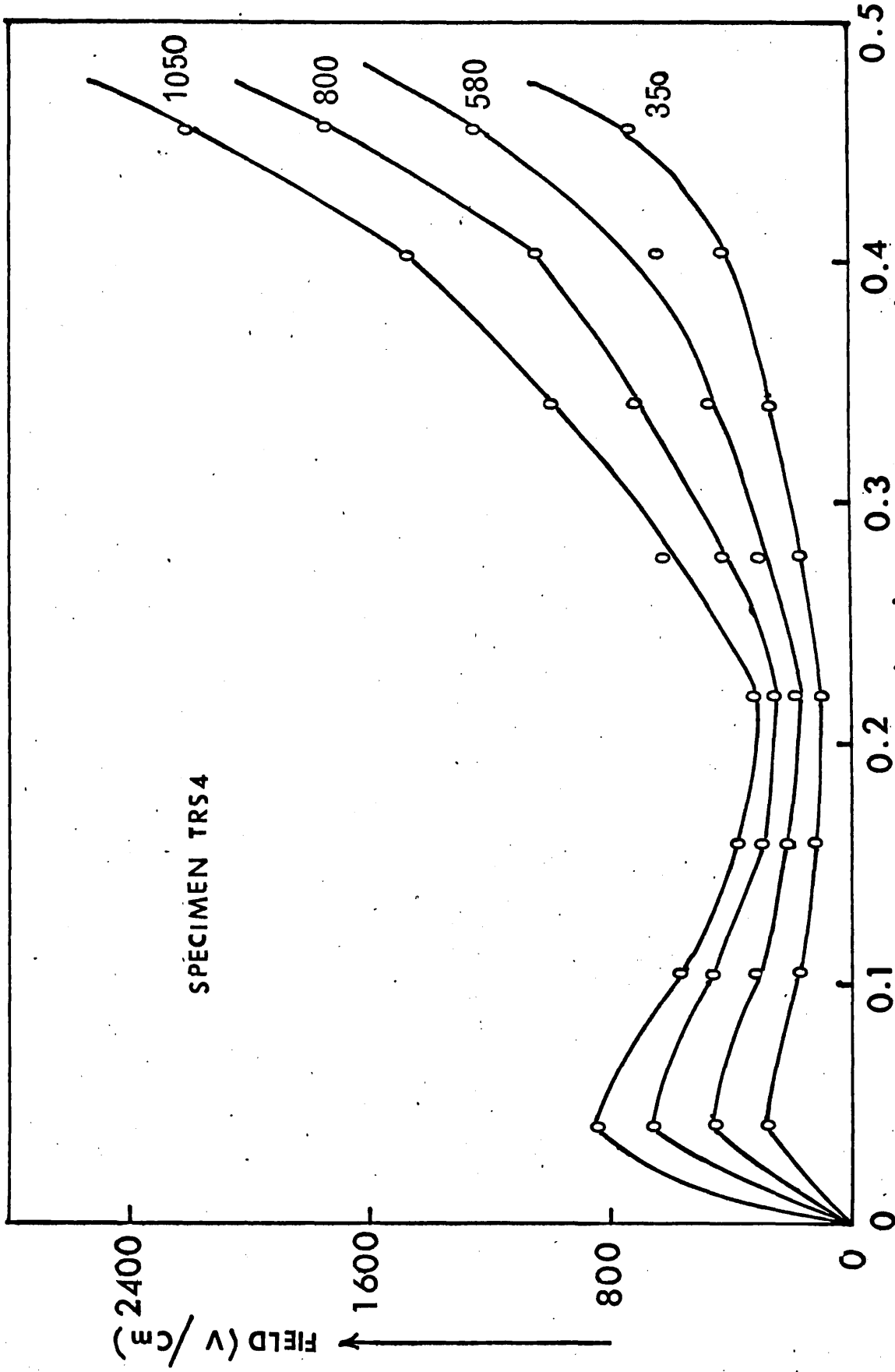

FIG. 33 b FIELD DISTRIBUTION

threshold field $Ec(\frac{V_s}{\mu_d})$ where V_s is the sound velocity in CdS and μ_d the electron drift mobility.

It is seen[58] that for the range of V when the field in L_l is below E_{th} but above E_{th} in L_h no marked saturation of current will occur. Considering L_l just a resistor put in series with L_h, then the possibility of current saturation is there at $J = \sigma_h E_{th}$ where σ_h is the conductivity of the high resistivity region L_h. The possible reason why the saturation in current does not occur can be explained with the aid of the conductivity distribution in the sample as shown in Fig. 34. There exists a region between L_l and L_h where the ohmic conductivity σ_z is between σ_h and σ_l. If, after equilibrium at a time t_s, the base of the stationary domain formed in L_h terminates at some point z_d in the region of varying conductivity , then the current through the specimen will be given by $J = \sigma_{(z_d)} E_{th}$. Since the amplification constants in the two regions are different because of different conductivities, the distribution of acoustic flux is different especially in L_h, but an explanation is attempted below. When the field in L_l is above E_{th}, continuous oscillations can occur. The period of oscillation depends on:

a) the length of the specimen L

b) the length of L_h

c) the conductivities σ_h and σ_l (higher conductivities give higher gain Appendix II, Fig.1A)

d) the acoustic reflectivity of the anode

e) the irregularities present in the sample.

So far very little is known about the magnitudes of the acoustic waves which may be generated by shock excitation at discontinuities etc., along the length of the specimen. Electrodes will generally be the

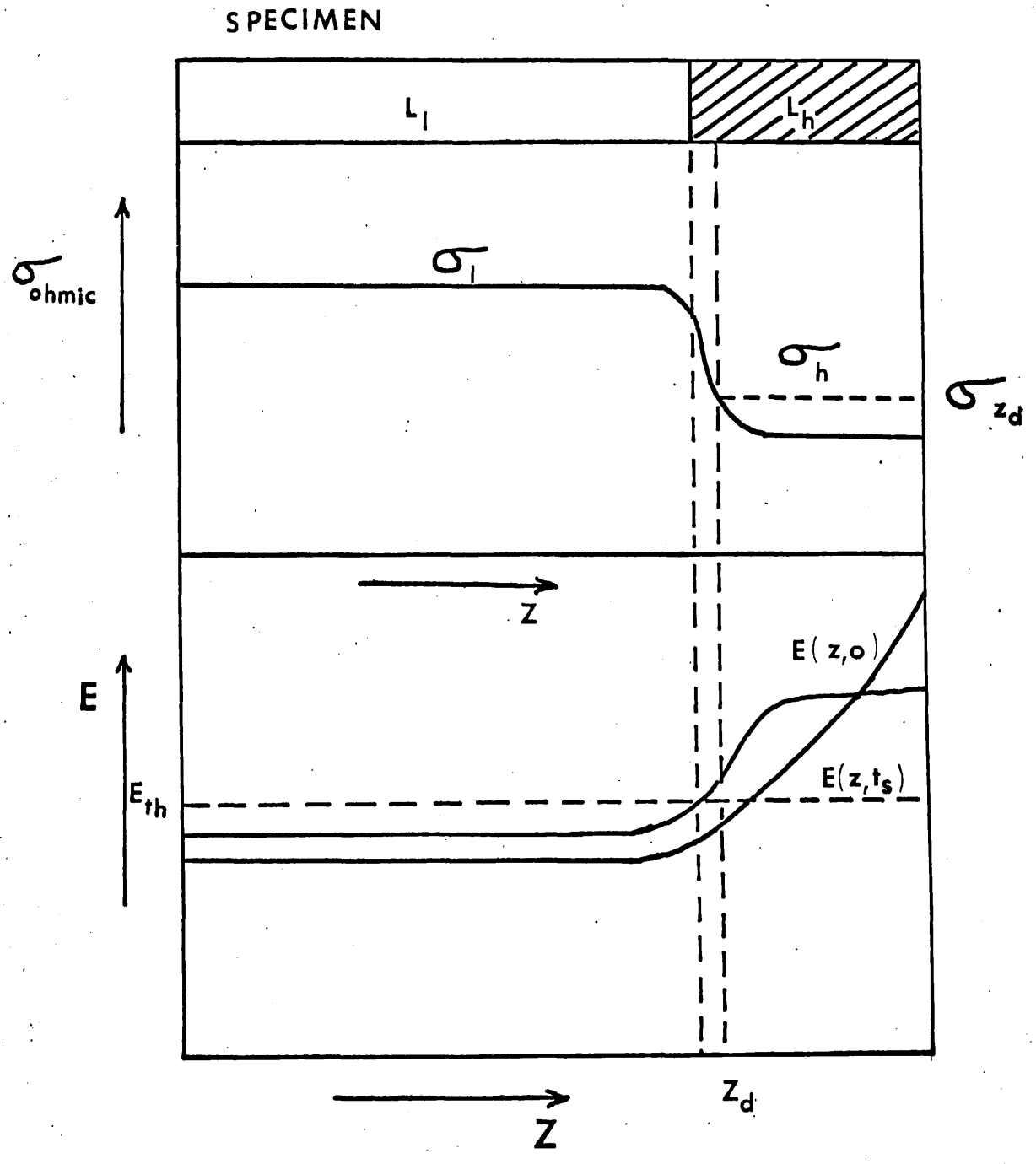

FIG. 34 CURRENT GIVEN BY σ_{z_d} E_{th}

regions of greatest discontinuity of the electric field. It is, therefore, assumed that domains are generated by shock excitation at the cathode only.

So, at the onset of the applied voltage pulse a domain forms at the cathode and is amplified as it travels through the low resistivity region. The thermal acoustic flux which is always present is amplified simultaneously at all points along the specimen. After amplification in the L_l region, a large amount of flux flows into the L_h region and results in a decrease of field in L_l and of current flowing in specimen. As the domain remains in L_l, the field there will not fall below E_{th}. But when the domain in L_h is further amplified, then the field in L_l may fall as low as $\frac{\sigma_h}{\sigma_l} E_{th}$. The field distribution is then bound to change in the specimen. The field E_l in the L_l region decreases while the field E_h in L_h region increases. When E_l decreases below threshold field E_{th}, the L_l region changes into an attenuator of ultrasonic flux. In[58] this situation, the flux is attenuated during travel in the L_l region and damped waves flow into the L_h region. But if the amplification in L_h is small, then the field in L_l will not fall far below E_{th}. The extinction of the domain at the anode will then cause the field in L_l to rise above E_{th} and a new domain to form at the cathode. The same process is repeated and continuous oscillation with a period of $\frac{L}{V_s}$ are obtained. Such oscillations were observed in specimens TRS_1-TRS_4. When the domain is in L_h, there is no amplifying condition in L_l as in this case the thermal acoustic flux cannot maintain a large stationary domain. The only amplified thermal flux present will be in L_h and this can maintain a small stationary domain near the anode as there is little amplification in L_h. This small stationary domain may be sufficient to cause the field in L_l to be perpetually below E_{th}, if the applied voltage is too low and oscillations will die out.

Table 5 Tabulation of results for specimens when anode end is shaded

Specimen Number	Applied Voltage (v) Volts	Length of low resistivity region (L_l) mm	Length of high resistivity region (L_h) mm	Oscillation frequency (f) KHz.	Period of oscillation (μ) sec.	Sonic transit time (T_s) μsec.	Amplitude mA
TRS_1	1100	2.8	0.48	550	1.8	1.8	3
TRS_2	1100	1.82	0.5	769	1.3	1.3	2
TRS_3	1000	1.81	0.5	833	1.2	1.3	2
TRS_4	1100	3.38	1.2	800	1.20	1.03	3
TRS_4	1100	2.48	2.1	760	1.3	1.03	2.5
TRS_4	1100	2.3	2.28	670	1.4	1.03	1.8

A large stationary domain can be maintained near the anode if high amplifying conditions are maintained in L_h. Being a larger domain, this causes a greater decrease of field in L_l. If the field in L_l can only rise slightly above E_{th}, when the first travelling domain from the cathode is extinguished at the anode, then the second domain will not reach the size attained by the first domain. Second, third and fourth domains will be smaller and smaller and oscillation due to these will eventually die out. The high amplifying conditions in L_h will enable oscillation of another kind to occur and it is these types of oscillation which cause the oscillation due to shock excitation to disappear.

These oscillations in current are maintained by thermal acoustic flux. L_l behaves as an input of thermal flux to the amplifier L_h. Then the amount of flux from L_l going into L_h rises when the field there is above E_{th}. However, the more amplification of this flux in L_h causes a fall of field in L_l and the input is decreased. It is when the domain travelling in L_h and on its extinction, that the field again rises above E_{th} in L_l. In this mechanism oscillation with a period of $\frac{L_h}{V_s}$ will then be observed.

While discussing the mechanism, it has been assumed that no reflection of acoustic flux occurs at the anode end of the specimen. The rise of field in other parts of the sample is due to the domain dissipated at the anode. The reflected part of the domain mainly reduces the total amount of electric field available to the rest of the specimen. But if there is much reflection the part of the domain which is extinguished may not be sufficient for the field in L_l to rise to E_{th}. The reflected part of the domain will, however, be attenuated rapidly and enable the field in L_l to rise above E_{th}. The period of oscillation will then by given by $\frac{L_h + r}{V_s}$, where r is the distance travelled by the reflected domain before the field in L_l reaches E_{th}.

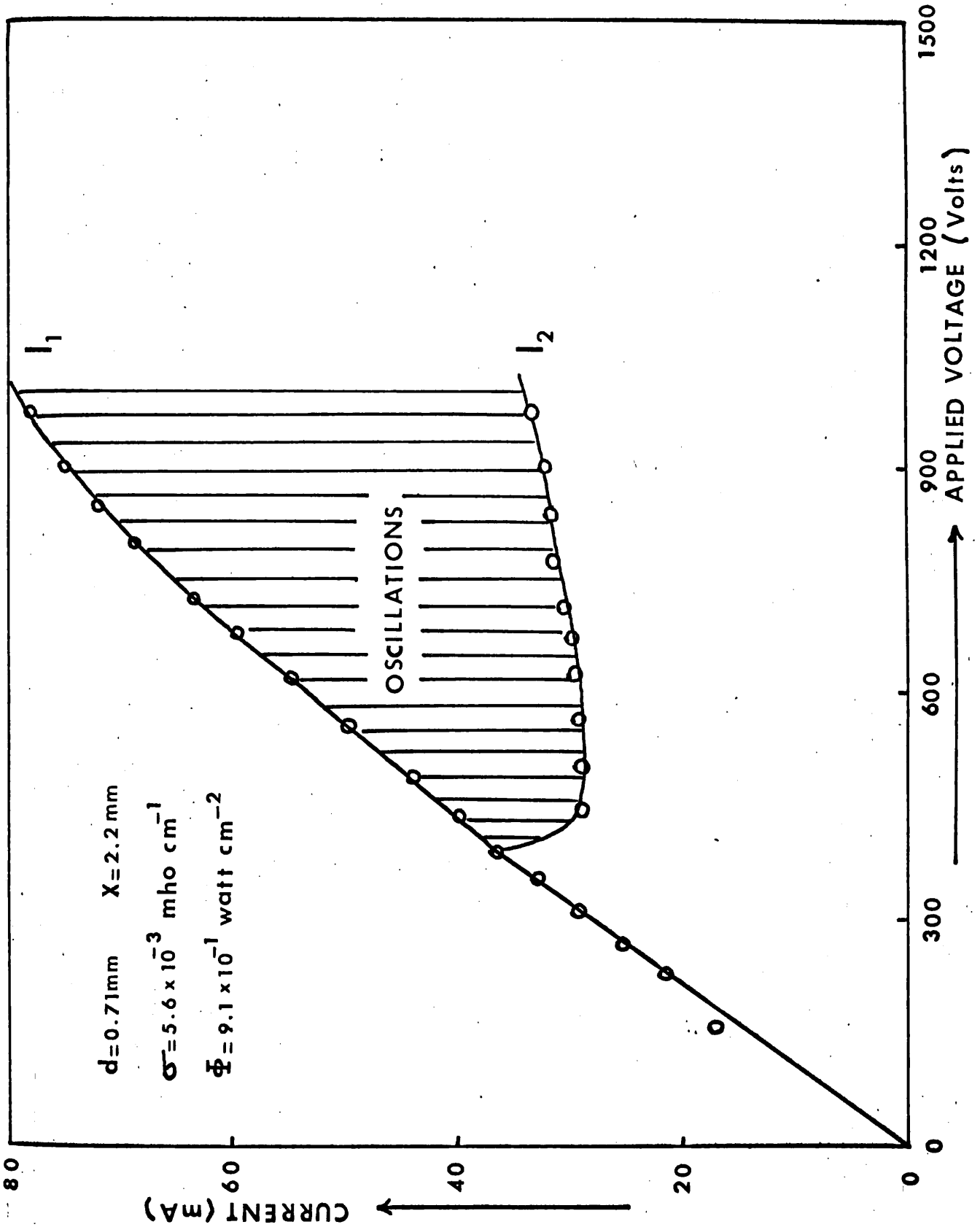

FIG. 35 I-V CHARACTERISTICS

5.3.4 Oscillations by obscuring a strip of the specimen by ceramic strip (Fig. 22)

Current oscillations in non-uniformly illuminated CdS when the mean drift velocity of the carriers exceeds the velocity of sound have been reported by several authors.[32,42] The phenomenon is related to ultrasonic amplification. This work demonstrates that different modes of oscillation can exist and show different local field variation down the specimen.

Specimens of semi-insulating CdS orientated with the c-axis perpendicular and parallel to the current flow were uniformly illuminated except for a narrow transverse strip perpendicular to its length as shown in Fig. 22. Work on CdS specimen when high voltage pulses were applied perpendicular to the c-axis of the crystal has been presented before, but the current oscillations obtained by using light strips in specimen having c-axis parallel to the length of the crystal have not been reported. Specimens chosen for this experiment had the dimensions, conductivities and illumination intensities given in Table 2. The frequency of oscillation depended on the position of the dark strip. Measurements of oscillation frequency, along with the field distribution, are made at different positions of the light strip on the specimen. Frequency measurements reveal the existence of two periods given by:

$$\tau = \frac{x + d}{V_s} \quad \text{or} \quad \frac{2(x + d)}{V_s} \quad \text{approximately}$$

where τ is the period of oscillation, x the distance of the light strip from the anode end of the specimen, d the width of the ceramic strip and V_s the sound velocity.

Current voltage characteristics under oscillatory conditions are shown in Fig. 35. Above the oscillation threshold voltage of 560 volts, the current oscillates periodically between the ohmic value I_1 and a lower value I_2.

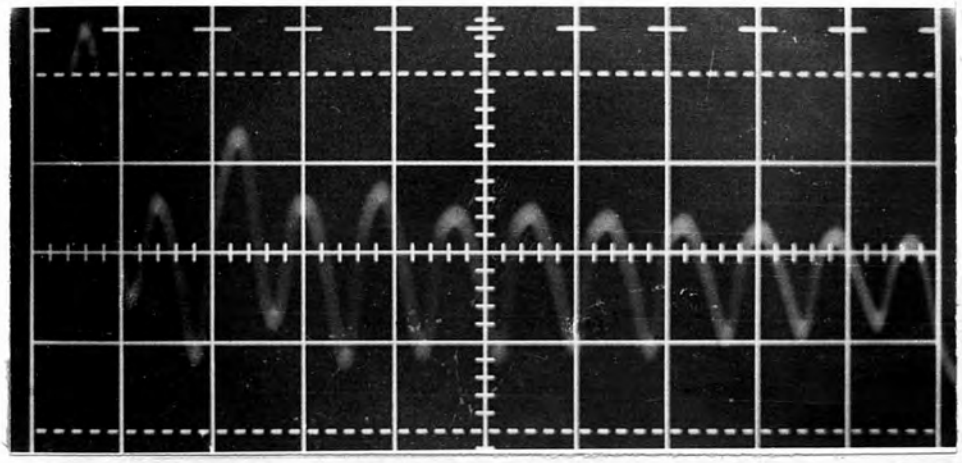

(a) x = 0mm ⟵ 4 μsec. ⟶

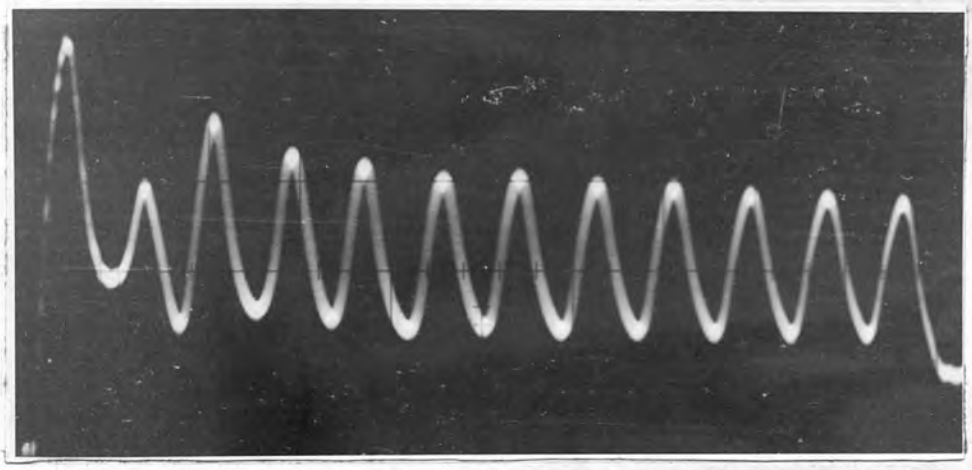

10 mA

(b) x = 0.2mm ⟵ 4.3 μsec. ⟶

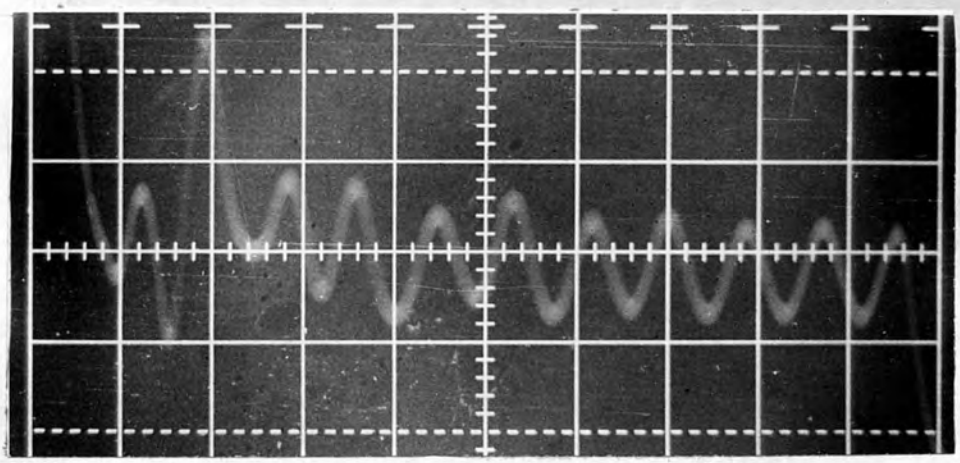

(c) x = 0.6mm ⟵ 4.45 μsec. ⟶

FIG.36 OSCILLATORY MODES IN TRS7

$\Phi = 4.2\ 10^{-3}$ watt cm^{-2} V = 800V d = 0.5mm

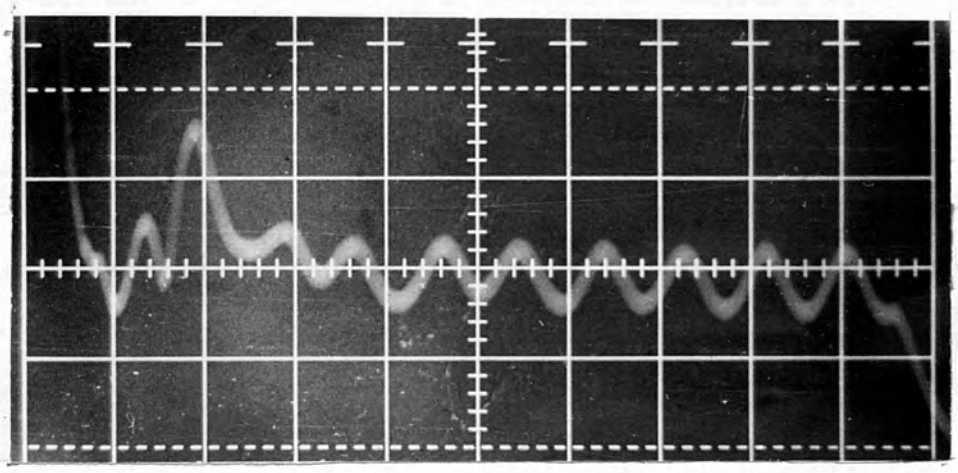

(d)=1.0mm ⟵ 6 μ sec. ⟶

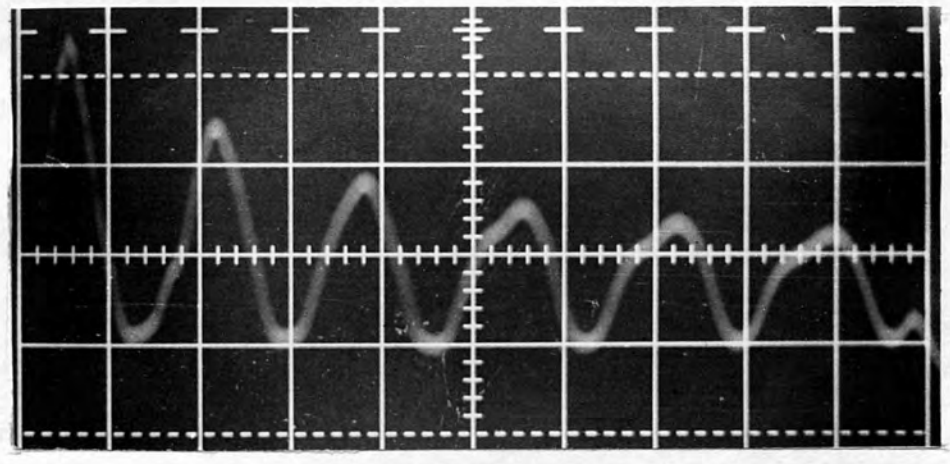

(e)=1.2mm ⟵ 4.8μsec. ⟶

FIG. 36

The oscillation wave forms of the current are shown in Fig. 36 for different positions of the ceramic strip in specimen TRS_7 and are seen to be between 800 and 1200 KHz. Initially the current exhibits the ohmic value, but oscillations appear after a few microseconds.

The results obtained with different specimens are summarised below:

Specimen TRS_5

For V = 1000 volts, d = 0.71mm and $\Phi = 9.1 \times 10^{-1}$ watt cm^{-2}, this specimen has given results shown in Fig. 37. The period of oscillation varies as $\tau = \frac{x + d}{v_s}$ approximately. For x = 0 to x = 2mm, no oscillations are observed. The oscillations obtained at x = 2.1mm are irregular in amplitude. It is observed that when the distance of the ceramic strip from the anode end increases, the oscillation frequency decreases as shown in Fig. 37. As the frequency decreases, the amplitude of oscillation increases all along the voltage pulse. At x = 2.8mm the amplitude of oscillation is 40mA. Oscillations disappeared at x = 3mm from the anode.

Reversal of the polarity of the specimen resulted in an increased frequency of:

$$f = 1500 KHz \quad \text{at} \quad x = 2.2mm$$

Using a ceramic strip of width 1.0mm, specimen TRS_5 has given results shown in Fig. 38. Again no oscillations are observed from x = 0 to x = 2mm. It is rather interesting to look at the current oscillations obtained between x = 4 to x = 6mm. The oscillations at these frequencies are of regular amplitude 40mA as shown in Fig. 39. These appear to be similar to those found in semi-conducting CdS[63] material but a closer examination showed that the sharp peaks of these oscillations were at the minimum current, whereas they are at maximum current in semi-conducting CdS. These oscillations resemble more or

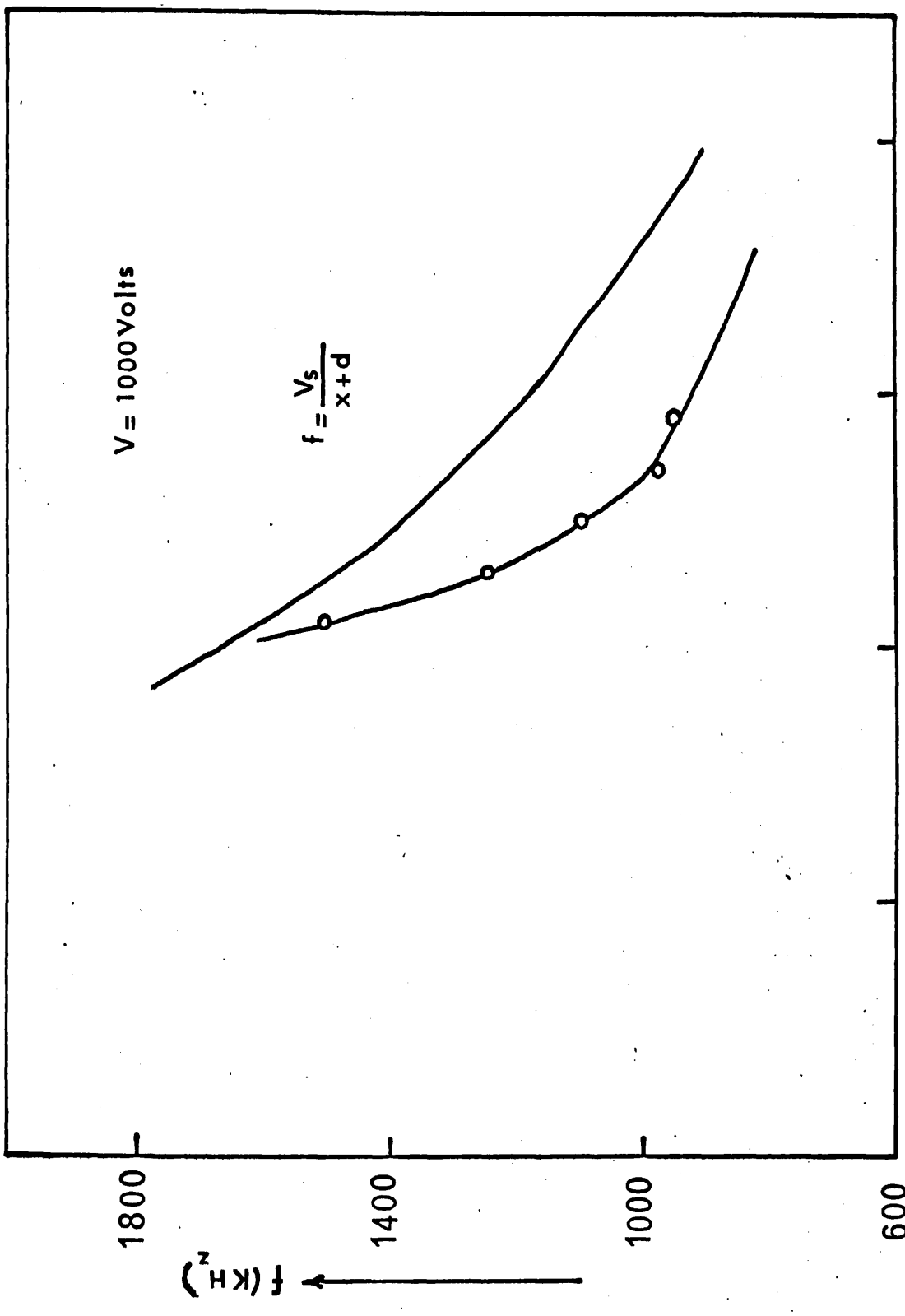
V = 1000 Volts
$f = \frac{V_s}{x+d}$
f (KHz)
1800
1400
1000
600
0
1
2
3
4
X (mm)
d=0.71mm
$\Phi = 9.1 \times 10^{-4}$ Watt Cm^{-2}
SPECIMEN IRS5

FIG. 37

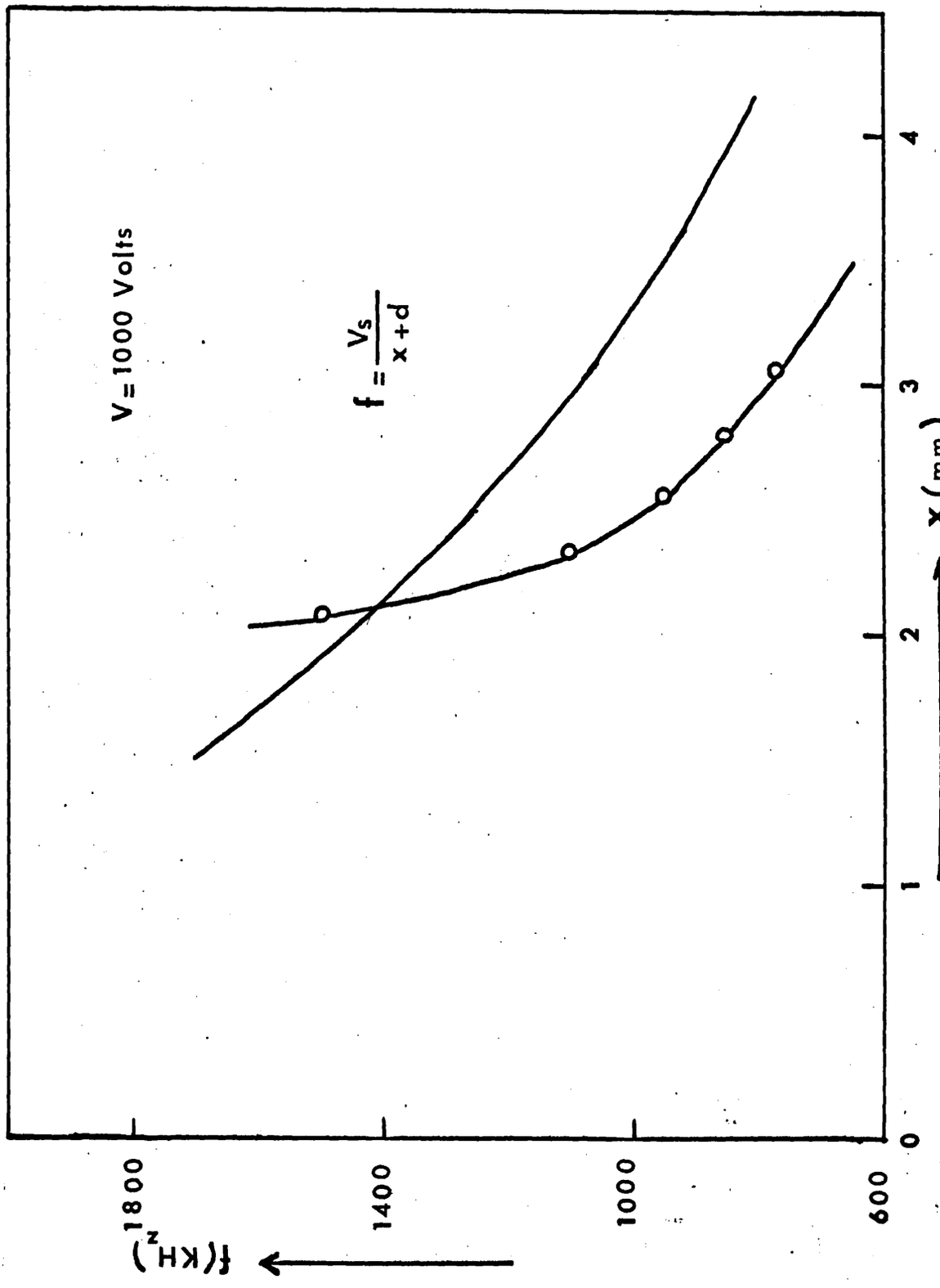
V = 1000 Volts
$f = \frac{V_s}{x+d}$
f (KHz)
1800
1400
1000
600
0
1
2
3
4
X (mm)
d = 1mm Φ = 9.1 x 10⁻¹ Watt cm⁻²
SPECIMEN TRS5

FIG. 38

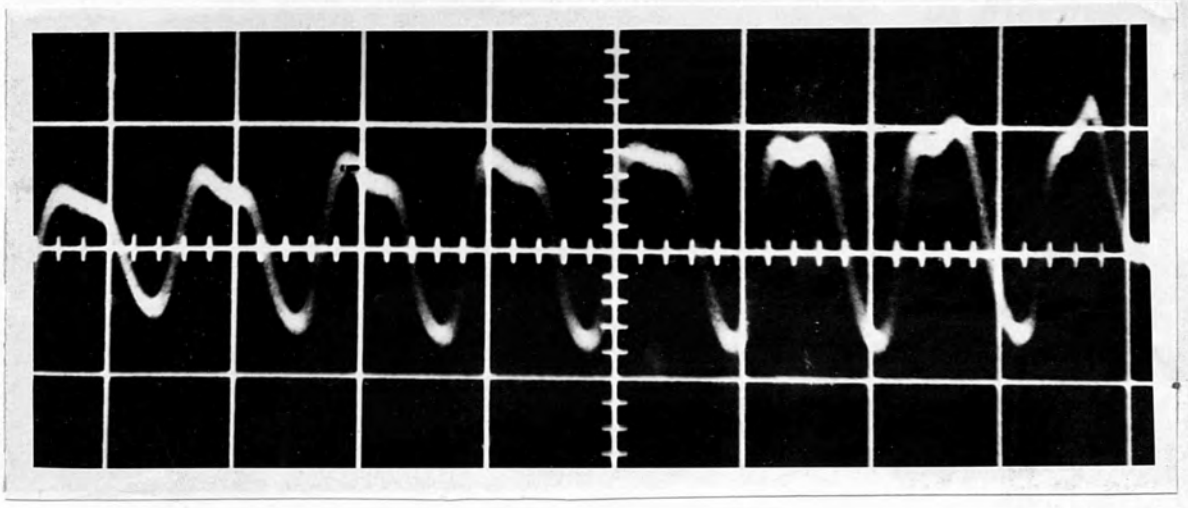

Fig.39 Current oscillations in TRS_5 when a strip of 1mm wide was position at 4mm from the anode end of uniformly illuminated specimen.

Horizontal scale = 1 μsec/div.
Vertical scale = 50 mA/div.

less those obtained by Bauduin and Buchy,[46] with the specimen narrowed at the negative end.

Reversing the polarity of the specimen and using d = 1mm, gave the following results:

$$f = 1100 \text{ KHz} \quad \text{at} \quad x = 2.0\text{mm}.$$

Using a narrow, ceramic strip of width d = 0.58mm and V = 1000 volts: $\Phi = 9.1 \times 10^{-1}$ watt cm^{-2} a similar graph is obtained as shown in Fig. 40. As this ceramic strip is moved from anode to the cathode end of the specimen, a range of frequencies is observed entirely different from the set of values obtained by using other widths of strip mentioned before.

Once again, for x = 0 to x = 2.1mm, no oscillations are observed. But on slightly increasing the distance of the strip from the anode end, the specimen breaks into oscillation. The oscillations observed at x = 2.2mm of frequency 1500 KHz are rather irregular in amplitude 12mA. But when the frequency decreases with distance from the anode end, the amplitude starts increasing. The oscillations at f = 1380 KHz are of regular amplitude of 33mA. When the ceramic strip crosses this point i.e. x = 2.8mm on the specimen, the amplitude of oscillations start falling. The amplitude of oscillation at x = 3.2mm for f = 1250 KH is 20mA.

At x = 3.4mm, f = 1050 KHz the distortion in oscillation starts taking place and this form persists until the ceramic strip reaches the point where minimum frequency of 870 KHz is observed at x = 3.6mm. The amplitude of oscillation at this frequency is fairly small 10mA. Nothing is observed after x = 3.6mm on the specimen.

Reversing the polarity of the specimen and using d = 0.58mm, the following results are obtained.

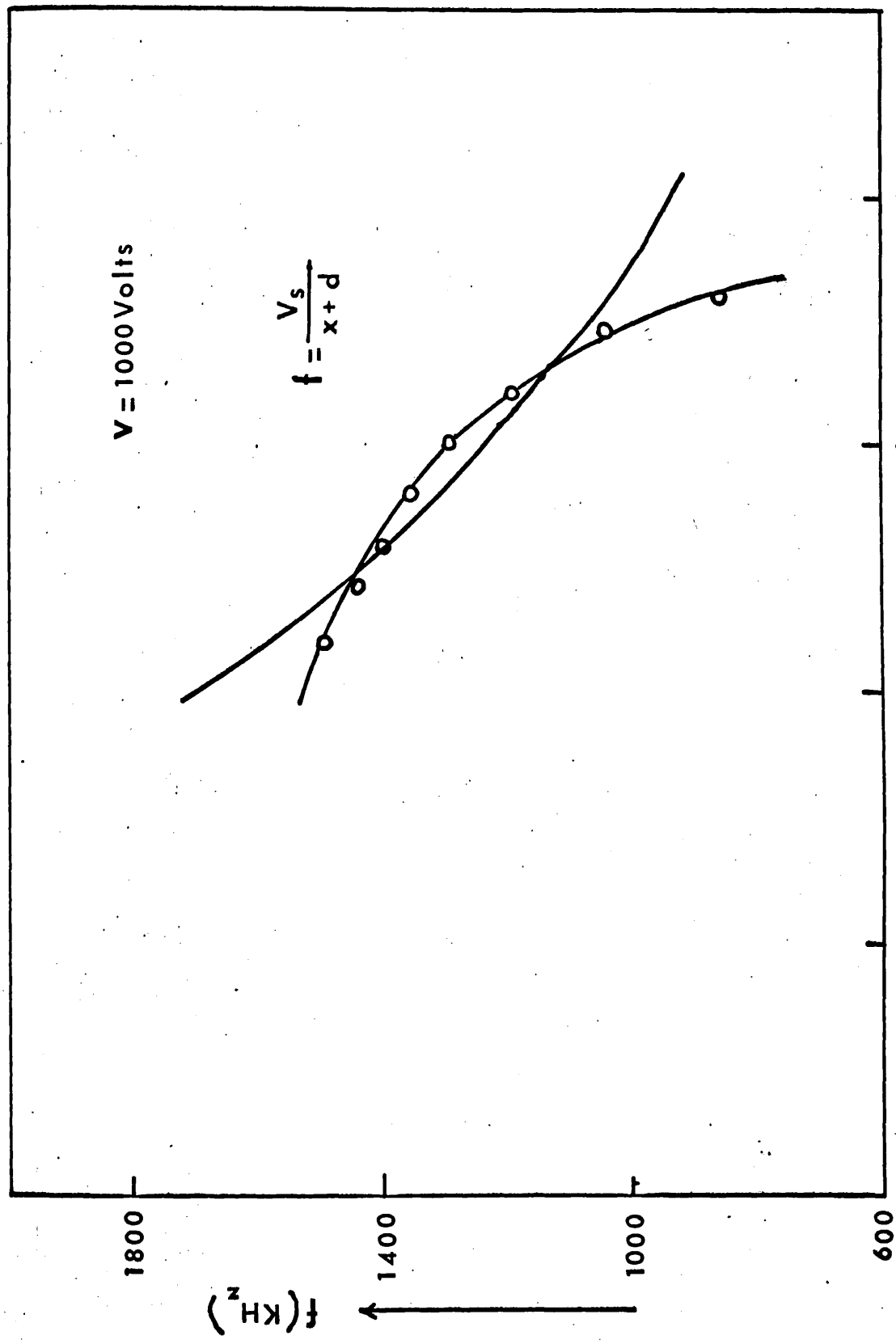
V = 1000 Volts
$f = \frac{V_s}{x+d}$
f (KHz)
1800
1400
1000
600
1
2
3
4
X (mm)
d = 0.58mm Φ = 9.1×10^{-1} Watt cm^{-2}
SPECIMEN TRS 5

FIG. 40

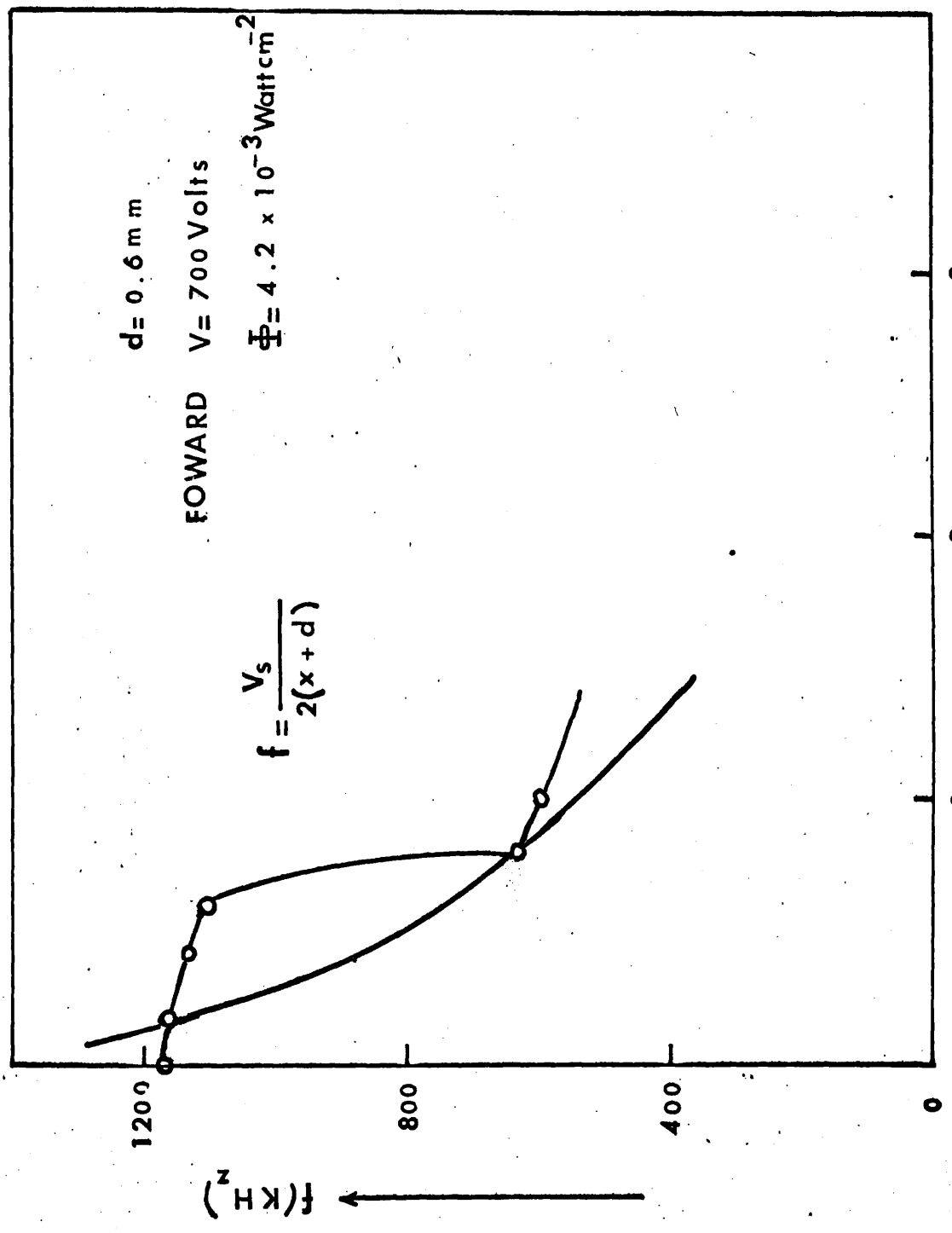

FIG.41 SPECIMEN TRS 7

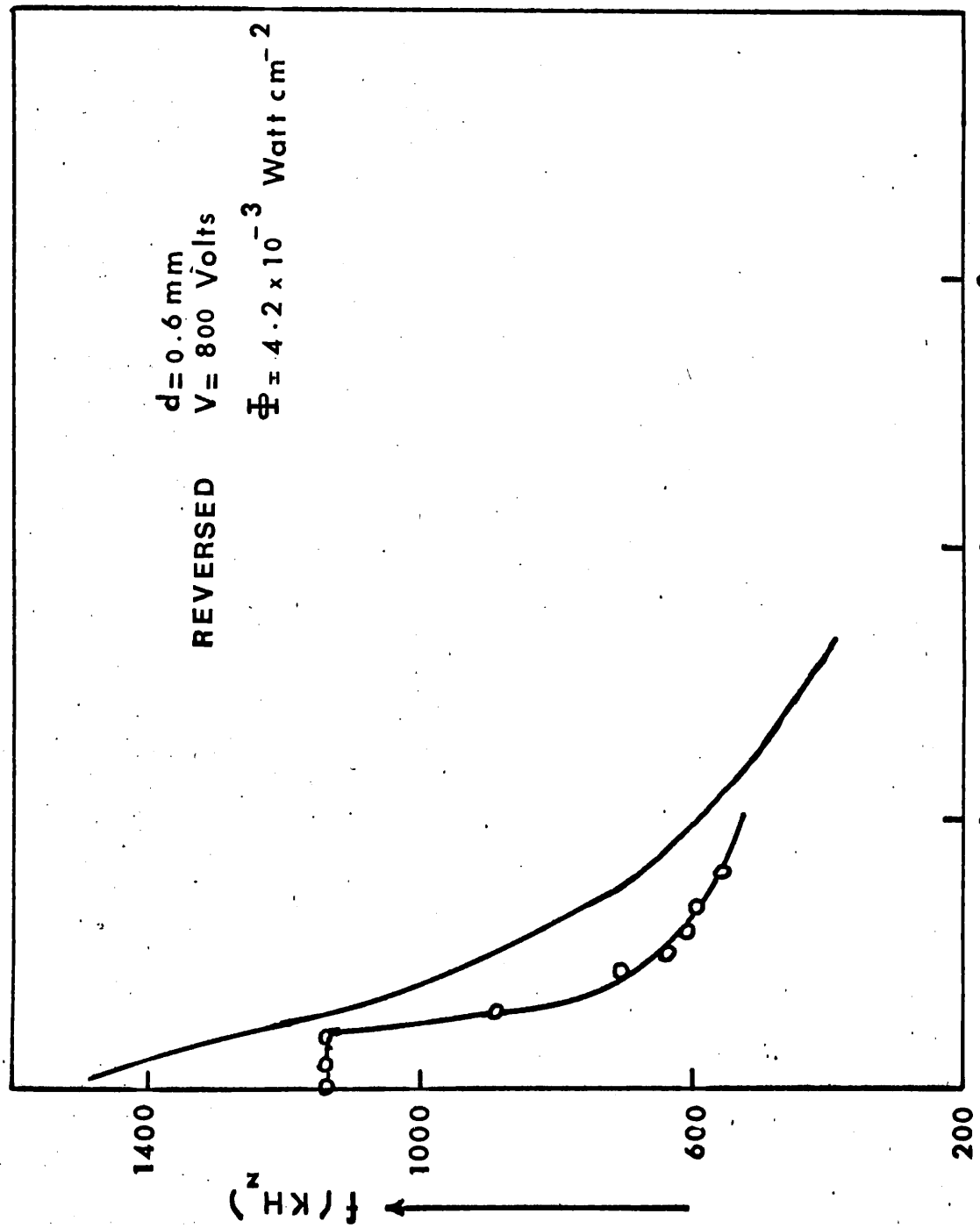
d = 0.6 mm
V = 800 Volts
Φ = 4·2 x 10⁻³ Watt cm⁻²
REVERSED
f (KHz)
1400
1000
600
200
1
2
3
X (mm)
SPECIMEN TRS 7

FIG. 42

f = 1450 KHz at x = 2.6mm

Specimen TRS_6

In this specimen no gradual fall in the oscillation frequency is observed by moving the strip from anode to cathode end, whereas ceramic strips of different widths are used for inducing different modes of oscillation. The results have been summarised in Table 6. The period of oscillation varies as $\tau = \frac{x + d}{V_s}$. It is noted from results that the frequency of oscillation not only depends on the distance of the strip from anode end of the specimen but also on the length of the shaded area, i.e. strip width. As the width of the strip increases, the frequency of oscillation decreases.

Reversing the polarity of the specimen, and using d = 0.4mm, 1.78mm; 1.4mm, the specimen gave no results.

Specimen TRS_7

In Fig. 41 the relationship between f and x for V = 700 volts; d = 0.6mm and $\Phi = 4.2 \times 10^{-3}$ watt cm^{-2} is shown. No oscillations are observed beyond 1mm from the anode end of the specimen. As the frequency of oscillation decreases, their amplitude decreases as well. At a higher frequency, i.e. x = 0, the amplitude at 1200 KHz is 3mA. It decreases to 2mA until the strip reaches x = 0.6mm. After crossing this point on the specimen the amplitude starts building up again and becomes a maximum at x = 1mm. The amplitude at a frequency of 600 KHz is 7mA.

Reversing the polarity of the specimen, the results obtained are shown in Fig. 42. Here no oscillations are obtained beyond x = 0.8mm from the anode end of the specimen. The amplitude at the frequencies mentioned in Fig. 42 are consistent, i.e. 3mA.

The results shown in Fig. 43 are for the same specimen, when strip width 0.5mm is used. No oscillations are observed beyond x = 1.2mm.

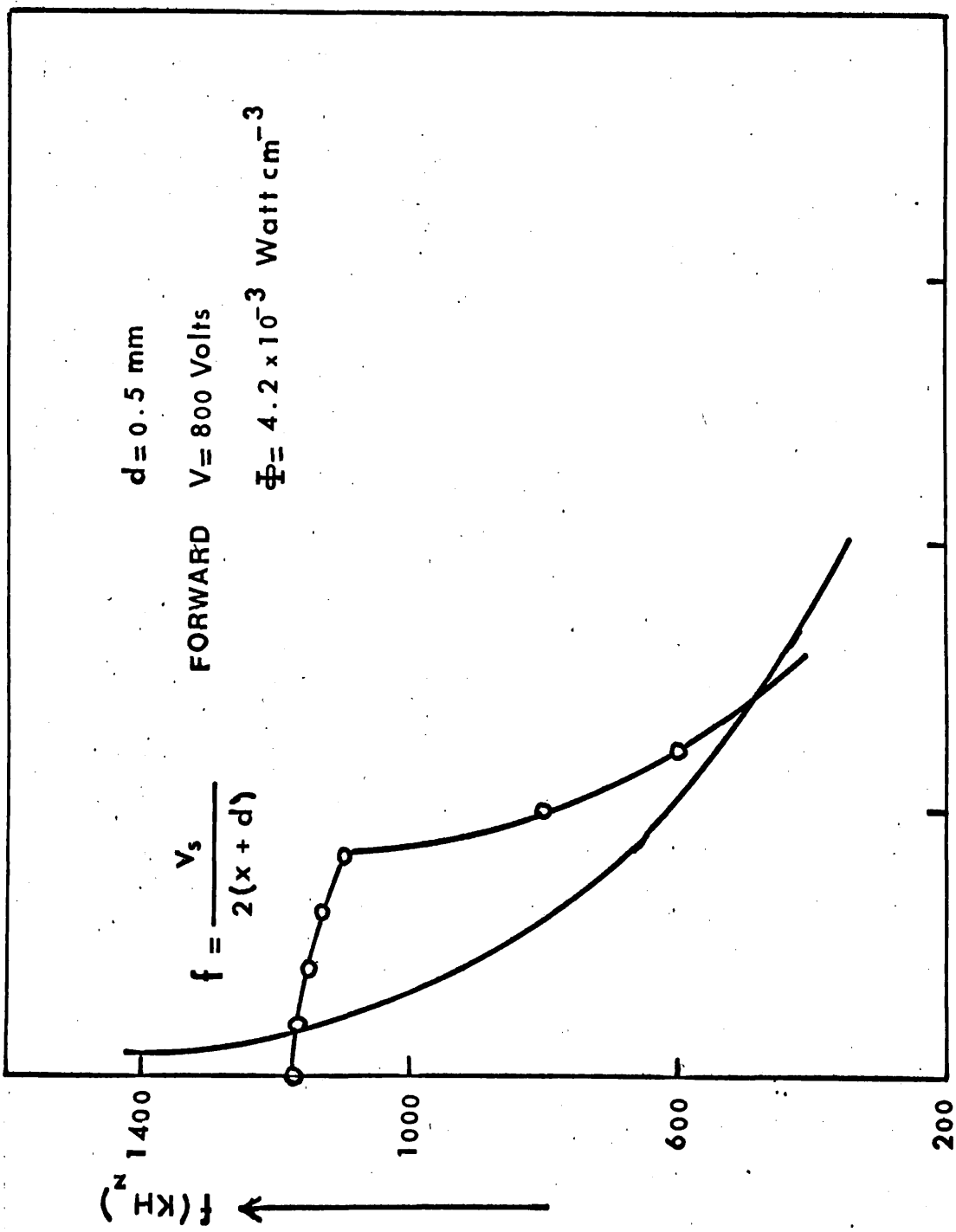

FIG. 43 SPECIMEN TRS 7

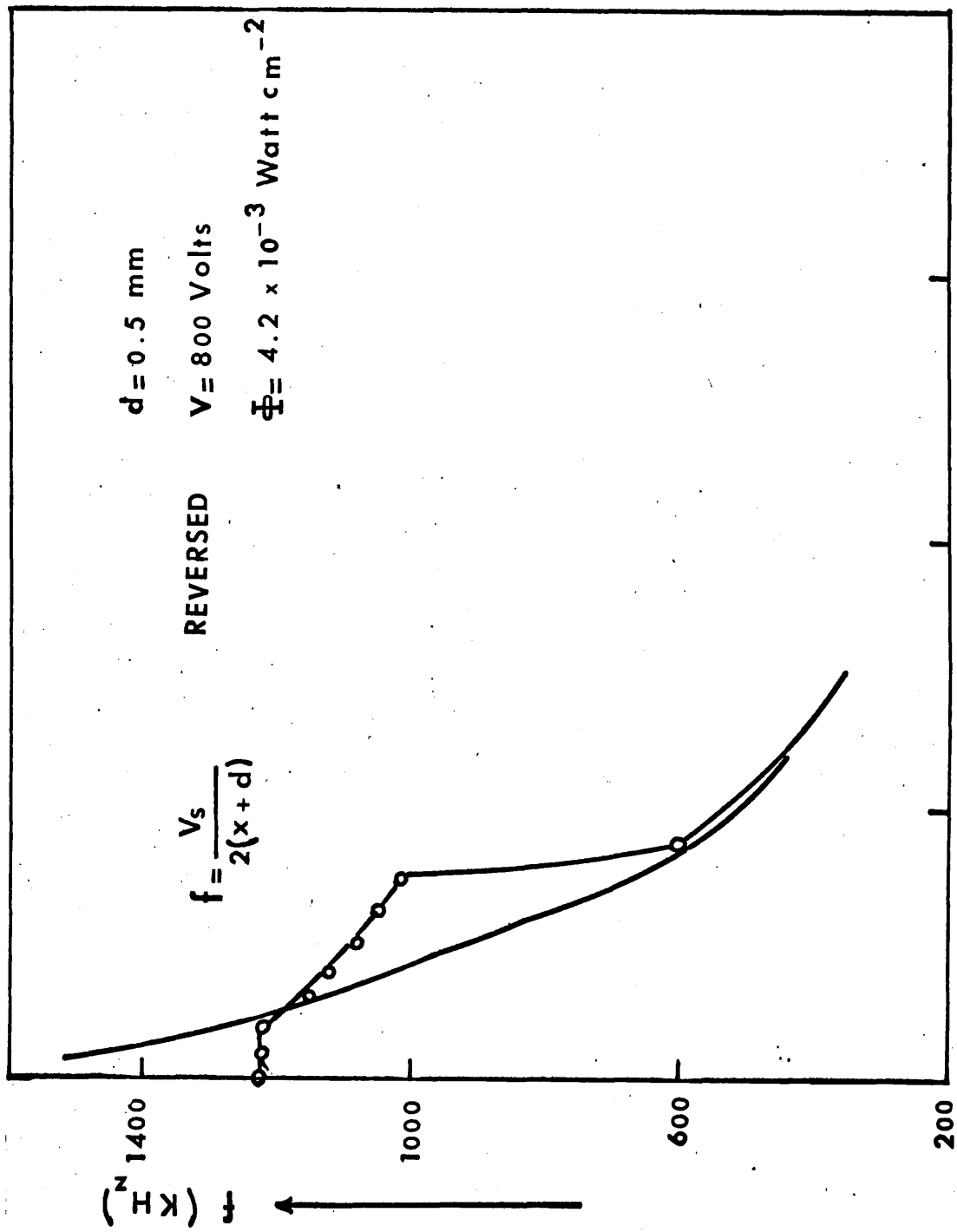
d = 0.5 mm
V = 800 Volts
Φ = 4.2 × 10⁻³ Watt cm⁻²
REVERSED
f = Vs / 2(x + d)
f (KHz)
1400
1000
600
200
1
2
3
X (mm)
SPECIMEN TRS 7

FIG. 44

The amplitude of oscillations observed are regular value, i.e. 5mA at all the frequencies observed.

Reversing the polarity of the specimen has given the results shown in Fig. 44. No oscillations are observed beyond x = 0.7mm from the anode end of the specimen. The amplitude of oscillation at frequencies observed was 5mA. Fig. 45 illustrates the distribution of field along the length of the specimen TRS_5. The current in the specimen is found to oscillate at an applied voltage of 560V (Fig. 35). Below 560V the current voltage characteristics are quite linear. Therefore, the plot in Fig. 45 corresponding to 350V applied represents the field distribution in the sample under ohmic conditions.

The other curves corresponding to V = 560, V = 720 and V = 900 volts give the field distribution obtained under oscillating conditions. In the current oscillating state (say at V = 900) a narrow high electric field domain appears near the position of the high resistivity region. This high field domain appears to form at the anode end of the high resistivity region. It is also observed that the position of high field domain can be controlled by varying the position of the light strip along the length of the specimen.

The field distribution at different times is shown in Figs. 46(a,b) for different positions of light strip on the same specimen. The initial state of successive cycles are not exactly equal to those at the instant of drift field application, but the electric field is concentrated near the positive edge of the high resistivity region. The domain seems to build up at the region of electric field concentration through amplification of the acoustic flux, but does not move out of this region. Domain propagation is triggered by shock excited acoustic waves. This acoustic flux is generated at regions of discontinuity or high field gradients by a time varying electric field.

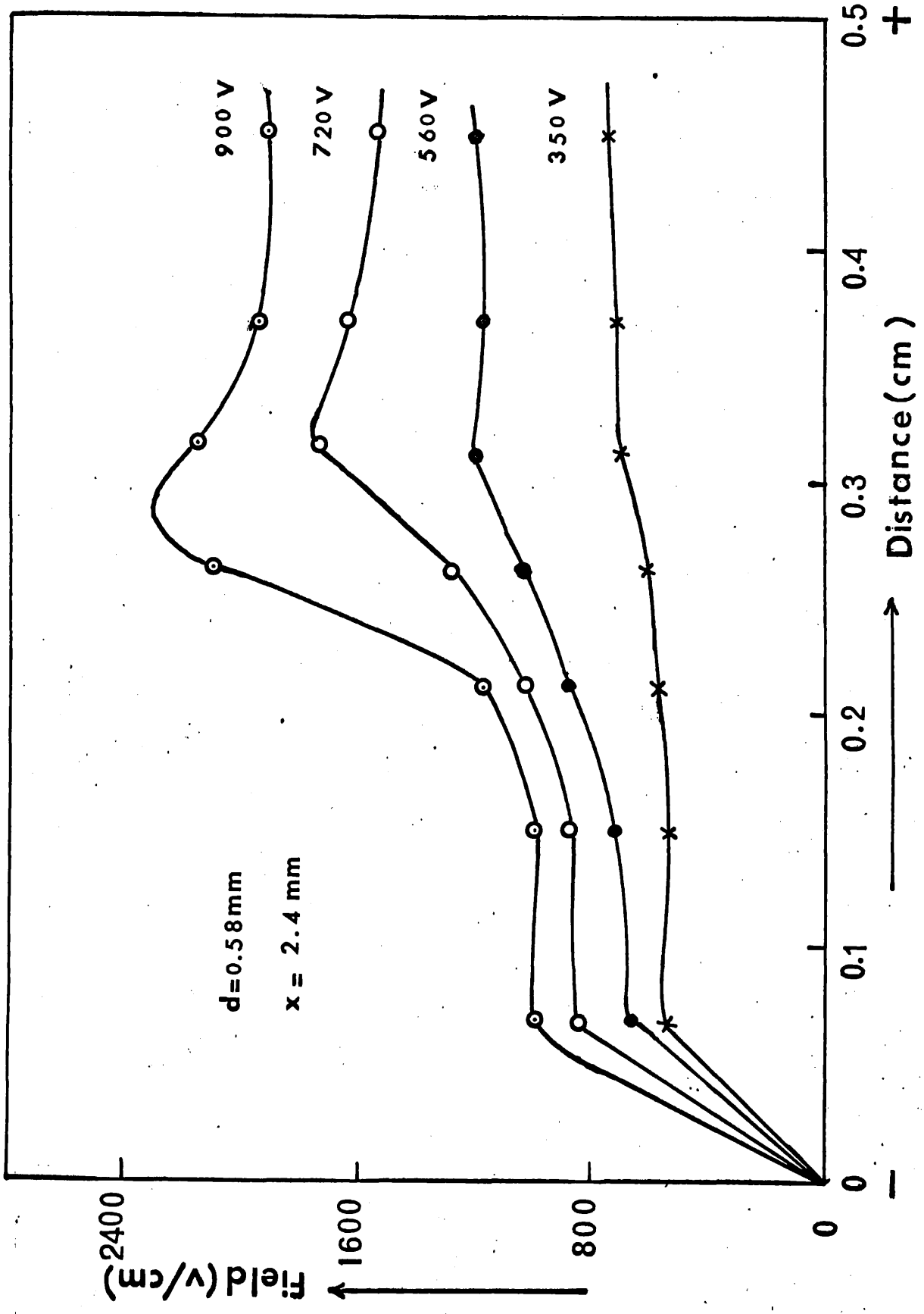

FIG. 45 DISTRIBUTUION OF ELECTRIC FIELD

These current oscillations can be explained along the same lines as with the high resistivity region near the anode end. The main difference between the two systems of non-uniform illumination is that the specimen has been divided into three different regions, L_c the region near to the cathode; Ld the shielded region by the ceramic strip; L_x the region closest to the anode, with their respective lengths lc, d and x. The presence of thermal acoustic flux maintains the region close to anode, i.e. Lx at a field above E_{th} under the oscillatory conditions. If the amplification of waves through the regions L_d and L_x is sufficient oscillation with period of $\frac{x + d}{V_s}$ is expected. The results obtained show that the periods are sometimes larger than this. It is therefore assumed that a considerable amount of reflection occurs at the anode. Under the circumstances it is expected that the frequency of oscillation would decrease gradually as x is increased and as shown in Figs. 36, 37, 39.

It is also possible that irregularities present in the specimen may also be responsible for the occurrence of this variation in frequency. The variation in the resistance of the specimens (Fig. 56) at various positions of the shielded strip showed that irregularities do exist, although they do not reveal the exact nature or effects of these. If it is considered that irregularities are present at different points, then the low field distribution should be as shown in Fig. 47a. Considering irregularities as the regions of higher resistivity in L_c, then they would cause the peaks of field at z_1, z_2. Under the oscillatory conditions, when the domain is being amplified in L_x (Fig. 47b), then the field in all parts of L_c region will be below E_{th}. The partial extinction of the domain at the anode raises the field in L_c, but not sufficiently. But the attenuation of the reflected part of the domain causes a continued rise of field in L_c, until eventually the fields in z_1

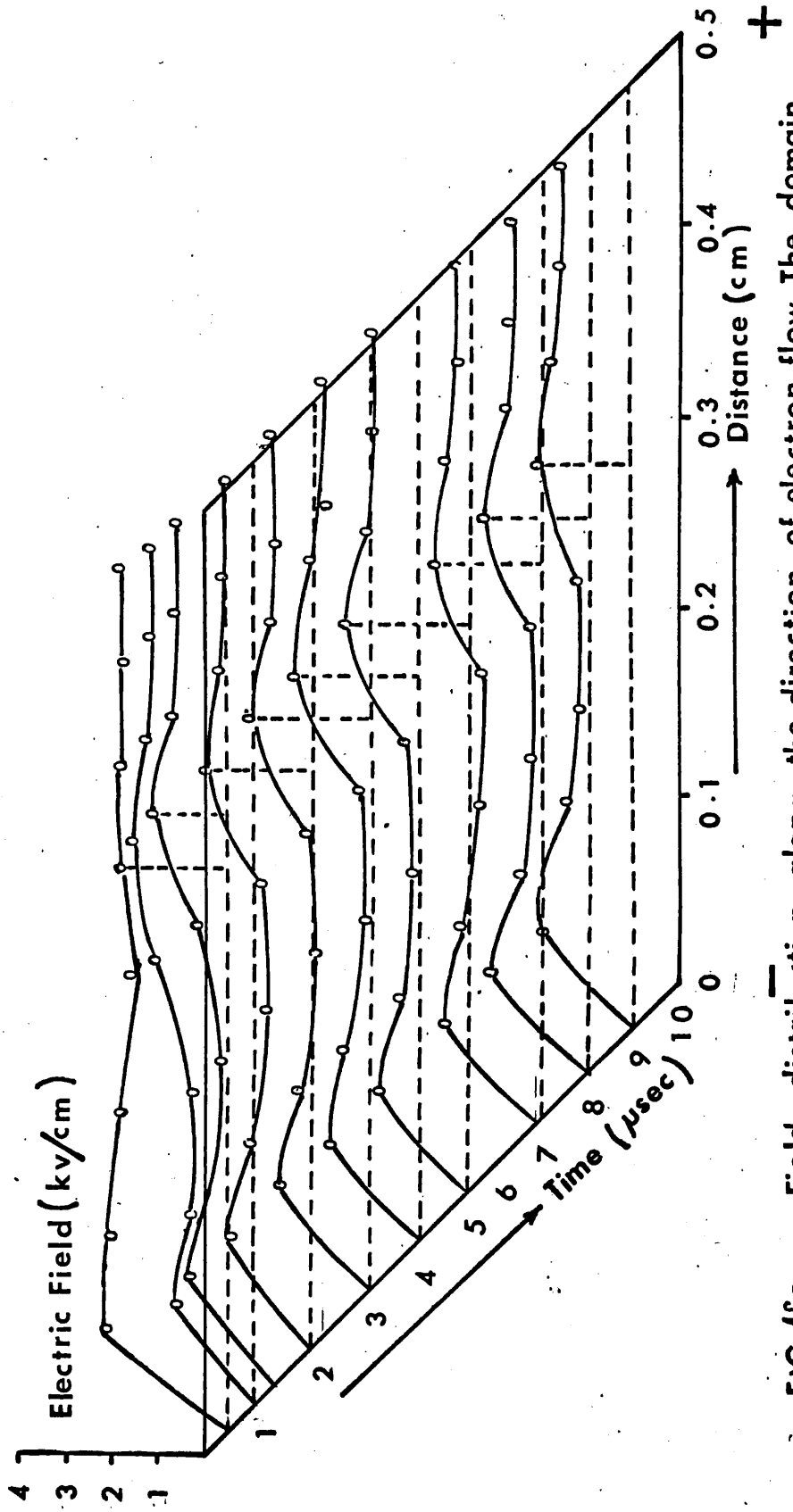

FIG. 46a Field distribution along the direction of electron flow. The domain is nucleated near the high resistivity region.

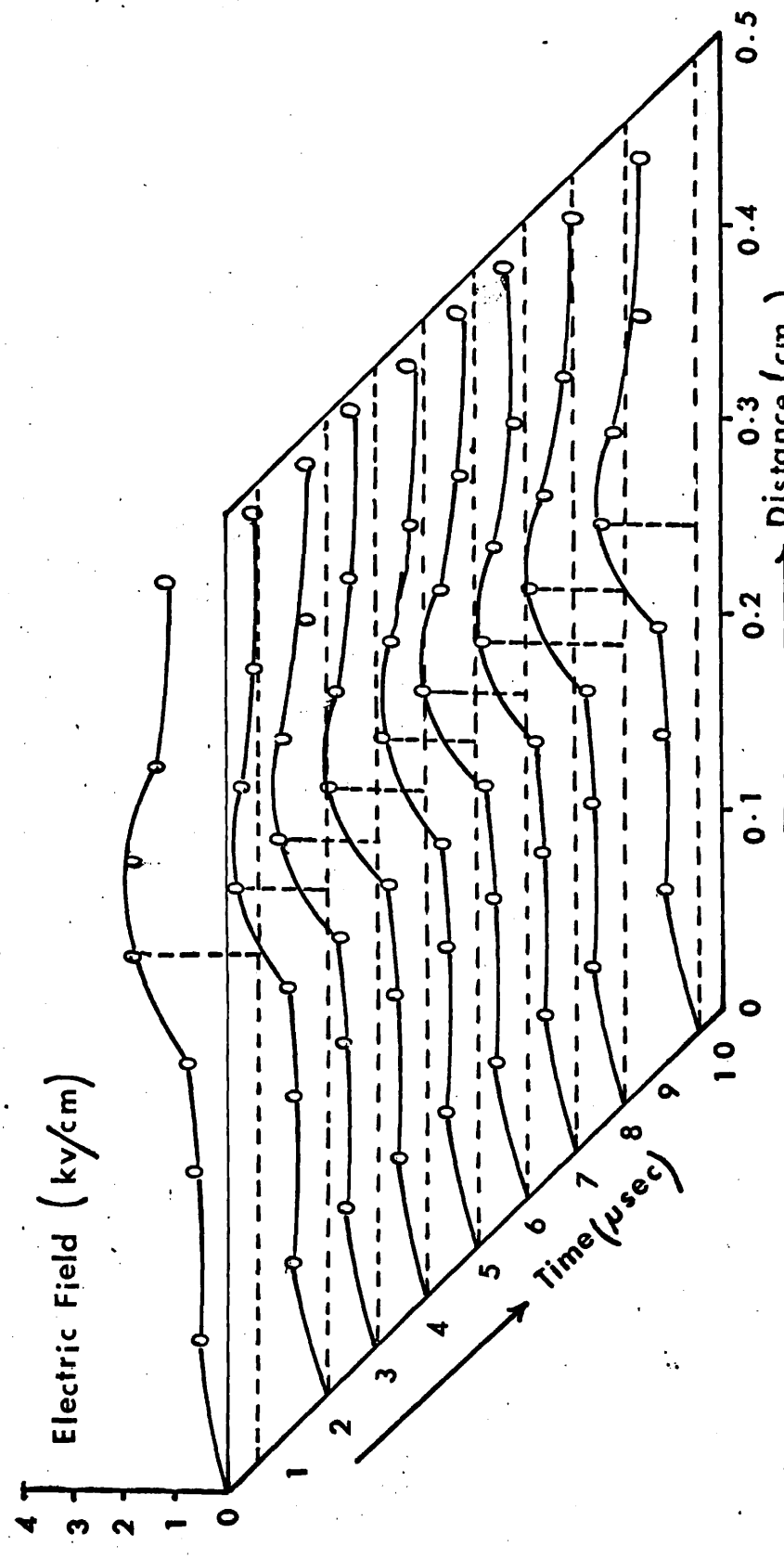

FIG. 46b Fieldddistribution along the direction of electron flow. The domain is nucleated near the high resistivity region.

and z_2 are above E_{th} (Fig. 47c).

Since z_2 is closest to the amplifying regions L_d and L_x, the amplified thermal flux from z_2 will arrive at first and be further amplified in L_d. A domain then grows from this point and damps out the flux from z_1, before it can be amplified. Considering the case, where attenuation of the reflected domain is slow, it is quite possible that its arrival at z_2 is the point at which the field at z_2 is raised above E_{th}. The oscillation frequency is then given by $\frac{2(x + d)}{V_s}$, where z_2 is at a junction A, between L_c and L_d. The curves for $f = \frac{V_s}{2(x + d)}$ have been drawn as shown in Figs. 40, 41, 42, 43.

If the distances of z_1, z_2 from the anode are given by l_1, l_2 respectively, then frequencies of $\frac{V_s}{2l_1}$; $\frac{V_s}{2l_2}$ would be obtained, when z_1, z_2 are near to point A. This could occur when the attenuation of the reflected domain is not very large. But, when the attenuation is large then the period of oscillation would be between $\frac{1}{V_s}$ and $\frac{2l}{V_s}$ where l is the distance of the irregularity from the anode.

It is possible to calculate the expected locations of irregularities from the simple relation: $f = \frac{V_s}{2l}$.

For d = 0.6mm, the locations are,

l = 0.72mm for f = 1200 KHz and

l = 1.4mm for f = 600 KHz

When the period of oscillation is less than $\frac{V_s}{2(x + d)}$ an approximate location can be found. If it is assumed that the minimum x, at which oscillations of particular frequency are seen, is when the irregularity responsible for them is at the junction A. The position of the irregularity is then given by:

. l = d + the minimum x at which a particular frequency mode is observed.

Using this relation for the results of Fig. 37 it is found that,

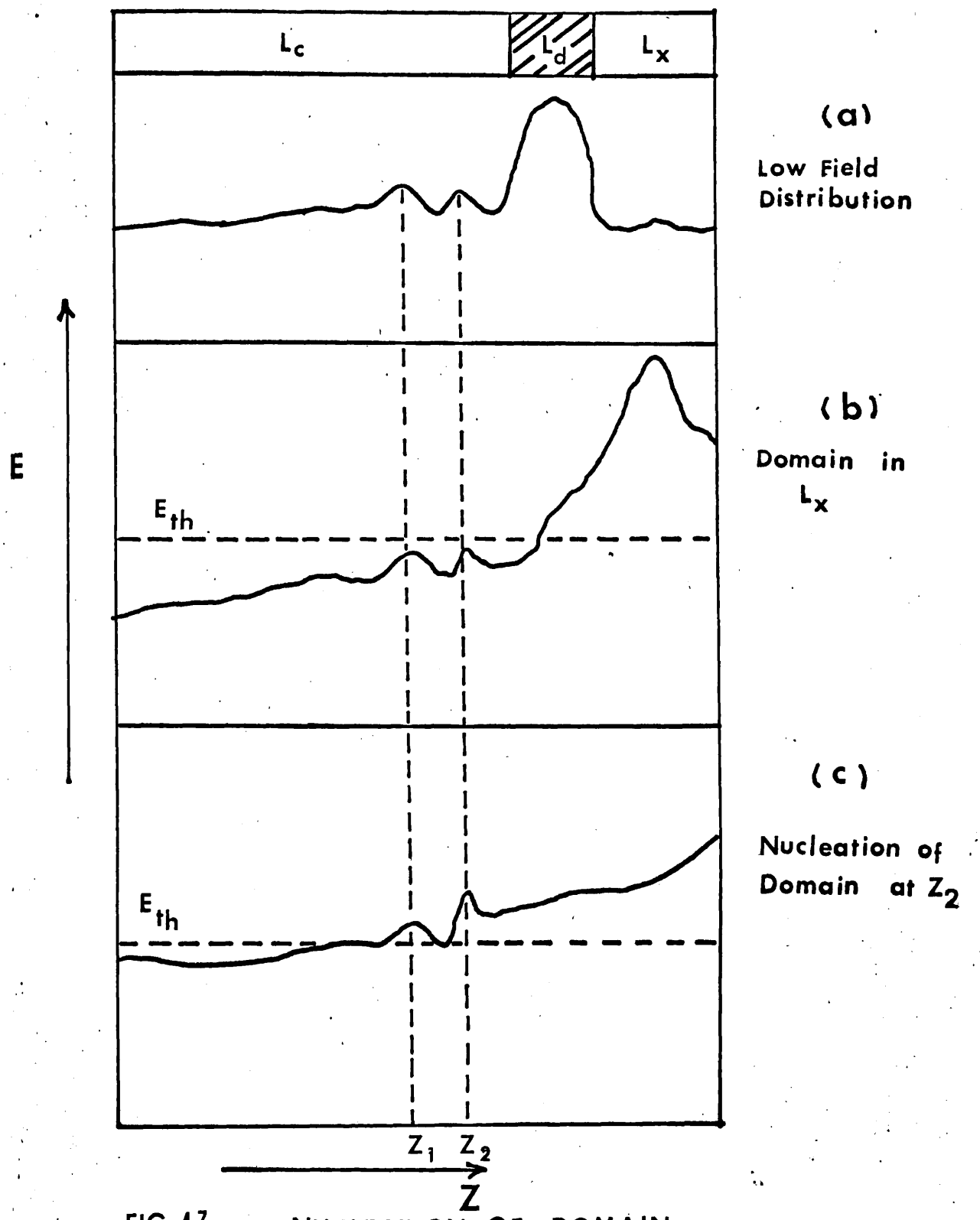

FIG. 47 NUCLEATION OF DOMAIN AT IRREGULARITIES.

l = 2.81mm for f = 1500 KHz,

l = 2.91mm for f = 1250 KHz and

l = 3.61mm for f = 950 KHz

In specimens where the direction of the applied voltage is parallel to c-axis of the crystal, no oscillations are observed until the ceramic strip reaches a definite distance from the anode (Figs. 36, 37,39). This means that the field in L_c cannot exceed E_{th} other than at the irregularities.

The transition from one mode of oscillation to another occurs with certain values of x the distance of the ceramic strip from the anode. This clearly indicates a shift of the nucleation point for domain from one irregularity to another. Firstly the irregularities present are the regions of higher resistivity and secondly shift is caused by change in field distribution as shown in Figs 45(a,b) at different positions of the light strip. Another reason for the shift from one mode to another can be caused by a change of field distribution, due to non-uniform heating of the specimen. The regions of higher field would be heated up more than other regions. This certainly would increase the resistivity in that region and raise the field there.

The manner in which the frequencies of oscillation change show that it is unlikely they are due to irregularities only. If lower value of V_s were assumed this condition would be satisfied reasonably as the experimental curves (Figs. 36, 37, 39, 40), are quite parallel to that given by $f = \frac{V_s}{x + d}$ and $f = \frac{V_s}{2(x + d)}$. However, it could be safely said that the velocity of sound in the specimens is affected by the intensity of illumination and the applied voltage.

When the distance of the light strip from the anode becomes too large, no oscillation occurs and a similar situation to that shown in

Fig. 12 is arrived at. Here L_x remains at an attenuating region. Moreover, the specimens gave different modes of oscillation when reversed. This confirms the belief that there are irregularities present within the material.

The majority of the specimens broke down during experiments as arcing and chipping at the surfaces occurred. When the fields in L_c are below E_{th}, very high fields do exist in L_d and L_x regions. From versus curves shown in Appendix II small gain should be expected at very high fields. However, it has been shown[69] that at fields above 2.1×10^3 V/cm, there is a decrease of mobility and corresponding increase of electrons. The drift velocity given by E_{th} will not exceed the velocity of sound by too large a factor and conditions of high gain may still be present at very high fields.

Table 6 Tabulation of results for specimen TRS_6 oscillating by using a light strip

Applied voltage (V)	Strip width (d)	Distance of strip from anode end (x)	Frequency of oscillation (f)	Intensity of illumination (Φ)
1050 volts	0.4mm	1.78mm	833KHz	2.4×10^{-3} watt cm^{-2}
1050 volts	1.4mm	1.4mm	752KHz	2.4×10^{-3} watt cm^{-2}
1050 volts	2.1mm	1.4mm	584KHz	2.4×10^{-3} watt cm^{-2}

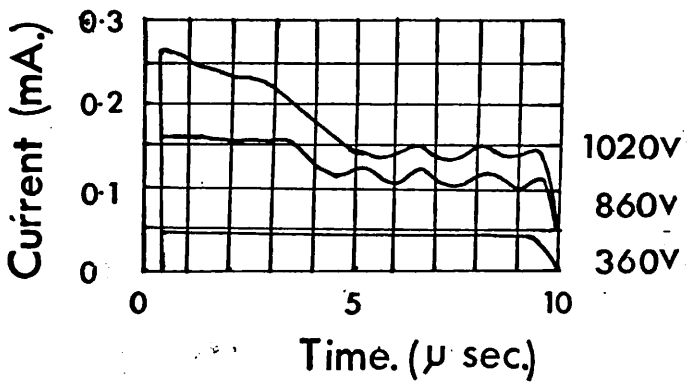

Fig. 48 Current obtained for various peak values of applied voltage pulses.
$\sigma_{dark} = 2.92 \times 10^{-6}$ ohm cm^{-1}

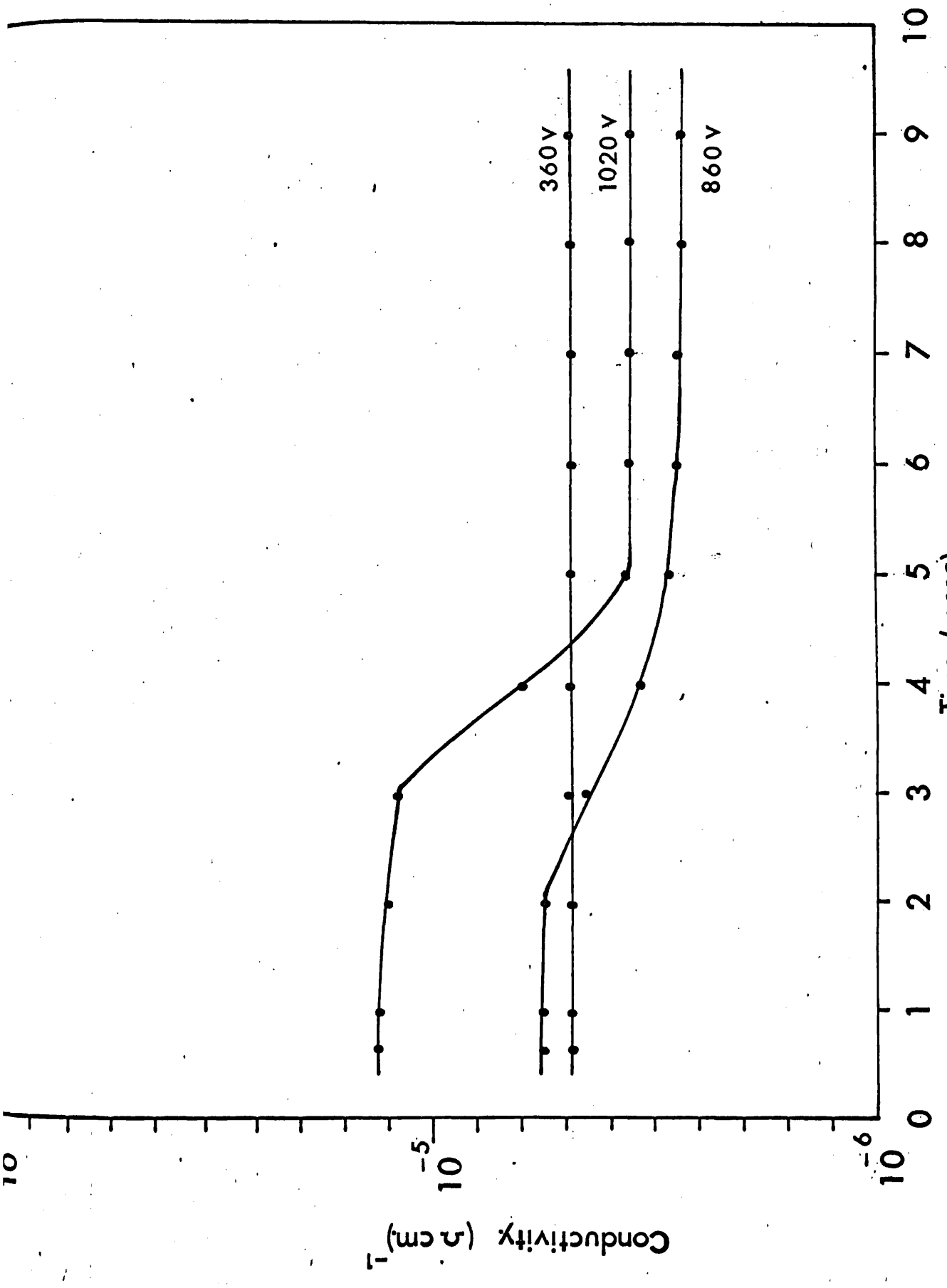

Fig. 49 Conductivity of the specimen at various times after the application of a voltage pulse of 10 microseconds duration.

5.3.5 Current oscillation with one or more major changes in amplitude

In studying the oscillations of the current obtained by applying a high voltage pulse to a cadmium sulphide crystal, a number of features have been obtained which differ from those previously reported.[72-73] A strip of ceramic 0.4mm wide was positioned accurately at 2.18mm from the anode end to obscure a strip of the crystal 0.4mm wide and perpendicular to the crystal axis.

When a voltage pulse lasting 10μsec was applied to the ends of the specimen TRS_{11}, the current varied as seen in Fig. 48. At voltages exceeding 300V, the current rose to a maximum in a few nanoseconds, dropped to a slightly lower value in about 2 microseconds and fell to another value after 5 microseconds. Oscillationsin current were observed after it had fallen to final stage as shown in Fig. 48. The conductivity of the material at various times after the application of the voltage pulse is seen in Fig. 49 to remain constant up to 360V and thereafter to differ from the ohmic low voltage value.

When the applied voltage was kept constant and the illumination intensity increased as in Fig. 50, changes in the current pulse were observed. Initially with an illumination intensity of 2.1×10^{-4} watt cm^{-2} the response was ohmic. At an intensity of 3.7×10^{-4} watt cm^{-2}, a single downward step appeared after 4 microseconds, but on increasing the intensity to 5.5×10^{-4} watt cm^{-2} a double step developed. At an intensity of 7.3×10^{-4} watt cm^{-2}, oscillations began and at 2.4×10^{-3} watt cm^{-2}, the steps disappeared with oscillations continuing throughout the voltage pulse.

Fig. 51 shows the dependence on illumination intensity of the conductivity of the specimen after the application of a high voltage pulse. Initially at an illumination intensity of 2.1×10^{-4} watt cm^{-2}, the conductivity of the specimen did not vary in time. At intensities

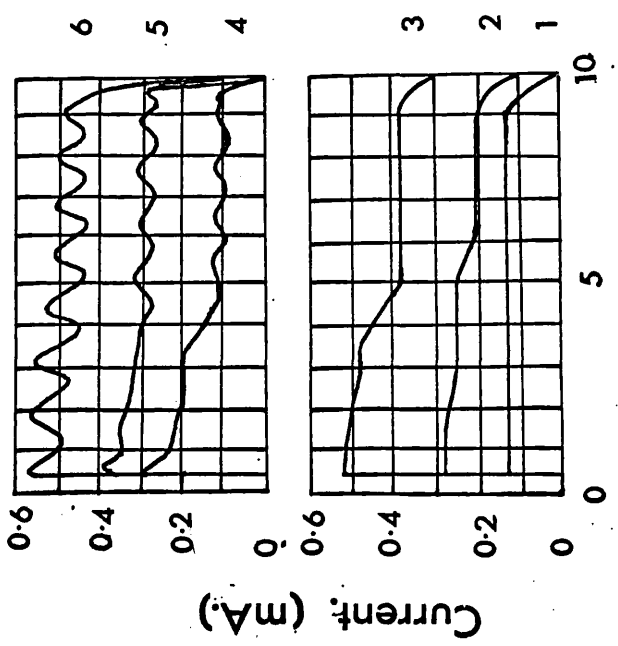

Fig.50 Shape of the current pulse for various illumination intensities and an average electric field of 2.22 kV/cm. Illumination intensity:- (1) $2.1\ 10^{-4}$ (2) $3.7\ 10^{-4}$ (3) $5.5\ 10^{-4}$ (4) $7.3\ 10^{-4}$ (5) $9.3\ 10^{-4}$ (6) $2.4\ 10^{-3}$ watt cm^{-2}.

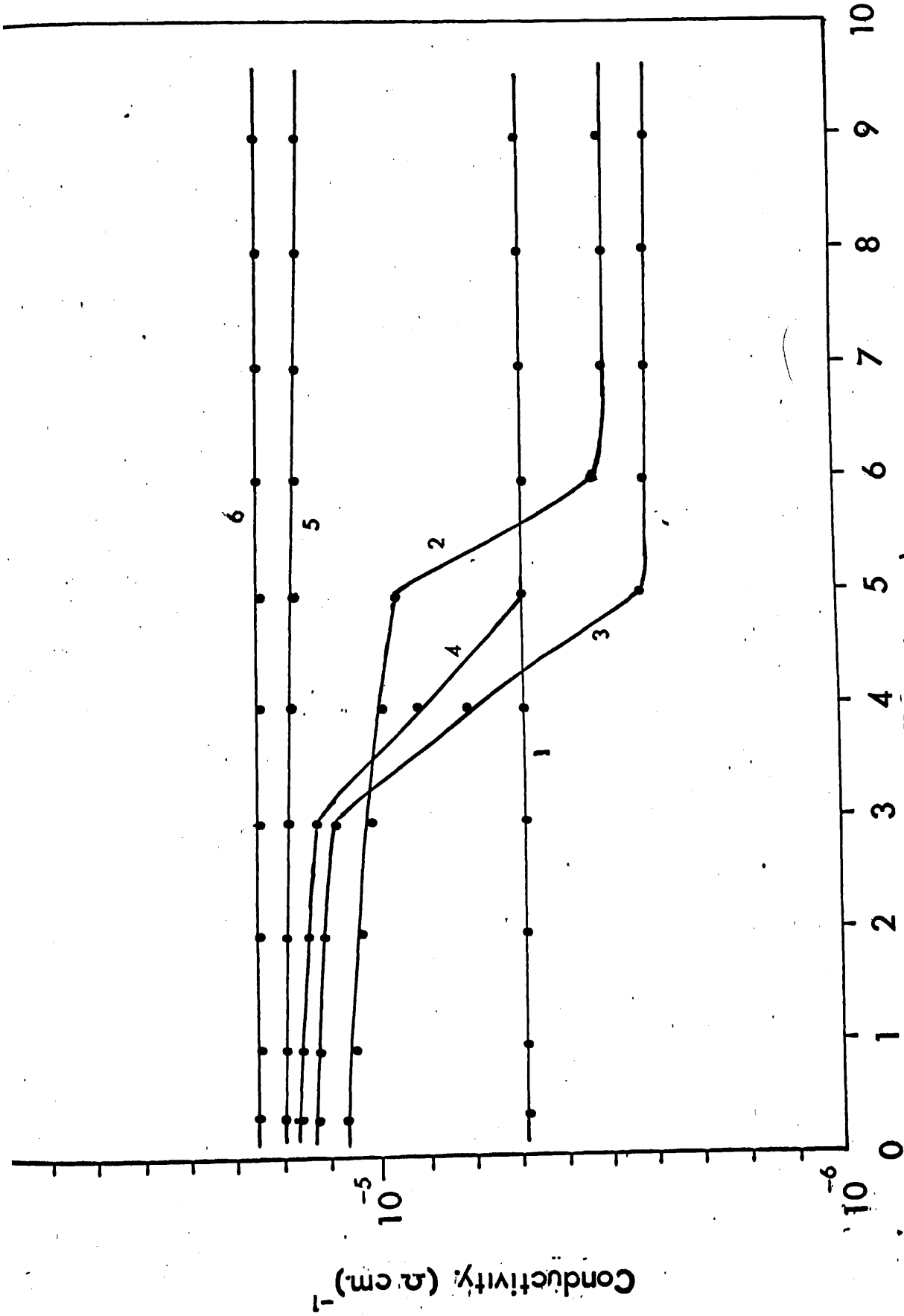

Fig.51 Conductivity of the specimen at various times after the application of a voltage pulse of 1020 V and 10 microseconds duration. Illumination intensity:- (1) $2.1\ 10^{-4}$ (2) $3.7\ 10^{-4}$ (3) $5.5\ 10^{-4}$ (4) $7.3\ 10^{-4}$ (5) $9.3\ 10^{-4}$ (6) $2.4\ 10^{-3}$ watt cm^{-2}.

of 3.7×10^{-4} watt cm^{-2} to 7.3×10^{-4} watt cm^{-2} the conductivity of the specimen exceeded the ohmic value initially, but its conductivity fell after about 3 microseconds to a value lower than the ohmic one. At intensities of 2.4×10^{-3} watt cm^{-2} and above, the conductivities fell only by a few percent. The electric field was determined by means of a voltage probe on the surface of the specimen and is shown in Fig. 52. It has maxima 0.5mm from the cathode and 1mm from the anode, whereas Autin et al[73] reported a step up near the cathode but did not see a maximum near the anode.

The first drop in the current at 3 microseconds appears to be due to the development of an acoustic field[56] which interacts with the drifting charge carriers leading to amplification. These processes lead to oscillations if the gain is adequate.[33] In a crystal of sufficiently high conductivity, the flux should attain its saturation level as soon as the drift field exceeds the threshold for ultrasonic amplification. In a crystal of lower conductivity such as the present CdS sample, where flux build-up time is long compared to the sample transit time, no appreciable flux build-up can occur until the amplification in the drift direction exceeds the loss in the opposite direction.

From the theory of linear ultrasonic amplification,[50,74] it has been shown that the condition for net round trip gain at the frequency of maximum gain

$$\omega = (\omega_C/\omega_D)^{\frac{1}{2}} \quad \text{is}$$

$$V_d \geq \left[1 + 4\,(\omega_C^2/\omega_D^2)\right]^{\frac{1}{2}} V_s$$

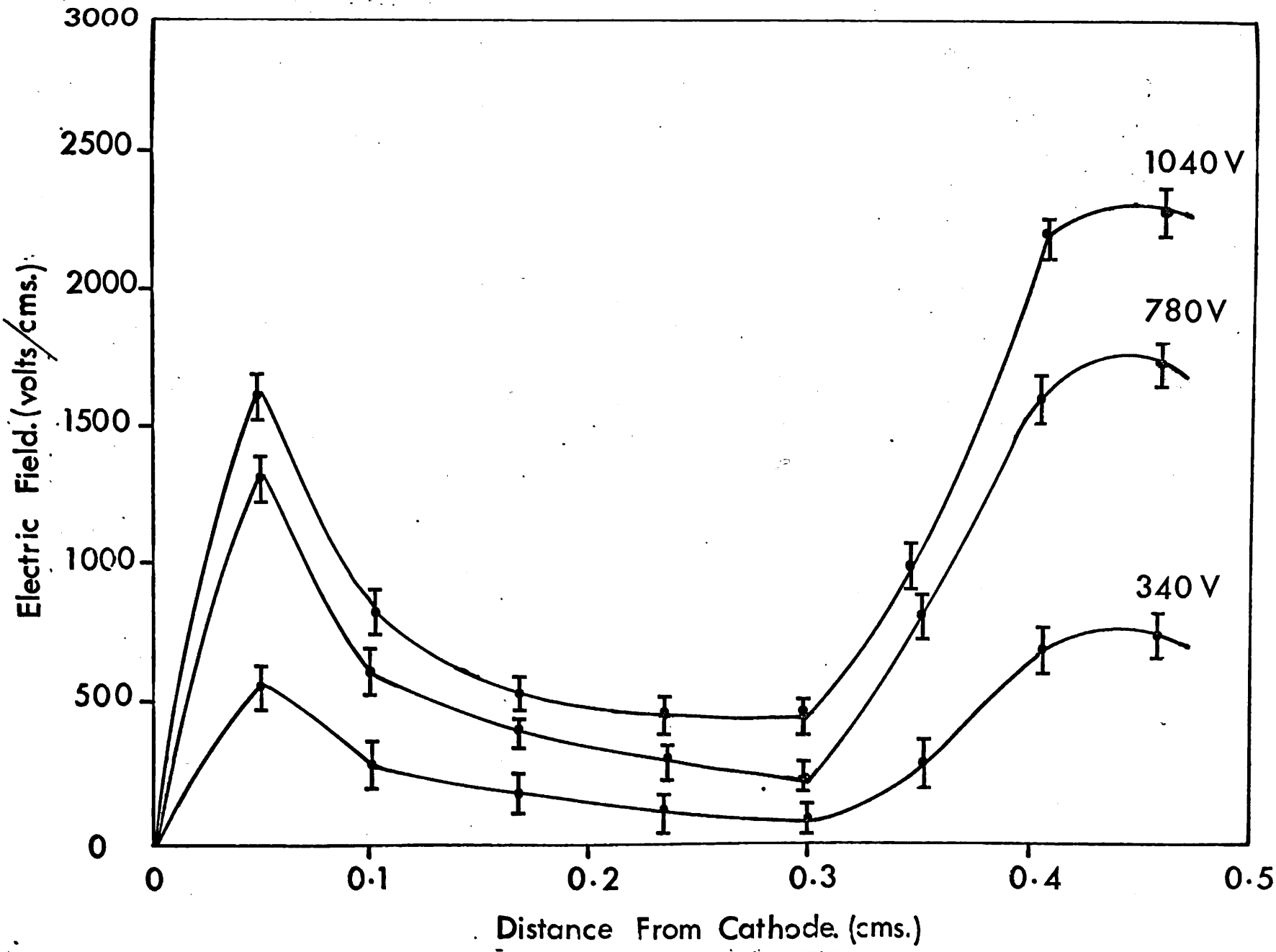

Fig.52 Electric field in the specimen.

Where,

V_d = is the drift velocity

V_s = is the sound velocity

$\omega_C = \frac{\sigma}{\epsilon}$ is the dielectric relaxation frequency

and $\omega_D = \frac{V_s^2}{D}$ is the 'diffusion' frequency.

In n-type CdS values of these frequencies[31] are,

$$\omega_C = 1.2 \times 10^{12} \sigma \text{ sec}^{-1}$$

In our specimen, $\sigma = 3 \times 10^{-5}$ ohm cm^{-1} so,

$$\omega_C = 3.6 \times 10^{7} \text{ sec}^{-1}$$

and

$$\omega_D = 2.9 \times 10^{10} \text{ sec}^{-1} \text{ at } 300^{\circ}\text{K}.$$

Then the drift velocity V_d must exceed $[1.000003]\ V_s$, as the condition for the sound trip gain to exceed unity.

The second step occurs at a time when the acoustic field intensity is increased by reflection from the anode. In an experiment to observe scattering of CW Helium Neon laser light by the acoustic wave packets generated in the specimen, it was noted that the transmitted light showed weak scintillations at a frequency of a few Hz, consistent with the existence of slowly moving domains.[75]

These are said to arise[76] when the crystal changes from n-type to P-type conductivity. Such injections of holes may occur from inhomogeneities and would produce the second step in the current.

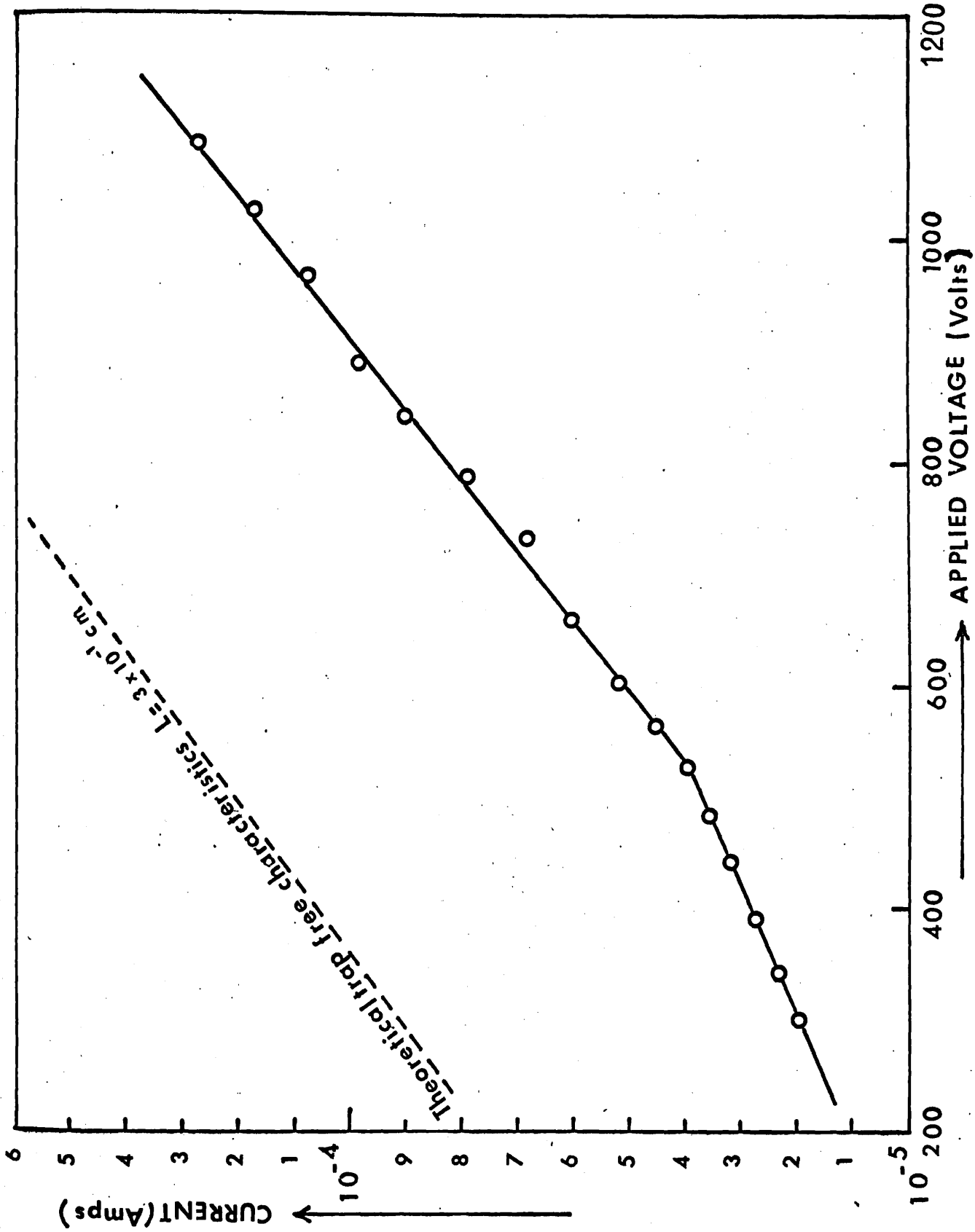

FIG. 53 I–V CHARACTERISTICS

5.3.6 Non-sinusodial oscillations induced with localised illumination using He-Ne laser beam (Fig. 7)

Many research workers[33,39,53,57] have reported numerous observations of sinusodial oscillations in CdS, CdSe and CdTe, when specimens are illuminated with a light spot at an experimentally found position along their length. These have been generally explained in terms of the regenerative propagation of amplified acoustic flux packets and the associated acoustoelectric current. In studying the current oscillations obtained by applying a high voltage pulse to CdS crystal which has been locally illuminated by He-Ne laser beam, a number of features have been observed which differ from those previously reported. The current oscillations observed are of high frequency and their wave form is non-sinusodial. Apart from low frequency sinusodial oscillations, their I-V characteristics showing current saturation behaviour above a certain critical voltage differ entirely from present measurements. Field measurements under oscillating conditions have revealed the existence of non-uniformity of electric field along the length of the specimen. Absorption spectra of these specimens in the range 2.5-25 micron showed absorption peaks. The range of frequencies reported here make a simple interpretation along the lines reported earlier unlikely. This phenomenon can be explained on the same lines as for a specimen illuminated uniformly. The only difference is that, here, a fraction of area 0.2mm near the centre of the sample has been illuminated by focussing the He-Ne laser beam. The specimens chosen for this experiment had the dimensions and conductivities at illumination intensity as given in Table 2. Experiments were performed mainly with the electric field applied perpendicular to the c-axis of the crystal.

The dependence of current on voltage for various applied voltages to specimen TRS_8 is shown in Fig. 53. It is observed that at low

voltages, the current voltage characteristics fall below the linear ohmic relation. After this, the sub-linear region changes in a stronger electric field to a dependence of $I \propto V^2$. The sub-linear portion of I-V curve can be explained on the basis of the charge formed in CdS when an electric current flows through it. This negative charge increases with the voltage applied and means that the cathode injects into the crystal more electrons than the number lost at the cathode. If the excess negative charge of the crystal is partly or completely localised (at traps) in the bound state, then these bound states may act as additional scattering centres. Thus, when voltage is increased, the number of charged traps acting as effective scattering centres increases and the mobility of free carriers decreases. This should gradually saturate the current. But the resulting I-V curve (Fig. 53) does not show such a saturation in current. The reason may be that if the shallow traps (present in material) which act as scattering centres are completely filled with electrons, the reduction in the mobility of free carriers is slight compared with an increase in the number of these carriers per unit volume, which makes a considerable contribution to the photocurrent. In such a case, the dependence of current saturation on voltage should be weak. The subsequent rapid rise in the current can be explained on the assumption that the process leading to the multiplication of free carriers by electric field takes place in CdS. Such a process may be the emptying of shallow traps by the field or impact ionization of these traps by fast electrons.

The full curve of I-V characteristics also exhibits the features of the Lampert theory for a single discrete trapping level. Fig. 53 also shows the Child's law relationship for the crystal, which was

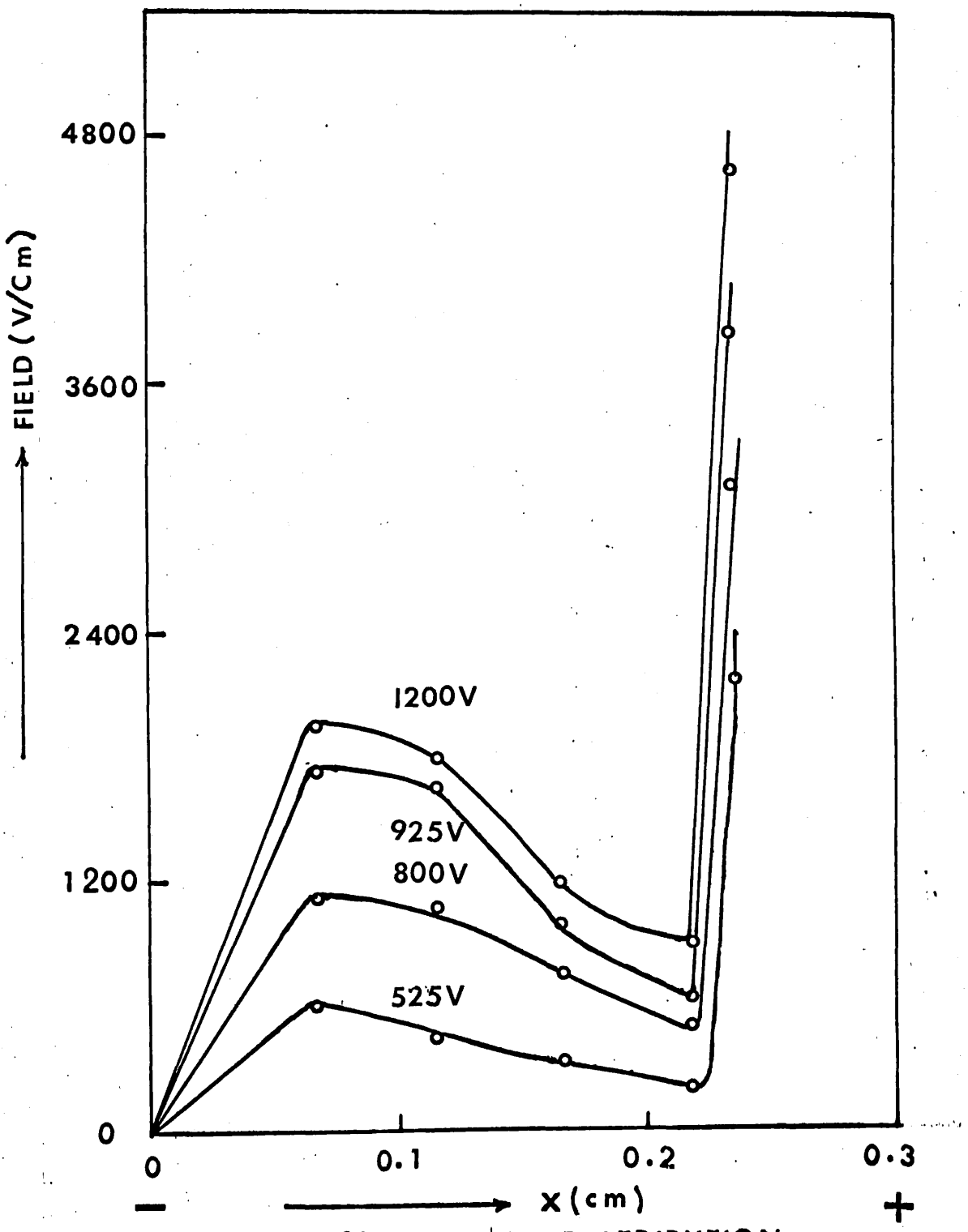

FIG. 54 FIELD DISTRIBUTION

calculated by assuming dielectric constant 10 and experimentally measured drift mobility of 300 $cm^2\ V^{-1}\ sec^{-1}$ at room temperature. The trap filled limit voltage and θ (ratio of the measured current to an appropriate voltage in the region considered to the Child's law current at that voltage) for the curves gave a trap density of $6.34 \times 10^{13}\ cm^{-3}$ at a level 0.19eV in specimens TRS_8, TRS_{10} and a trap density of $1.66 \times 10^{14} cm^{-3}$ at a level 0.21eV below the bottom of the conduction band in specimen TRS_9. The traps into which these electrons decay may have the same or different cross-sections. The values of cross-section obtained were $1.5 \times 10^{-14} cm^2$ and $1.4 \times 10^{-15}\ cm^2$ respectively.

The electric field measurement is shown in Fig. 54 and it disclosed the non-uniformity of electric field present along the length of the specimen. There is a step up near the cathode and a definite high electric field region existing near the positive end of the specimen. Such a situation exists in all the specimens given in Table 7. Such presence of non-uniformity of electric field can result in current oscillations.

It is, however, reasonable to mention that since 6328A^o light lies well below the normal absorption edge energy of CdS (2.35eV), the photoconductivity observed must arise from the excitation of deep lying levels in the energy gap. Such levels have been shown to be associated with the presence of cu, Ag and of defects and vacancies in CdS;[110] cu, for example, can give a pronounced photoconductivity maximum at around 6000A^o.

Fig. 55a shows the current oscillations obtained when 1100 volts pulse of 100μsec duration is applied to specimen TRS_8. The results for this type of illumination have been summarised in Table 7. The wave form of oscillation is shown in Fig. 55b. It is seen that the application of the voltage difference from lower ohmic region to the region when

(a)

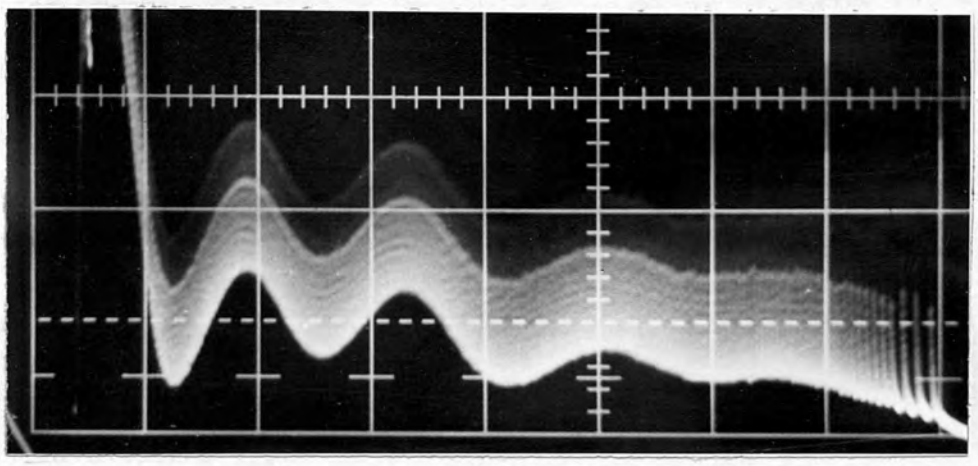

(b)

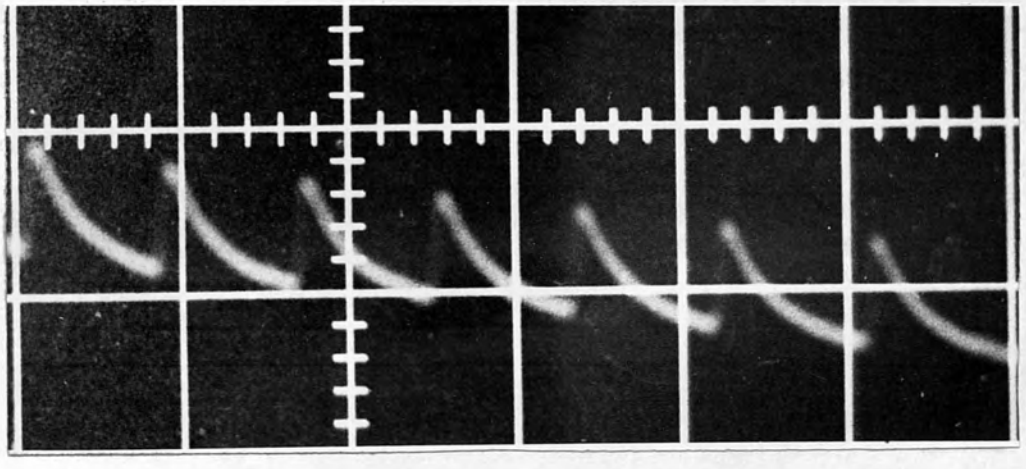

Fig.55 Continuous current oscillations in specimen TRS_8 under localised illumination with red laser light.

(a) Horizontal scale = 10 μsec./div.
Vertical scale = 50 μA/div.

(b) Horizontal scale = 0.1 μsec./div.
Vertical scale = 50 μA/div.

$I \propto V^2$, to the locally illuminated crystal lead to a discontinuous increase in current followed by a fall-off, which continued for a few microseconds. It clearly shows that the process of electrons capture by traps is playing an important role in the observed phenomena. Thus the appearance of these oscillations can be explained on the emptying and filling of these traps in the crystals. Such a localised type of illumination decreases the resistance of that part of the crystal making possible a concentration of field near the electrodes. Thus the increase in the resistance of the contact part of the crystal leads to a redistribution of potential over the length of the sample. So the occupied traps are in an electric field of increased intensity which increases the probability of their being emptied. This avalanche type liberation of electrons from the traps leads to an instantaneous increase of the current which is flowing through the sample after which occupation and decrease of the mobility of free carriers recommences.

Table 7 Tabulation of results when the specimen is illuminated with laser beam

Specimen Number	Applied Voltage (volts)	Oscillation frequency (MHz)	Period of oscillation (μsec.)	Amplitude of oscillation (μA)	Illuminated area near the centre of the specimen (mm)
TRS_8	1100	11	0.09	50	0.2
TRS_9	1000	3	0.33	20	0.22
TRS_{10}	1000	2.5	0.4	20	0.21

5.4 Other measurements

5.4.1 Current Saturation

Current saturation under uniform illumination (see Fig. 56) was observed in specimens shown in Table 3. Many samples displayed rapidly damped oscillations before the onset of saturation in current. The threshold field varied between 550 volt/cm to 800 volt/cm for specimens having their length perpendicular to c-axis, whereas for specimens having their length parallel to c-axis, the variation recorded was from 1400 volt/cm to 1600 volt/cm.

The value of E_{th} was calculated from the relation $E_{th} = \frac{V_s}{\mu}$ is 583 volt/cm for $V_s = 1.75 \times 10^5$ cm sec^{-1} and 1470 volt/cm for $V_s = 4.41 \times 10^5$ cm sec^{-1}. The drift mobility μ, measured experimentally is 300 cm^2 $volt^{-1}$ sec^{-1} at room temperature.

5.4.2 Variation in the resistance of the specimen using light strip

The resistances of TRS_4 for various values of Φ and d are shown as functions of α in Fig. 57(a,b). These measurements were made under ohmic conditions. It clearly indicates that the resistivity of the shielded region does effect the average resistance of the sample. This average resistance is different at different positions of the light strip.

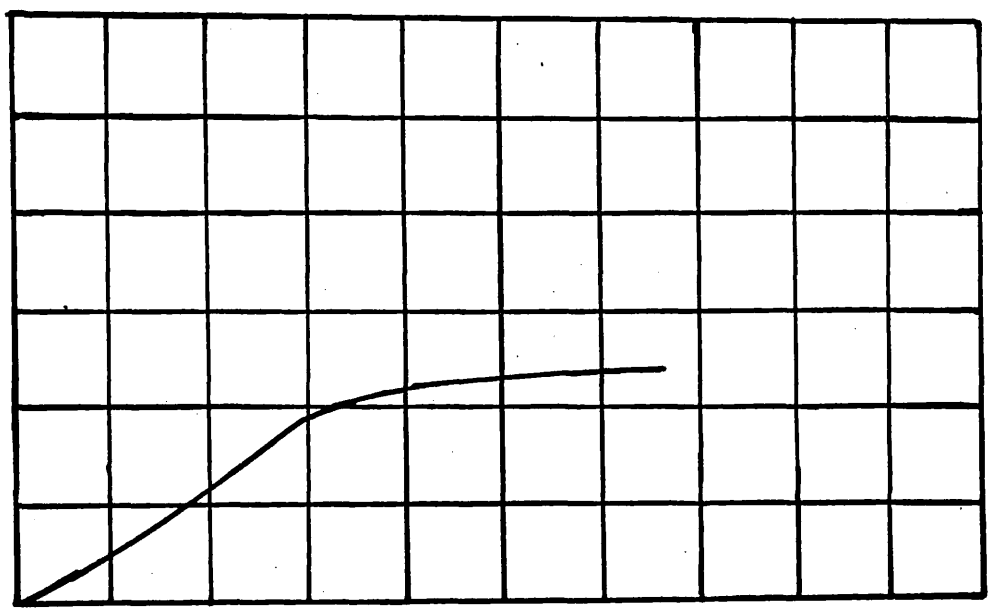

Fig.56 I-V characteristics for CdS specimen TRS_1 under Uniform illumination L = 3.28mm;

a = 0.74 x 0.88mm^2 V = 200 volts /div (horizontal scale)

I = 2mA/div (vertical scale) and L $\perp$ c-axis

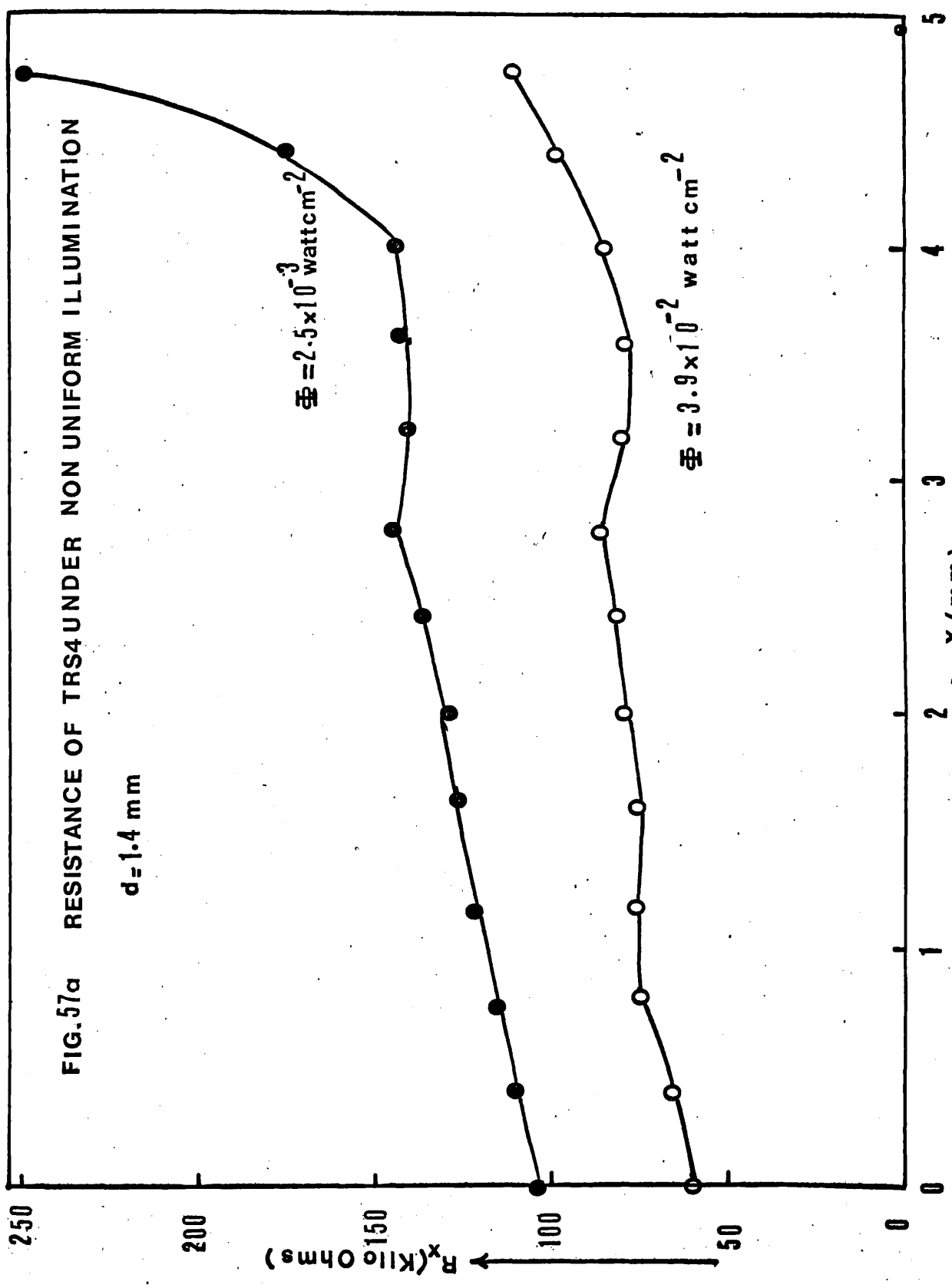

FIG. 57a RESISTANCE OF TRS4 UNDER NON UNIFORM ILLUMINATION

$d = 1.4$ mm

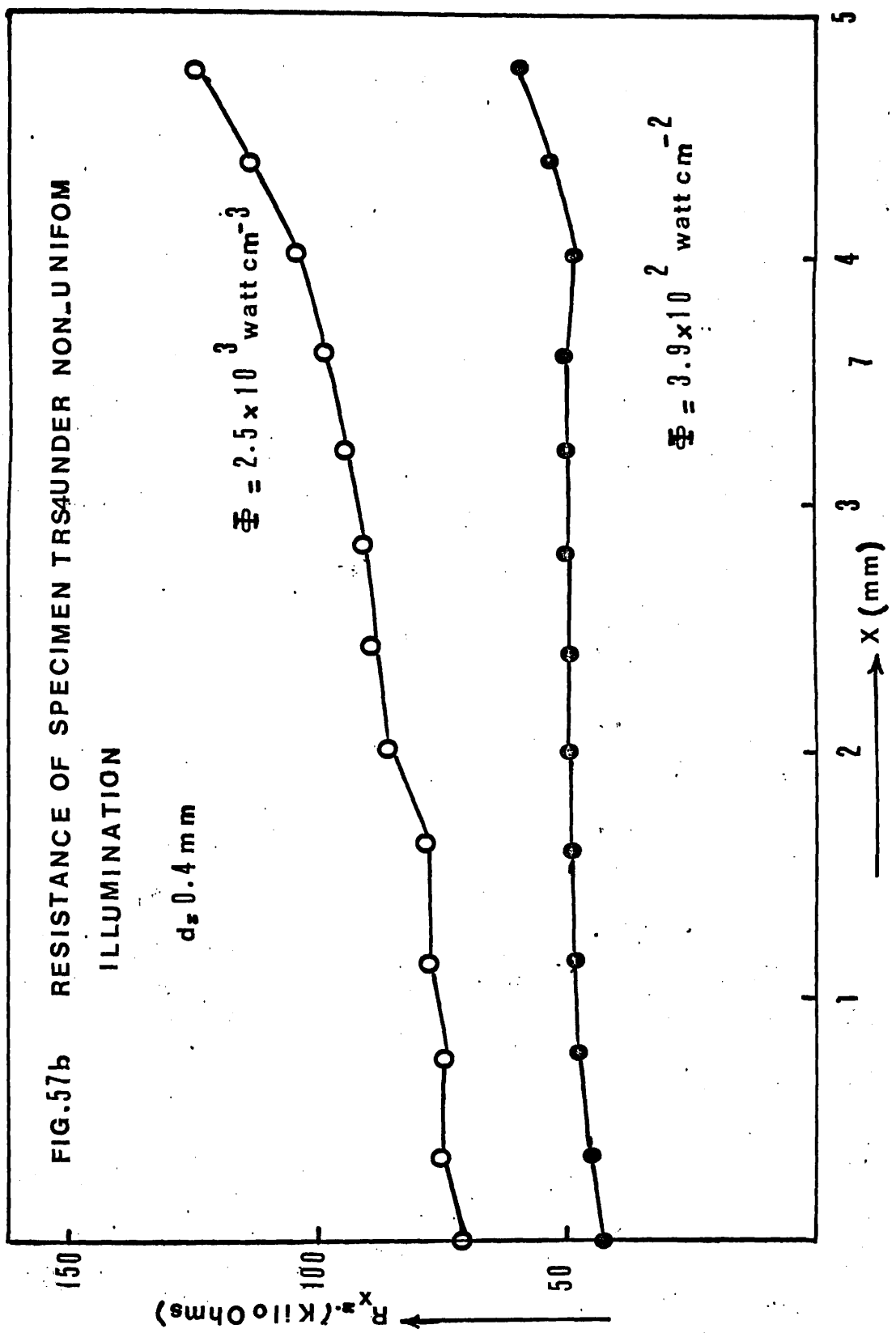
FIG.57b RESISTANCE OF SPECIMEN TRS4UNDER NON_UNIFOM ILLUMINATION
d_s 0.4 mm
$\Phi = 2.5 \times 10^{3}$ watt cm^{-3}
$\Phi = 3.9 \times 10^{2}$ watt cm^{-2}
R_x (Kilo Ohms)
150
100
50
1
2
3
7
4
5
X (mm)

6. Discussion

6.1 Introduction

The results presented in Chapter 5 show a considerable variation in the behaviour of different specimens under seemingly identical circumstances. It was difficult whilst discussing the results to isolate the effects of each of the numerous factors involved, but an attempt has been made to give qualitative explanations of the physical phenomena that may occur. It is worthwhile considering the theoretical background, the effects of traps and the variability of the CdS material whilst discussing the phenomena observed.

Current oscillations and current saturation are caused by the presence of an amplified acoustic flux, which is generated spontaneously at regions of discontinuity. Three types of discontinuities exist. At electrodes, the electric field changes rapidly. In the material, field discontinuities result from conductivity gradients caused by the varying intensity of illumination and because of the difficulties in the production of single crystals of cadmium sulphide. There are defects which give rise to changes in the piezoelectric constants.

Despite the variability of the material, it has been possible to examine a wide range of physical phenomena in small bars of single cadmium sulphide crystal. The effects observed are:

a) Oscillations in complete darkness

b) Non-sinusodial oscillations with uniform illumination

c) Oscillations with the anode end shielded

d) Oscillations with an intermediate shielded strip

e) Oscillations with one or more major changes in amplitude

f) Oscillations with localised illumination using an He-Ne laser beam

g) Current saturation

The effects (c), (d) and (g) have been reported before, but the remainder appear to be novel. Some explanation of these phenomena was given in the previous chapter, but it is useful to examine the applicability of existing theories and develop new explanations where necessary. The remainder of this chapter is devoted to discussion of the mode of injection of charge carriers; excitation and amplification of acoustic waves; acousto-electric instabilities, relaxation effects, limits of the linear theory; the role of traps; electrical instabilities and the material variability.

6.2 Injection of charge carriers

The current voltage characteristics recorded when the specimen is uniformly illuminated (b) or locally illuminated with a laser beam (f) showed no current saturation effect, but instead the current increased with increasing applied voltage. Such I-V characteristics have been reported previously for semi-insulating CdS platelets and the rise in the current has been attributed to the injection of charge carriers at the electrodes.[101] Obviously, with an increase of the applied voltage, the density of injected charge increases and the quasi-Fermi electron level at the cathode is displaced into the conduction band. This non-equilibrium charge is partially captured at traps which thereby change their charge distribution and become effective scattering centres for conduction electrons.

6.3 Excitation of acoustic waves

Acoustic waves in solids can be obtained either by injection from a transducer or by amplifying the thermally generated waves already present. The latter process depends on the interaction between a mobile

electron and an acoustic wave, and is possible in semi-conductors consisting of II-VI compounds such as CdS (or ZnO and III-V compounds such as GaAs and InSb). The criterion which determines whether or not a crystal is piezoelectric is the existence of a centre of symmetry. If a crystal lacks this property, the application of stress can separate the centres of the positive and negative charges and a dipole is produced. The converse effect also exists in that an electric field produces a stress within the crystal. CdS has a wurtzite structure (point group symmetry 6mm), and consists of two interpenetrating hexagonal lattices, one of cadmium atoms and the other of sulphur atoms. The basal plane of sulphur atoms does not lie mid-way between two basal planes of Cd atoms, and so this crystal has an obvious lack of symmetry, and the opposite directions of the hexagonal axis are not equivalent. Thus, the sign of an induced piezoelectric field is reversed by changing the sign of an applied stress. Each atom sits at the centre of a tetrahedron of atoms of the other type under equilibrium conditions, but the charge centres separate when stress is applied. In the case of hexagonal crystal the c-axis is the polar axis, and acoustic waves, longitudinal or transverse to that axis, produce electron displacements in the c-direction. So an acoustic wave with the appropriate strain propagating in a piezoelectric solid can affect the free electron not only by disturbing the periodicity of the lattice but also by producing a macroscopic electric field.

The coupling between mechanical and electrical stored energy in a particular crystal can be described in terms of an electromechanical coupling constant K, where

$$K^2 = e^2/\epsilon C$$

e, ϵ and C are piezoelectric, dielectric and elastic constants respectively

for the crystal.[45] K^2 arises in a calculation involving coupling between mechanical and electrical energy in piezoelectric materials.[31] The K^2 for II-VI compounds increases as the relative weights of the atoms increases.

In a semi-conductor, the carriers are free to move under the action of a piezoelectric field and if the frequency ω of the acoustic wave is much lower than the dielectric relaxation frequency $\omega_c (=\sigma/\epsilon$ where σ is the conductivity and ϵ is the permittivity) the carriers will be able to redistribute themselves quickly enough for their space charge field to cancel out the piezoelectric field of the acoustic wave. The crystal then behaves as if it were non-piezoelectric, although the carriers will be oscillating about their mean position with a frequency ω, and the acoustic wave is attenuated much more rapidly than in an insulator as joule heating is produced by the space charge field. However, the condition $\omega > \omega_c$ is more directly relevant to the present experiments where the electrons do not move fast enough to cancel out the piezoelectric field except in effects (b) and (f).

6.4 Ultrasonic wave amplification

Amplification of an acoustic wave has been observed in all the experiments described (a) to (g). The way in which an acoustic wave is amplified or attenuated by piezoelectric interaction depends on the scattering mechanism affecting the electrons. A measure of the strength of the latter is the collisional mean free path l, and this length must be compared with the wave length $\frac{1}{K}$ of the wave. If $Kl \gg 1$ the problem is essentially one of the electron and wave interacting in isolation. Near to room temperature it is found that $Kl \ll 1$ so that many scattering events occur per wave length, the electric field

associated with the wave then produces a macroscopic ohmic current which tends to pile electrons in the potential troughs of the wave and denude the crest. The resultant space charge tends to screen electrostatically the wave field and to reduce the electron-acoustic flux interaction. The characteristic length is the Debye length $L = (K_B T \epsilon / q^2 n_0)^{\frac{1}{2}}$ where K_B is the Boltzmann constant, n_0 the equilibrium electron density and T is the temperature. If $KL \ll 1$, the piezoelectric field is largely screened out, whereas if $KL \gg 1$, the field is unscreened but an electron is influenced by many waves at once and since the fields are oscillatory, the net effect tends to zero. In both cases, the piezoelectric interaction is weak. Thus, although the mere interaction is frequency independent, the effect of screening is to maximise the interaction for waves with $KL \approx 1$. The electron density in the material examined is of the order of 10^{12}-10^{13} cm^{-3} giving a Debye length at room temperature of around 10^{-5} cm. The frequency at which the interaction is a maximum is about 10^9 Hz.

A major factor affecting the net transfer of momentum between electron and wave is the average drift velocity of the electrons relative to the velocity of sound. If the drift velocity is less than V_s (velocity of sound in solid) the wave attempts to drag the electrons along with it and becomes attenuated as a result. On the other hand, if the drift velocity is greater than V_s, electrons attempt to increase the momentum of the wave and the wave is amplified in the absence of lattice loss. The formal expression for the attenuation is given in Equation (32). The maximum attenuation (or gain) is realized at the frequency $\omega_m^2 = \omega_C \omega_D$ (Appendix II). Fig. 1A shows curves of attenuation plotted against for various conductivities, at frequency ω_m.

The high mobilities of electrons in III-V compounds appears at first sight to reduce the threshold field E_{th}. In bulk grown GaAs, $\mu \simeq 6{,}000$ $cm^2V^{-1}sec^{-1}$ and E_{th} is about $60V/cm^{-1}$ whereas in CdS, where $\mu \simeq 300$ $cm^2V^{-1}sec^{-1}$, E_{th} is about 800 V/cm^{-1}. However, this advantage is opposed by the greater lattice loss in GaAs and the drift velocity required to reach the maximum amplification condition at a given electron density is about 24 times greater in GaAs than in CdS, since the diffusion constant D is 24 times as large. With n, the electron density is about $10^{13}cm^{-3}$, V_o in GaAs must be greater than $10^7 cm\ s^{-1}$. At such high velocities the electrons pick up so much energy from the electric field in a mean-free path that they are no longer in thermodynamical equilibrium with the lattice. Then hot-electron effects such as Gunn effect and impact ionization make the achievement of the resonant amplification condition impracticable. Despite these effects it is many times easier to study acousto-electric instabilities in III-V compounds since the amplification process is less rapid and is more amenable to detailed study. On the other hand, the large amplification of thermal waves in CdS has been found to result very easily in permanent damage or complete destruction of the specimen.

6.5 Acousto-electric instabilities

In the course of investigation this type of instability has been observed in all the cases except (b) and (f). It has been seen that by applying a high voltage pulse to produce an electric field in a CdS specimen parallel to the $< 110 >$ direction, the transverse acoustic waves propagating along the length of the specimen axis produce a longitudinal electric field by the piezoelectric effect. Below the

threshold voltage for acoustic amplification, the current at all times is proportional to the applied field. Above the threshold voltage the current remains ohmic for an incubation time of the order of 1μsec, but which often decreases with increasing field. The current then drops to about its value at the threshold field and remains more or less constant for a short period before rising to about the ohmic value. This variation with time is then repeated for as long as the voltage pulse is applied. The period of oscillations has been seen to be the time for an ultrasonic wave to travel from one end of the crystal to another; the time taken by the acoustic wave to travel from the position of the high field region to the anode end of the specimen. Probing the electric field along the crystal while the current is saturated at its low level shows the electron flow with the velocity of sound. An acousto-electric domain comparable in size with the specimen, is spontaneously generated by the acoustic amplification process and is destroyed when it reaches the anode. Its periodic generation and destruction is responsible for the current oscillation in semi-insulating CdS. During domain propagation, the current maintains the saturation value and returns to the ohmic value when the domain arrives at the anode and disappears. It was seen in the experiments that the domains produced in the samples were so intense that the crystal was often permanently damaged near the anode, where collision with the boundary takes place. One can understand the mechanical effects which are produced by the intense packets of acoustic flux, associated with the domain. All waves carry momentum, so it is not surprising that the anode end is subject to an intense "radiation" pressure when it reflects the domain. An intense acoustic flux may form by interaction with drifting electrons in the direction of the acoustic

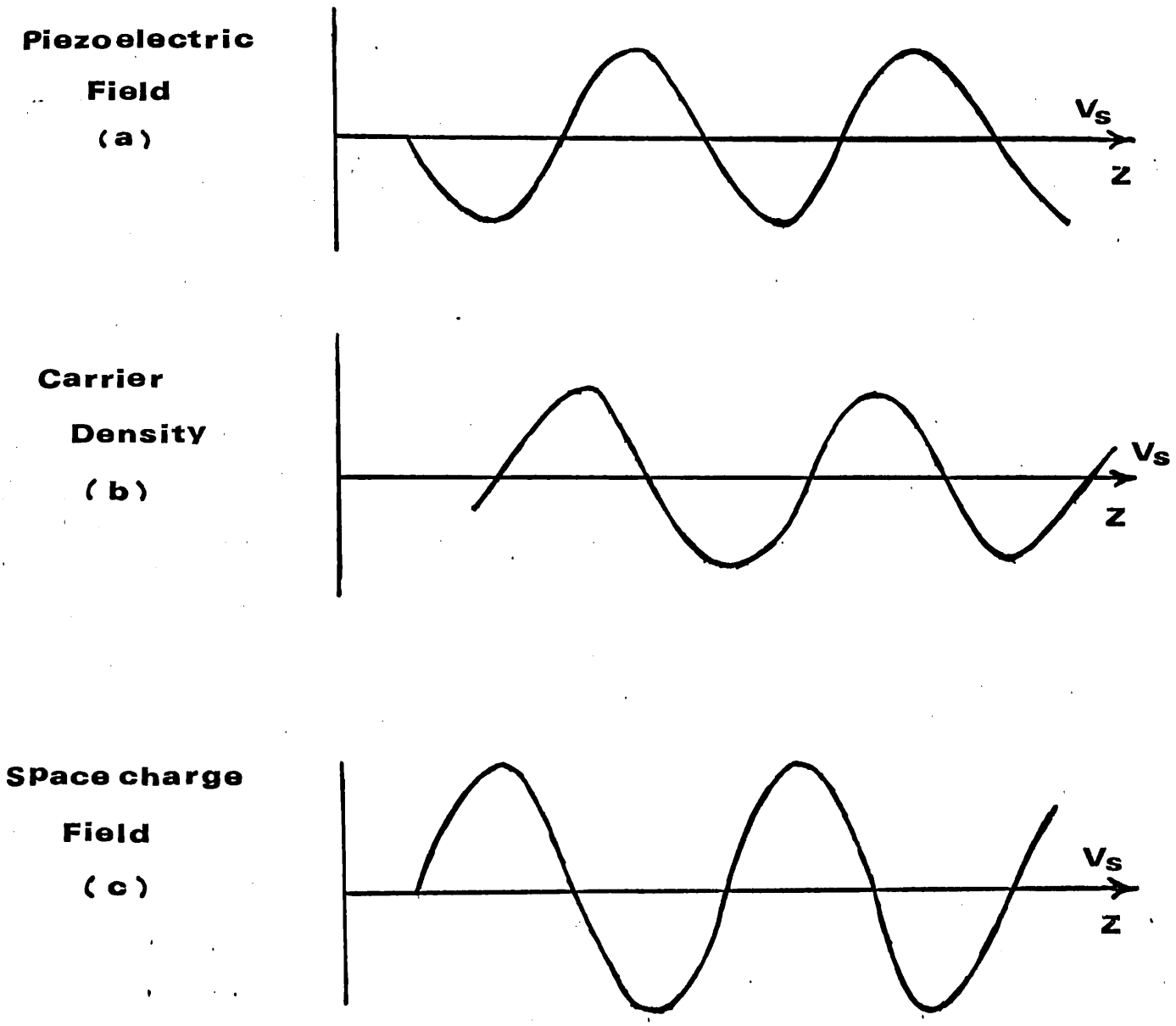

Fig.58 An piezoelectric semi-conductor, with the carriers drifting at the velocity of sound.

wave, the position of the carrier bunches with respect to net piezoelectric field is changed, and so the energy transfer is altered. When the carriers drift at the velocity of sound, they are bunched at the position of minimum potential energy, and there is no energy transfer. The situation for a longitudinal piezoelectric field is shown in Fig. 58, which shows the piezoelectric field, the carriers density modulation it produces and the space charge field due to the bunched carriers, which opposes the applied piezoelectric field. The density of carrier varies about a mean value, and the piezoelectric field is $-\frac{\partial V}{\partial x}$, where V is the potential of the wave. In Fig. 58 the electric field and the space charge wave are 90^{o} out of phase, so that no energy dissipation is taking place. If the phase is not 90^{o}, energy and momentum transfer take place. When the drift velocity of the carriers V_d, is greater than the acoustic velocity, then the carriers lose momentum to the acoustic wave and it is amplified.

The forward momentum of the carriers is depleted by an amplification process.[110] This effect produces flow counter to the direction of drift, and is known as the acousto-electric current. Consequently, the I-V characteristics of a semi-insulating CdS specimen has a saturation region[74] which develops when the carriers are drifting faster than the velocity of sound as shown in Fig. 56. This is what has happened when the momentum given up by the electrons drifting faster than the velocity of sound amplifies the random motion of the lattice, and results in a high level of acoustic noise. In 1957 Weinreich[110] first showed that the momentum given by the electrons to the waves may be described in terms of an acousto-electric current J_{ae}, to be added algebraically to

the ohmic current and of strength $J_{ae} = -\mu aW$, where μ is the mobility, a the electronic power gain coefficient and W the energy density of the wave. Thus, when a is positive, the acousto-electric current is opposed to the ohmic current. When there is attenuation, a is negative and the acousto-electric current reinforces the ohmic current. The measurement of the acousto-electric current provides a measure of the intensity of the flux, if the mobility and gain coefficient are known.

6.6 Relaxation Effects

In a piezoelectric semi-conductor, the available acoustic gain is a function of the conductivity modulation. Any type of influence which tends to debunch the carriers therefore tries to reduce the gain. The important mechanism involved are the dielectric relaxation and diffusion. The dielectric relaxation frequency $\omega_c (= \frac{\sigma}{\epsilon}$, where σ is the conductivity and ϵ is the dielectric constant) defines the rate at which charged carriers in a solid can move, under the influence of a local electric field, in an attempt to cancel that field.

Considering an acoustic wave with angular frequency ω, which is to propagate in a solid, in the absence of a drift field.

If $\omega \ll \omega_c$, the carriers can move fast enough to cancel the piezoelectric field, and sit exactly in the potential wells, so that they do not interact with the acoustic wave. On the other hand, if $\omega \gg \omega_c$ the distribution of carriers is not disturbed by the wave. When the drift field and diffusion effects are absent, the interaction between the acoustic waves and bunched carriers is maximised when $\omega = \omega_c$.[50] In CdS material, at frequencies of 1GHz and above, a suitable resistivity is $10^3 \Omega\text{-cm}^{-1}$ when a drift field is present, the condition for maximum interaction appears to be $(1 - \frac{V_d}{V_s})\omega = \omega_c$.

The random motion of the carriers tends to cause the bunches to decay by outward diffusion. When the frequency increases and the

acoustic wave length , falls the concentration gradient between carrier bunches increases and diffusion out of bunches become significant. If the number of carriers crossing unit area per unit time is N_c, and the concentration gradient is grad (N), where N is the particle density then $N_c = D_n \cdot \text{grad}\ (N)$, where D_n is the diffusion constant and is defined as $D_n (= \mu K T_B / q$ where μ is the carrier mobility, K_B is Boltzmann's constant, T is the absolute temperature and q is the charge on an electron).[111] There is then the possibility of local non-equilibrium concentration of carriers to decay with a time constant $\tau_d \sim \lambda^2 / D_n$, where λ is the distance over which a concentration gardient exists and it can be identified with the acoustic wave length.

Diffusion effects become important if τ_D (diffusion time) becomes less than the period of the ultrasonic wave, i.e. $\frac{\lambda^2}{D_n} < \frac{1}{\omega}$ or $\frac{\omega^2 \lambda^2}{D_n} < \omega$, where $\omega\lambda$ is the order of the acoustic wave velocity V_s, and (V_s^2 / D_n) has been defined as the diffusion frequency, ω_D. Diffusion becomes important when $\omega > \omega_D$. Deep understanding of the relaxation effects can be visualised by evaluating,

$$\frac{\omega_c \omega_D}{\omega^2} = \frac{\sigma}{\epsilon} \cdot \frac{V_s^2}{D_n} \cdot \frac{1}{\omega^2} = \left(\frac{\lambda}{2\pi L_D}\right)^2 \quad \text{where}$$

$L_D = (\epsilon K_B T / q_n^2)$ is the Debye length.[74]

When $\lambda \sim L_D$ diffusion effects become important and bunching of carriers on a scale much smaller than L_D (i.e. $\lambda \ll L_D$) will tend to be smeared out by the thermal motion of the carriers. When $\lambda \ll L_D$ the piezoelectric field is not screened by the carrier bunches and momentum transfer between the carriers and acoustic wave starts to decrease when $L_D > \lambda$ i.e. when $\omega > (\omega_c \omega_D)^{\frac{1}{2}}$.

6.7 Effects of trapping

The linear theory has been derived by assuming that the relaxation time of the carriers in the trap is much less than the period of the acoustic wave. If it is not, then the bunched carriers in traps are out of phase with those in the conduction band. So the trapping factor f_t becomes complex and Ishiguro, Uchida, Sasaki and Suski[112,113] have applied this condition to the White theory. The imaginary part of f_t leads to a phase shift between current density J and the net piezoelectric field E_p, which reduces the magnitude of the interaction. The size of the out of phase component is proportional to the drift field, so that the reduction in the electron phonon is more marked in the gaining region than in the attenuating region.

If only one kind of trap is assumed to exist and n_1 and n_2 are the concentrations of the free and trapped bunched electrons respectively, τ is taken as the trap relaxation time and the o subscript refers to the parameters when $\tau \ll \frac{1}{\omega}$

$$n_s = n_1 + n_2 \qquad n_{so} = n_{10} + n_{20}$$

$$n_1 = f_t \cdot n_s \qquad n_{10} = f_{to} \cdot n_{so}$$

$$n_2 = (1 - f_t)n_s \qquad n_{20} = (1 - f_{to})n_{so}$$

$$\frac{\partial n_s}{\partial t} = -\frac{(n_2 - n_{20})}{\tau}$$

By using $$\frac{\partial}{\partial t} = j\omega$$

$$f_t = \frac{f_{to} - j\omega\tau}{1 - j\omega\tau} = \frac{b.f_{to}}{1 + ja}$$

f_{to} is real and is defined by Hutson and White[5] as the ratio of the change mobile space charge to the change of total space charge, when the latter causes a small change of the electron Fermi level.

When $\omega\tau \ll f_{to}$, then $f_t \approx f_{to}$

The second statement in the Equation is written for convenience, so that $\gamma = 1 + bf_{to}\mu E_o/V_s$ and a is the ratio of $Re(f_t)/Im(f_t)$.

Therefore Equation (35) is modified and it can be shown that,

$$\frac{\alpha_{max}\ (gain)}{\alpha_{min}\ (loss)} = \frac{\sqrt{1 + a^2} - a}{\sqrt{1 + a^2} + a}$$

White suggested that variation in resistivity in the path of the acoustic wave would tend to reduce the gain more than the loss. But in practice, both effects are likely to be present.

6.8 Limits of the linear theory

White's analysis is valid only if the bunched electrons must be only a small fraction of the total free carrier concentration in the conduction band,[50] i.e. $f_t.n_s \ll n$

Using the equations $\sigma = nq\mu$ and

$$n_s = \frac{\omega_{Ce}}{q.V_s} \cdot \frac{S}{r + j(\frac{\omega_C}{\omega} + \frac{\omega}{\omega_D})}$$

it can be proved that this condition is equivalent to $S \ll V_s/f_t.\mu.e$

In practice this means that the value of strain must be less than 10^{-5}.

The condition for linearity, i.e. $|\alpha| \ll \omega/V_s$, which means that the gain per unit length must be small. For linear approximation it is essential to neglect the term $q\mu n_s E$ from the current density expression J, given by:-

$$J = q(n_o + f_t\ n_s)\ \mu E + q\ D_n \frac{\partial n_s}{\partial x}$$

But, when bunching of electrons is large, this term cannot be ignored. Pure harmonic wave is no longer a solution and each variable is then determined by a Fourier series. Each frequency component may interact with the others by virtue of the non-linearity and appreciable harmonic generation may occur.

6.9 Electrical instabilities

During the course of investigation, relaxation type of high frequency current oscillations have been observed when a high voltage is applied to a specimen and its inter-electrode area as in Case (b) is uniformly illuminated or in Case (f) with local illumination. It was seen that below the threshold voltage for current oscillation the current falls below the linear ohmic relation, but at high voltages the current becomes above the linear value, with an exponent nearly equal to 2. Such a current voltage dependence could occur with a non-uniformity in electric field along the length of the crystal. The existence of this non-uniformity is indicated by the electric field distribution in the specimen. The proposed mechanism in Chapter 5 is in agreement with a whole series of experimental results. The appearance of these current pulses can be explained by occupation and emptying of trap states in the crystal.

The avalanche type of increase in the current followed by a fall off suggests that electron capture by traps plays an important role. This avalanche type liberation of electron from the traps leads to an instantaneous increase of the current flowing through the sample, followed by occupation of traps and a decrease in the mobility of the free carrier.

6.10 Material variability

In all experiments it was found that the material inhomogeneity had conductivity influence on the phenomena observed. Semi-insulating CdS material with a dark conductivity about $10^{-7}\Omega^{-1}cm^{-1}$ is commercially available and since such material is generally photo-conductive, the required conductivity in the range of 10^{-3} to $10^{-5}\Omega^{-1}cm^{-1}$ can be easily achieved with suitable illumination shown in Table 2.

Two sources of material were used in the present investigation, namely G.E.C. and Imperial College, London. The photoconductivity in both materials has been achieved by controlling the stoichiometry of the crystal during its growth.[104]

During the present investigation it has been seen in experiment type (a) that two specimens, TRS_{12} and TRS_{13}, cut from a single crystal had dark conductivities as high as $10^{-4}\Omega^{-1}cm^{-1}$. It seems quite possible to grow CdS crystals of any required conductivity in order to obtain oscillations without illumination.

Material used from both sources is soft and data supplied by G.E.C. shows a dislocation count of about $10^{14}/cm^2$. Such a value makes the crystal rather more difficult to cut and polish as it is prone to damage. The mechanical handling involved such as lapping and polishing can produce damage to the crystal, involving the regions of structural disorder very close to the surface and rather deeper regions of high dislocation density, which tend to introduce a region of low conductivity which affects both the conductivity and the value of K^2. Above all there is every possibility that trapping levels are being introduced affecting μ_p and μ_n via a scattering process.

7. Conclusions

During the course of the present investigation a wide range of physical phenomena have been produced by different experimental conditions. Despite the variability of the material, some new phenomena have been observed and the rest have been compared with the results of other workers. An attempt has been made to discuss all the major phenomena observed and to explain the effects observed with various types of illumination.

One of the contributions of the present investigation is to an understanding of the phenomenon of current oscillations in a single semi-insulating CdS crystal when a high voltage pulse is applied in complete darkness. Measurement of the electric field shows that the period of oscillation is approximately equal to the time taken for a sound wave to travel between the position of the observed high field and the anode end of the specimen. The accompanying current saturation has been attributed to the formation of a stationary high field domain. It is suggested that one of the trapping levels observed in Fig. 27(a,b) plays an important role in the phenomena observed. Such traps are produced if, during the growth of crystal, the appropriate impurity is introduced into the material. The slow ionization rate, accompanying the slow rise of current with applied voltage, has been attributed to the majority carriers travelling at the sound velocity and being unable to take part in the ionization process. The additional carriers created by fast electrons are also velocity limited and the ionization rate is reduced by the ratio of the velocities of fast electrons to that of sound limited electrons. However, the phenomena observed confirm the possibility of growing CdS crystals of conductivity of 10^{-5}-10^{-3} ohm^{-1} cm^{-1} in order to dispense with the use of illumination increase the conductivity of the material to the range where maximum acoustoelectric interaction

occurs.

The results of investigations on semi-insulating CdS material obtained from different sources showed considerable variation of behaviour. Reversing the polarity of the voltage pulse applied produced results which differed from one specimen to another, indicating that irregularities are present in the material. Measurements of the resistance of the specimens using light obscuring strips at different positions showed similar variations. These irregularities affect the frequency of the current oscillations. In specimens having the anode end masked, the period of the current oscillations is simply the one-way transit-time of the acoustic flux.

When oscillations were produced by obscuring a strip of the specimen an irregularity in the material near to the negative edge of the shielded region caused a particular frequency of oscillation. The frequency depends to some extent on the width of the shielded region. The oscillation frequency often decreased as the distance of the shielding strip from the anode increased. The current oscillations often become damped and disappear eventually when the distance is between $\frac{L}{3}$ and $\frac{L}{4}$.

The field measurements under amplifying conditions revealed the existence of extremely high electric fields near to the anode end of the specimen when the positive end was shaded. However, in specimens where non-uniform illumination was produced by a ceramic strip, high electric fields do exist in the shaded region. These high fields produced arcing in these regions followed by electrical breakdown of the material.

Obscuring a narrow strip perpendicular to the length of the specimen and applying a high voltage pulse resulted in oscillations with major changes in current. Low frequency current oscillations were recorded after the current had fallen to its final steady state value. The measurements of the conductivity of the material made after the

application of a high voltage pulse and its dependence on the various illumination intensities also indicate the presence of inhomogeneities in the material. CdS specimens showed field instabilities when the applied voltage was high enough to cause the differential resistivity to become negative, because the carrier mobility decreased with the electric field. In an experiment to observe the scattering of light from an He-Ne laser by acoustic wave packets produced in the specimen the transmitted light showed weak scintillations at a frequency of a few Hz, consistent with the existence of slowly moving domains. These are said[75] to arise when the crystal changes from n-type to p-type conductivity. Injection of holes may occur from inhomogeneities present in the material. The electric field increased suddenly near the cathode and also at 1mm from the anode.

The best way at present to increase the conductivity of cadmium sulphide crystal is by introducing shallow donors during its growth. During the investigation, shallow donors at concentrations of 10^{10} to $10^{13}/cm^{-3}$ have been observed at various levels close to the conduction band. Apparently the inclusion of these donors has not increased the conductivity 10^{-7}-10^{-6}ohm^{-1}cm^{-1} to 10^{-5}-10^{-3}ohm^{-1}cm^{-1} apart from the few specimens already mentioned. The trapping levels affect μ_D and possibly μ_n via a scattering mechanism.

High frequency non-sinusodial current oscillations were obtained when the specimens were uniformly illuminated or locally illuminated with an He-Ne laser beam. The recorded I-V characteristics showed no current saturation. Instead, the current increased with increasing applied voltage. The rise of the current is attributed to the injection of charge carriers at the electrodes. With the increase of the applied voltage, the density of the injected charge increases and the quasi-Fermi

level at the cathode is displaced into the conduction band. Such non-equilibrium charge is partially captured at traps which thereby change their charge distribution and become effective scattering centres for conduction electrons. The appearance of these high-frequency saw-tooth current oscillations is attributed to the occupation and emptying of trap states. The absorption spectra of specimens indicated the presence of active trapping centres at levels as low as 0.08eV with a continuous band between 0.19eV and 0.21eV. The occupation of these states by charge carriers leads to a decrease of the electrical conductivity of the material as a result of a change in the mobility of free carriers. A consequence of the decrease in mobility could be the field liberation of electrons from traps. The very large increase in the resistance of the contact region of the specimen leads to a redistribution of the potential over its length. The occupied traps are in an electric field of increased intensity which increases the probability of their being emptied. The relaxation type of oscillations in CdS can exist as long as the traps are filled by injected charge and subsequently emptied by field ionization or impact ionization. These oscillations are dependent on temperature, illumination intensity and field intensity.

Numerous investigations have been carried out on the study of the amplification of ultrasonic waves in single cadmium sulphide crystals and the process of the interaction between acoustic waves and conduction electrons. If the electrons in n-type material were given a drift velocity V_d greater than the velocity of sound V_s by an external electric field E, the attenuation of the ultrasonic waves became negative and amplification resulted. This amplification process applies both to acoustic waves, which are introduced into the crystal using suitable

transducers, and to the fundamental lattice vibration or phonons which exists within the crystal. An effect of this electron-phonon interaction can be demonstrated very easily by measuring the current/voltage curve of specimens. In the present work it was seen that an abrupt change in I/V slope occurred at the critical field E_C corresponding to $V_d = V_s$. This is current saturation which was first reported by Smith and is due to the energy being transferred from the drifting electrons to certain of the lattice vibrations in the crystal under uniform illumination.

Several compounds of II-VI and III-V groups are piezoelectric and their theoretical behaviour as acoustic amplifiers can be compared. The significant properties are the electromechanical coupling constants, available gain and power handling capacity. The drift power consumed per unit gain for the optimum condition is

$$\frac{P_{dc}}{G} = \frac{\epsilon V_s^3}{4.34(\mu K^2)} \times \frac{\omega}{\omega_D}$$

The quantity μK^2, which occurs in the denominator, is described as the merit factor and a high merit factor indicates low power consumption per unit gain. With CdS the value of μK^2 is 11, whereas for ZnO it is 18. The important advantages of ZnO in acoustoelectric interaction can be listed below:

(i) The value of K = 0.3 is higher compared to CdS, whereas K = 0.19, so has the ability to gain higher power outputs. Alternately thinner crystals can be used. The higher gain also results in a much shorter build up time for oscillations (in the range of 1μsec.,).

(ii) The shear velocity of sound is greater which means higher frequency operation at a given frequency.

(iii) The lattice attenuation is not serious up to frequencies of about 14GHz.[105]

(iv) The material is harder than CdS and therefore easier to process.

For acoustoelectric interaction ZnO crystals doped with lithium or copper are commercially[106] available in the range 10^{-5}-10^{-3} ohm^{-1} cm^{-1}, so that an external light source is no longer required. Recent reports[114] have appeared of an acoustoelectric oscillator made from doped ZnO and operated in the continuous wave mode at room temperature at frequencies up to about 5GHz. However, ZnO is not without material problem since grown crystals of ZnO also show a marked non-uniformity in conductivity up to four orders of magnitude and a careful heating process is required to reduce the non-uniformity to within one order of magnitude.[107] Also, Hemphill[108] has reported significant K^2, variation in insulating ZnO. It is however concluded that much emphasis on the growth of the material has to be made in order to achieve the best results from CdS as a photoconductor and acoustoelectric oscillator.

APPENDIX I

Acoustoelectric currents

The current density J, if we neglect the carrier diffusion, is given by:

$$J = q\mu\left[n(z) + f\, n_s(z)\right]\left[E(z) + E_1(z)\right] \qquad (1)$$

$n(z)$ = carrier density at z

We assume a space time dependence of $e^{j(Kz-\omega t)}$. The d.c on steady state part of J is then given by:

$$J_{d.c} = q\mu n(z)\, Ez + q\mu \tfrac{1}{2}\, Re(f n_s E_1^*) \qquad (2)$$

The second term is the acoustoelectric current J_{ae};

$$J_{ae} = q\mu \tfrac{1}{2} Re(f n_s\, E_1^*)$$

From equation , the amplitude of the time varying part of J is given by,

$$J_1 = -q\left(\frac{K}{\omega}\right)^{-1} n_s = -qV_s n_s$$

When weak coupling is assumed, i.e. $V_s \approx \left(\frac{K}{\omega}\right)^{-1}$ then

$$J_{ae} = -\tfrac{1}{2}\frac{\mu}{V_s} Re(f\, J_1\, E_1^*) \qquad (3)$$

Acoustoelectric current considered here is due to a single acoustic mode of frequency ω. But if there is a whole range of frequencies as is the case with thermal acoustic noise, then the acoustoelectric current would be the sum of all the acoustoelectric currents due to each frequency mode.

Then we have

$$J_{ae} = -\tfrac{1}{2}\frac{\mu}{V_s} Re \sum f\, (J_1 \omega E_1 \omega^*) \qquad (4)$$

If $f\omega$ is real and constant over all frequencies then,

$$J_{ae} = -\tfrac{1}{2} f \frac{\mu}{V_s} \mathrm{Re} \sum (J_1 \omega E_1 \overset{*}{\omega})$$

By the principle of energy conservation, the average electrical power absorbed or delivered by the carriers is equal to the rate at which acoustic power increases or decreases.

This is given by:

$$\frac{dU}{dt} = -\tfrac{1}{2} \mathrm{Re} \sum_{\omega} (J_1 \omega E_1 \overset{*}{\omega}) \tag{5}$$

Where U = acoustic energy intensity

Therefore

$$J_{ae} = f \frac{\mu}{V_s} \frac{dU}{dt} \tag{6}$$

which is the Weinreich's relation.

So,

$$\begin{aligned} J &= q\mu n_{(z)} E_{(z)} + J_{ae} \\ &= q\mu n_{(z)} E_{(z)} + f \frac{\mu}{V_s} \frac{dU}{dt} \end{aligned} \tag{7}$$

It follows that when the carrier drift and the acoustic waves are travelling in the same direction J_{ae} will oppose J when the acoustic waves are growing. J_{ae} will also oppose J if the acoustic waves are being attenuated while travelling in the opposite direction to the carriers.

APPENDIX II

The maximum gain condition for acoustic wave amplification[50]

The maximum gain which occurs at a frequency can be found by putting

$$\frac{\partial \alpha}{\partial \omega} = 0$$

and solving it for ω.

$$= \frac{K^2 \omega_C}{2V_s \gamma}\left[\frac{1}{1 + \frac{\omega_C^2}{\gamma^2 \omega^2}\left(1 + \frac{\omega^2}{\omega_C \omega_D}\right)^2}\right]$$

$$\therefore \quad \frac{\partial \alpha}{\partial \omega} = \frac{K^2 \omega_C \gamma}{2V_s} \frac{\partial}{\partial \omega}\left[\frac{\omega^2}{\omega_C^2 + \left(\gamma^2 + \frac{2\omega_C}{\omega_D}\right)^2 + \frac{\omega^4}{\omega_D^2}}\right] = 0$$

Therefore,

$$2\omega\left[\omega_C^2 + \left(\gamma^2 + 2\frac{\omega_C}{\omega_D}\right)\omega^2 + \frac{\omega^4}{\omega_D^2}\right]$$

$$- \omega^2\left[2\left(\gamma^2 + 2\frac{\omega_C}{\omega_D}\right)\omega + 4\frac{\omega^3}{\omega_D^2}\right] = 0$$

From where we get,

$$\boxed{\omega^2 = \omega_C \omega_D}$$

Fig. 1A shows the V_s curves for various conductivities with this condition.

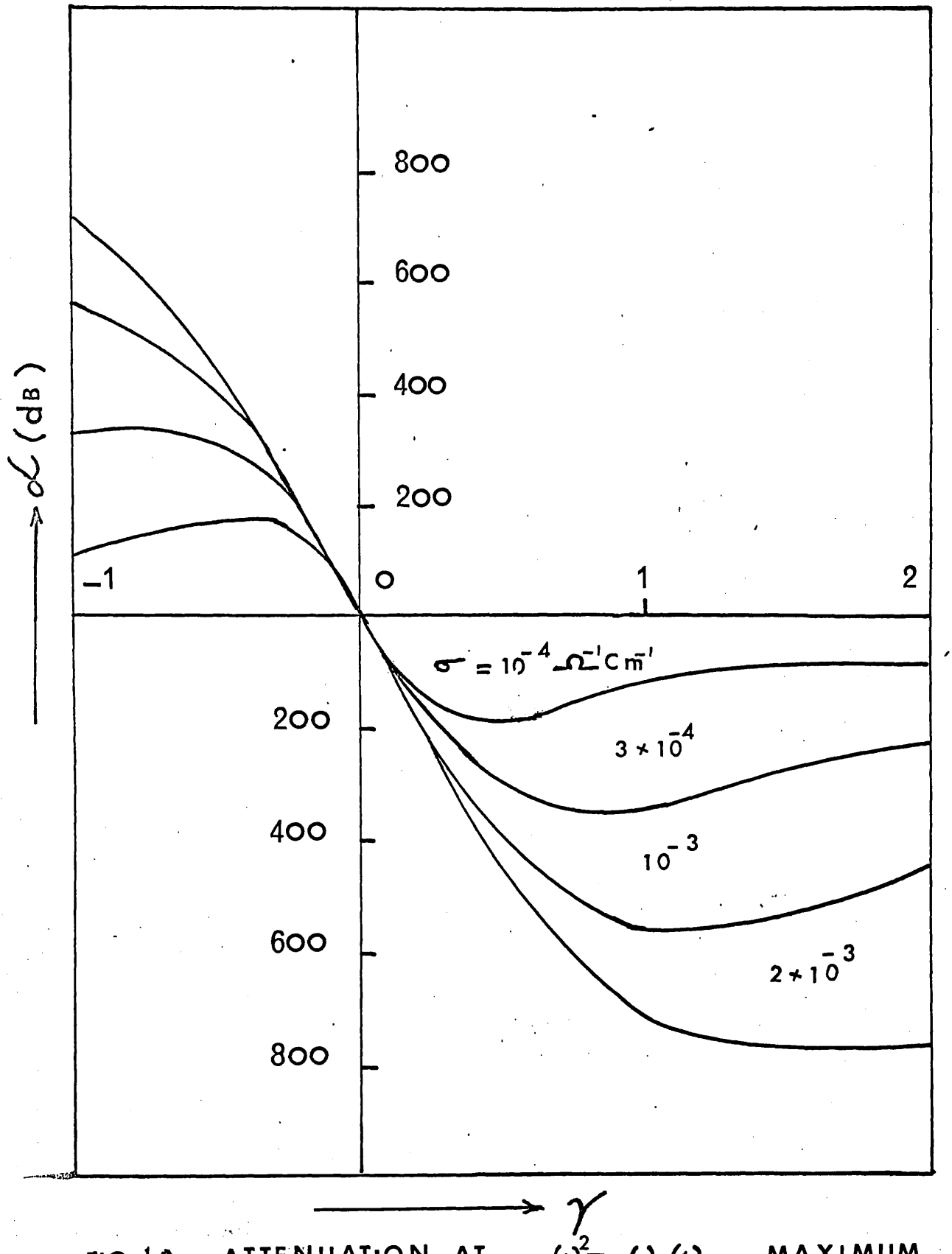

FIG. 1A ATTENUATION AT $\omega^2 = \omega_c \omega_d$ MAXIMUM GAIN CONDITION

APPENDIX III

High voltage pulse generator

A positive input square pulse of +33V is taken from Pulse Generator "SOLARTRON" type GO 1101-2 and is amplified by the help of a conventional pulse amplifier, using an EL34. Its associated circuit is shown on the lefthand side of Fig. 2A. A floating D.C voltage of about +500V for EL34 is supplied from a separate unit, with its circuit shown in Fig. 3A. The H.V. Pulse Generator using a thyeetron type FX2505 with its associated circuit is shown in Fig. 2A. The pulse length has been adjusted to 100μsec., by using the lumped delay line shown in circuit diagram 2A. The high impedence delay cable RG-65A/U is used to obtain a 10μsec., pulse. The characteristics of this cable are:

Impedence = 950 Ω

Capacitance = 44 $\mu\mu$F/ft

Normal delay time = 0.042μ sec. per foot

Maximum operating voltage = 2KV

Outer diameter = 0.405"

The H.T. supply for FX2505 is taken from another unit and its associated circuit is shown in Fig. 4A.

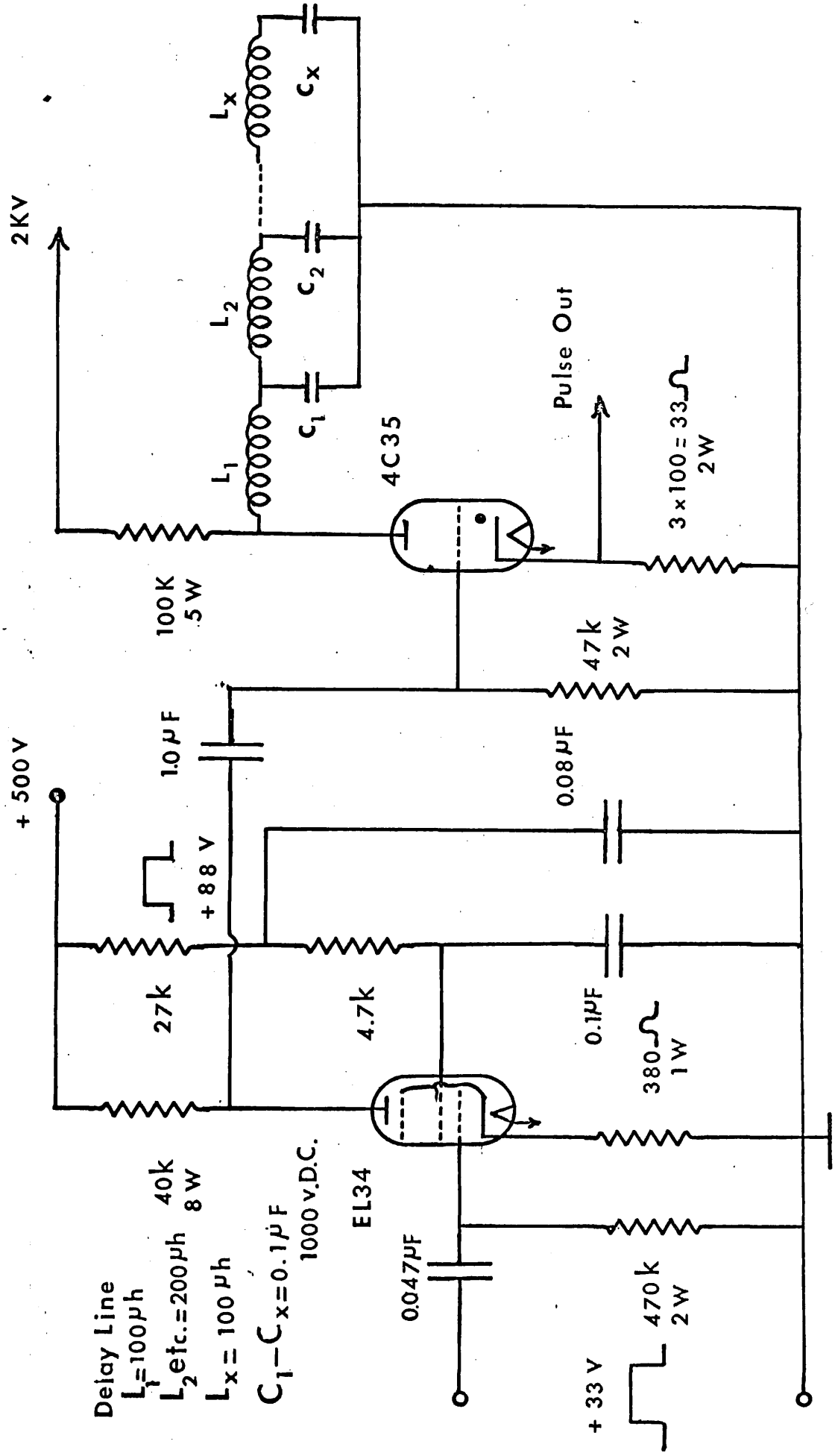

Fig. 2A H.V. Pulse Generator Circuit

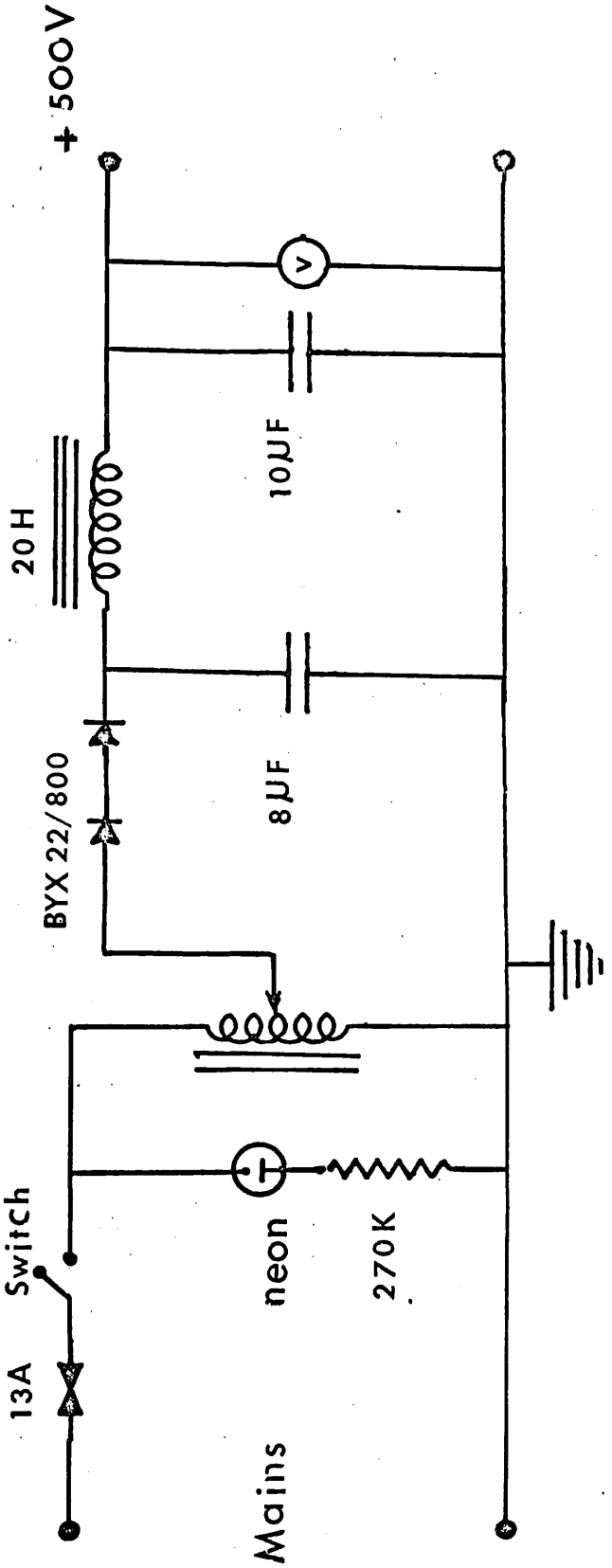

FIG. 3A D.C. POWER SUPPLY

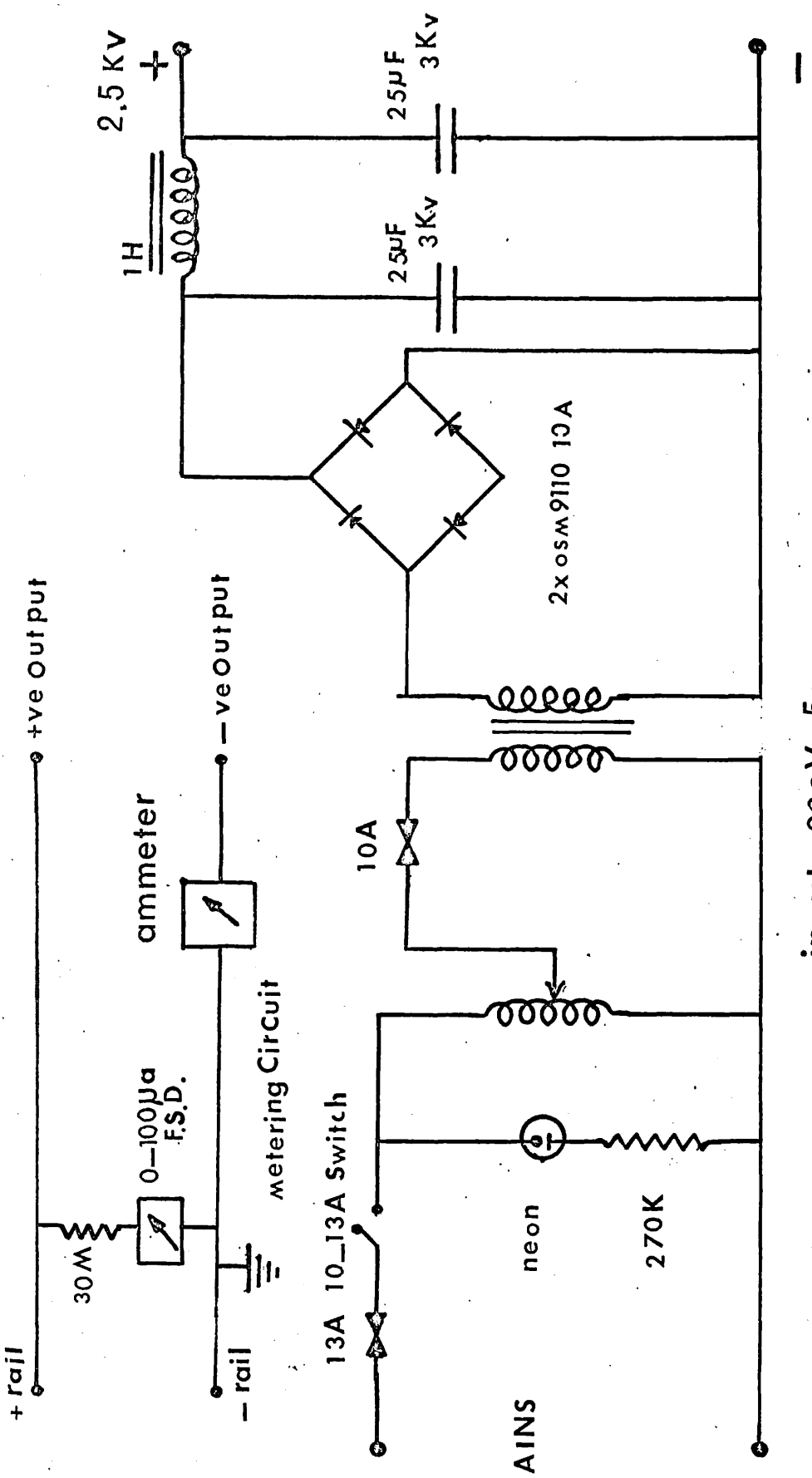

FIG. 4A H.T. POWER SUPPLY

REFERENCES

1. Ancker-Johnson, B., R.W. Cohen and M. Glicksman; Phys. Rev., 124, 1745 (1961)
2. Glicksman, M. and M.C. Steele; Phys. Rev., 110, 1204 (1958)
3. Steele, M.C.; Bull. Am. Phys. Soc., Ser. 11,4: 28 (1959)
4. Steele, M.C. and Toshima; Japan J. Appl. Phys, 2, 381 (1963)
5. Mackay, K.G. and K.B. McFee; Phys. Rev., 91, 1079 (1953)
6. Glicksman, M. and M.C. Steele; Phys. Rev. Letters, 2, 461 (1959)
7. Louisell, W.H. "Radiation and Noise in Quantum Electronics", McGraw Hill, New York.
8. Sclar, N. and E.J. Burstein; Phys. Chem. Solids, 2, 1, (1957)
9. Bragg, W.L.; Phil. Mag., 39, 647 (1920)
10. Aminoff, G., Z. Krist; 58, 203 (1923)
11. Ulrich, F. and W. Zachariasen; Z. Krist., 62, 260 (1925)
12. Keffer, F. and A.M. Portis; J. Chem. Phys., 27, 675 (1957)
13. Jeffrey, G.A., G.S. Parry and R.L. Mozzi; J. Chem. Phys., 25, 1024 (1956)
14. Cesella, M.L.; Phys. Rev., 114, 1514 (1959)
15. Glasser, M.L.; J. Phys. Chem. Solids; 10, 229 (1959)
16. Rashba, E.I. and B.I. Sheka; Fiz. Tver. Tela, Collected Articles, 2, 162 (1959)
17. Birman, J.L.; Phys. Rev., 115, 1493 (1959)
18. Hopfield, J.J.; J. Phys. Chem. Solids, 15, 97 (1960)
19. Wilson, A.H.; 1953 'The Theory of Metals', (Cambridge University Press, Cambridge) p.8.
20. Rashiba, E.I.; Soviet Phys. Solid State 1, 368 (1959)
21. Thomas, D.G. and J.J. Hopfield; Phys. Rev., 116, 573 (1959)
22. Piper, W.W. and D.T.F. Marple; J. Appl. Phys. Suppl., 32, 2237 (1961)

23. Balkanski, M. and J.J. Hopfield; Phys. State Solidi, 2, 623 (1962)

24. Hopfield, J.J. and D.G. Thomas; Phys. Rev., 122, 35 (1961)

25. Piper, W.W. and R.E. Halsted, in: Proc. Intern. Conf. Semiconductor Physics, Prague, 1960

26. Samamoto, K; J. Phys. Soc., Japan, 18, 1224 (1963)

27. Bear, W.S. and R.N. Dexter; Phys. Rev., 135, A 1388 (1964)

28. Mahan, G.D. and J.J. Hopfield; Phys. Rev., Letters, 12, 241 (1964a); 135, A428 (1964b)

29. Thomas, D.G. and J.J. Hopfield; Phys. Rev., 116, 573 (1959)

30. Weinreich, G.; Phys. Rev., 104, 321 (1956)

31. Hutson, A.R. and D.L. White; J. Appl. Phys., 33, 40 (1962)

32. Weinreich, G.; Phys. Rev., 114, 33 (1959)

33. Hutson, A.R., J.H. McFee and D.L. White; Phys. Rev. Letters, 7, 237 (1961)

34. Pomerantz, M.; Phys. Rev. Letters, 13, 308 (1964)

35. Okada, J. and M. Matina; Jap. J. Appl. Phys., 3, 698 (1964)

36. Wang, W.C.; App. Phys. Letters, 6, 81 (1965)

37. Kikuchi, M.; Jap. J. Appl. Phys., 2, 812 (1963)

38. Kikuchi, M.; Jap. J. Appl. Phys., 3, 448 (1964)

39. Kikuchi, M.; Jap. J. Appl. Phys., 4, 233 (1965)

40. Hayakawa, H., M. Kikuchi and Y. Abe; Jap. J. Appl. Phys., 5, 734 (1966)

41. Silva, P.O. and R. Bray; Phys. Rev. Letters, 14, 372 (1965)

42. Okada, J. and H. Matino; Jap. J. Appl. Phys., 2, 736 (1963)

43. Ibuki, S. and K. Nojima; Jap. J. Appl. Phys., 4, 71 (1965)

44. Miya, M. and M. Terai; Jap. J. Appl. Phys., 5, 186 (1966)

45. Mason, W.P.; "Piezoelectric crystals and their application to ultrasonic", New York, Van Nostrand, 1950

46. Bauduin, P. and F. Buchi; Phys. Stat. Solidi, 17, 517 (1966)

47. Bauduin, P.; Phys. Letters, 23, 12 (1966)

48. Hartnagel, H. and R. Gay; Phys. Letters, 24A, 158 (1967)

49. Gay, R.K.L. and H. Hartnagel; Sol. Stat. Electr., 11, 407 (1968)

50. White, D.L.; J. Appl. Phys., 33, 2547 (1962)

51. Greebe, C.A.A.; J. Philips Res. Repts., 21, 1 (1966)

52. Blötekjaer, K. and C.F. Quate; Proc. I.E.E.E., 52, 360 (1964)

53. Smith, R.W.; Phys. Rev., Letters, 9, 87 (1962)

54. Ishida, A., C. Hamaguchi and Y. Inuishi; J. Phys. Soc. Japan, 20, 964 (1965)

55. McFee, J.H. and P.K. Tien; J. Appl. Phys., 37, 2754 (1966)

56. McFee, J.H.; J. Appl. Phys., 34, 1548 (1963)

57. Kikuchi, M.; Jap. J. Appl. Phys., 2, 807 (1963)

58. Yamamomoto, R.; Jap. J. Appl. Phys., 5, 351 (1966)

59. Ishida, A., C. Hamaguchi and Y. Inuishi; J. Phys. Soc. Japan, 21 Suppl., 469 (1966)

60. Haydl, W.H. and C.F. Quate; Phys. Letters, 20, 463 (1966)

61. Haydl, W.H.; Appl. Phys. Letters, 10, 36, (1967)

62. Many, A. and I. Balberg; Phys. Letters, 21, 486 (1966)

63. Stanley, I.W.; Appl. Phys. Letters, 10, 76 (1967)

64. Zucker, J. and S. Zemon; Appl. Phys. Letters, 9, 398 (1966)

65. Bömmel, H.E. and K. Dransfield; Phys. Rev., 117, 1245 (1960)

66. Jacobson, E.H.; J. Acoust. Soc. Am., 32, 949 (1960)

67. Haydl, W.H. and C.F. Quate; Appl. Phys. Letters, 7, 45 (1965)

68. Maines, J.D.; Sol. Stat. Comm., 4, 215 (1966)

69. Miyaka, J. and M. Onuki; Appl. Phys. Letters, 4, 128 (1967)

70. Lampert, M.A.; Phys. Rev., 103 1648 (1956)

71. Chynoweth, A.G.; "Progress in Semiconductor", 4, 103 (1960)

72. Ishiguro, T. and I. Uchida; J. Phys. Soc. Japan, 22, 934 (1967)

73. Autin, B., O. Cahen, E. Dieulesaint, D. Gouvernelle, J. Tavernier and P. Bauduin; Phys. Stat. Sol., 22, K(135) (1967)

74. Hutson, A.R.; Phys. Rev. Letters, 9, 296 (1962)

75. Böer, K.W. and J.J. Ward; Phys. Rev., 154, 757 (1967)

76. Böer, K.W. and J.J. Ward; Solid Stat. Comm., 5, 467 (1967)

77. Das, P. and A.J. Steckl; Appl. Phys. Letters, 16, 163 (1970)

78. Ramestad, A.; Phys. Rev., 155, 744 (1967)

79. Wang, W.C.; Phys. Rev., 155, 744 (1967)

80. Ellis, D.J. and M.G. Cornwall; Phys. Letters, 25A, 135 (1967)

81. Fossum, H.J. and A. Rannested; J. Appl. Phys., 38, 5177 (1967)

82. Haydl, W.H., K. Harker and C.F. Quate; J. Appl. Phys., 38, 4295 (1967)

83. Wettling, W.; Phys. Letters, 25A, 193 (1967)

84. Hobson, G.S. and E.G.S. Paige; Proc. Inter. Conf. Phys. Semicond., Koyoto, Japan, 1966.

85. Pohlendt, E. and W. Wettling; Phys. Letters, 25A, 22 (1967)

86. Zemon, S. et al., App. Phys. Letter, 11, 40, (1967)

87. Miyaka, T. and M. Onuki; Appl. Phys. Letters, 10, 128 (1967)

88. Hervouet, C.; Phys. Stat. Sol., 21, 117 (1967)

89. Ishida, A. and Y. Inuishi; Appl. Phys. Letters, 8, 235 (1966)

90. Nine, H.D.; Phys. Rev., Letters, 4, 359 (1960)

91. Ishida, A., C. Hamaguchi and Y. Inuishi; J. Phys. Soc. Japan, 21, 192 (1966)

92. Moore, A.R.; J. Appl. Phys., 38, 2327 (1967)

93. Ozaki, H. and N. Mikoshiba; J. Phys. Soc. Jap., 21, 2486 (1966)

94. Quentin, G. and J.M. Thuillier; Phys. Letters, 23, 42 (1966)

95. Zilberman, P.E.; Sov. Phys. Sol. St., 9, 231 (1967)

96. Ishida, A. and Y. Inuishi; J. Phys. Soc., Japan, 21, 2078 (1966)

97. Miyaka, T.; Jap. J. Appl. Phys., 5, 728 (1966)

98. Böer, K.W. and U. Kümmel; Z. Naturforsch, 13A, 698 (1958)

99. Böer, K.W. and U. Kümmel; Ann. Physik, 6, 303 (1957)

100. Kallmann, H. and P. Mark; Phys. Rev., 105, 1445 (1957)

101. Trodden, W.G.; Brit. J. Appl. Phys., 18, 401 (1967)

102. Smith, R.W. and A. Rose; Phys. Rev., 97, 1531 (1955)

103. Smith, R.W.; Phys. Rev., 105, 900 (1957); RCA Rev., 20, 69 (1959)

104. Fochs, P.D., W. George and P.D. Augustus; J. Crystal Growth, 3, 4, 122 (1968)

105. Maines, J.D. and E.G.S. Paige; Elect. Letters, 3, 10, 549 (1967)

106. Airtron, A division of Litton Industries, Morris Plaines, Jersey.

107. Monchamp, R.R., R.C. Puttback and J.W. Nielson; U.S.A.F. Technical Report, No. AFML-TR-67-144, June 1967.

108. Hamphill, R.B.; Appl. Phys. Letters, 9 (1), 35 (1966)

109. Bube, R.H.; "Photoconductivity in Solids".

110. Weinreich, G.; Phys. Rev., 107, 317 (1957)

111. Smith, R.A. "Semiconductors", Cambridge University Press (1959)

112. Ishiguro et al.; J. Phys. Soc. Japan, 19, 674 (1964)

113. Uchida et al.; I.E.E.E. Trans. on Sonics and Ultrasonics Su-12, 9 (1965)

114. Maines, J.D., F. Marshall, E.G.S. Paige and R.A. Stuart; Phys. Letters, 26A (8), 388, (1969)

LIST OF SYMBOLS

α Attenuation constant

a Cross sectional area of specimen

A Negative edge of shielded strip

C Elastic constant

C Modified elastic constant

D_n Diffusion constant for electrons

D Electric displacement

d Width of light strip

e Piezoelectric constant

E Electric field

E_o Applied d.c. field

E_1 Amplitude of a.c. field due to ultrasonic wave

E_{th} Threshold field

ϵ Dielectric permittivity

f Frequency of oscillations

f Fraction of space charge due to mobile carriers in derivation of and J_{ae}

$\gamma = 1 - \frac{V_d}{V_s}$

I Current

J Current density

J_{ae} Acoustoelectric current density

K Propagation constant

K Electromechanical coupling constant

L Length of the specimen

L_1 Low resistivity region in the specimen

L_h High resistivity region in the specimen

L_c Length of the shielded region from the cathode end of the specimen

L_d Length of the shaded region

L_x Length of specimen from the anode end of the specimen

l Distance of irregularity from anode

l_h Length of L_h

l_c Length of L_c

l_o Incubation distance defined in Fig. 9

l_1, l_2 Distances of z_1, z_2 from the anode

n Carrier density

n_e Density of electrons in the conduction band

n_o Equilibrium number of electrons which give electrical neutrality in the absence of an ultrasonic wave

n_s Number of electrons per unit volume required to produce the charge Q

q Magnitude of charge on an electron

Q Space charge density

ρ Mass density

S Strain

σ Conductivity

T Stress

t Time

τ Period of oscillations

τ_s Sonic transit time

τ_o Incubation time

τ_R Dielectric relaxation time

τ_d Time during which domain observed

τ_g Duration of shock excitation

λ_D Debye length

μ Drift mobility of electrons

u	Lattice displacement
U	Acoustic power
V	Applied voltage
V_{th}	Threshold voltage
V_d	Drift velocity of carriers
θ	Ratio of the measured current to the Child's Law current at V_{tf}
V	Phase velocity
V_s	Sonic shear wave velocity
V_ϕ	Phase velocity of wave
V_{tf}	Trapped filled voltage
ω_R	Dielectric relaxation frequency
ω_C	Dielectric relaxation frequency given as 1.25×10^{12} for shear waves and 1.2×10^{12} for longitudinal waves as given in reference (31)
ω_D	Diffusion frequency given as 4.8×10^9 for shear waves and 2.9×10^9 for longitudinal waves (at $300^\circ K$) in reference (31)
ω	Acoustic wave frequency
x	Distance of the light strip from the anode end of the specimen
z	Direction of propagation, also the distance from the cathode
z_1, z_2	Regions of irregularities